Spring 2021

Stretching the Limits in Thermoplastic Forming of Bulk Metallic Glasses

Rodrigo Miguel Ojeda Mota

Yale University Graduate School of Arts and Sciences, r.ojeda@tutanota.com

Abstract

Stretching the Limits in Thermoplastic Forming of Bulk Metallic Glasses

Rodrigo Miguel Ojeda Mota

2021

Metallic glasses (MG) suggest that superb mechanical properties can be paired with plastic-like processing. Their high strength and elasticity are often paired with fracture toughness. Their supercooled liquid region gives rise to plastic-like processing and suggests parts and shapes that can otherwise not be obtained for crystalline metals. However, current processing techniques only allow for limited options in terms of geometry, thicknesses uniformity, and shape complexity. In the first part of my thesis, I introduce the form-giving aspect of metallic glass thermoforming, by introducing stretch blow molding, to expand the geometries that can be fabricated with metallic glasses. For this I developed a model, which allows to quantify stretch blow molding and provides insight into its potential use and limitations. We demonstrate that with stretch blow molding overall strains exceeding 2000% are achievable, significantly higher than the previously reported ~150% of blow molding. In the second part of my thesis, I focused on the effect of the processing on metallic glasses properties. This is motivated by the current understanding that most metallic glasses lack sufficient ductility or toughness when fabricated under conditions resulting in bulk glass formation. To address this shortcoming, I used strain rate to excite the liquid while simultaneously cooling it to freeze the excited liquid into a glass with a higher fictive temperature. Microscopically, straining causes the structure to dilate, hence

"pulls" the structure energetically up the potential energy landscape. Upon further cooling,

the resulting excited liquid freezes into an excited glass that exhibits enhanced ductility. I

used $Zr_{44}Ti_{11}Cu_{10}Ni_{10}Be_{25}$ as an example to pull metallic glasses through this excited liquid

cooling method, which can lead to the tripling of bending ductility.

Stretching the Limits in Thermoplastic Forming of Bulk Metallic Glasses

A Dissertation
Presented to the Faculty of the Graduate School
Of
Yale University
In Candidacy for the Degree of
Doctor of Philosophy

By
Rodrigo Miguel Ojeda Mota

Dissertation Director: Jan Schroers

June 2021

Contents

Chapter 4. Processing Aspects on the Metallic Glass Properties

Chapter 5. Improving Ductility Through Straining 64

Table of figures

Acknowledgments

I want to show my gratitude to all the people that were part of this journey. To my committee members Corey O'Hern, Madhusudhan Venkadesan and Rui Yamada for the time taken to review and provide feedback to my research.

To the staff at Yale who always went the extra length, Vinnie Bernardo and Bill Samela for their help machining parts and pieces; Nick Bernardo for teaching me against his will how to machine pieces and parts, but even more for being a friend always willing to listen. To Victor Padilla-Taylor for his mentorship outside the world of engineering and metallic glasses and Vincent Wilczynski for providing support in order to explore new paths. Andy Morcus, Janet O'Dell, Mary MacNicholl, and Cara Gibilisco for having all the answers related to administrative support and always had a friendly face.

To all the great and amazing people I met during my time for the Ph.D. at Yale until today. Since my first year as a research assistant, I Would like to thank Wen Chen, Ze Liu, and Yanhui Liu for always making me feel welcomed and part of the group. To Jittissa Ketkaew and Punnathat Bordeenithikasem, they always provided a helping hand when research did not go as it should.

To all who visited Yale even if for a brief moment, I had a blast and enjoyed every second we worked together, Victoria Kaban, Witor Wolf, Yannic Duc, Shaofan Shao, Ling Shao, and David Browne.

To current Schroer's lab members, Salena Huang, Guannan Liu, Naijia Liu, and Arindam Raj. To my sailing mate Sebastian Kube who has the best "perreo" I have seen among scientists. To Ethen Lund for providing the energy and drive this research required. To

To my mother, who was always there to listen.

To my father, for whom I started this journey.

Chapter 1. Motivation, Background, and Key Contributions

1.1 Motivation, Metals, Plastics, and the Best of Both Worlds

In the ever-evolving need for new products and intricate designs, materials scientists have been developing new materials and processes to meet these needs. In the past 150 years two types of materials; plastics and metals, have become the leading options in industrial design.

Plastics can be readily processed and shaped. Techniques include die forming, extrusion, injection molding, compression molding, and blow molding [1], which allow a wide range of shapes. Something as familiar as a soda bottle can be processed to have undercuts, stamping, and be made in asymmetric shapes. They can be shaped very fast and at the cost of a few cents. Yet, plastics often exhibit insufficient strength and toughness. In contrast, metals are the archetype of a structural material with high strength and toughness. They are used from centimeter-sized pins that hold you on the ride of an amusement park to meter-sized beams and planks that provide support to buildings and vessels. Although there is a considerable amount of processing techniques for metals such as casting, drawing, hydroforming, CNC machining and others; metals processing has always been limited to a few simple symmetric geometries, such as sheets, bars, tubes, and cylinders. While CNC machining increases the opportunity of shapes obtained, as the part's complexity increases, the amount of wasted material does so proportionally. Although 3D printing has seen major breakthroughs in current years, there is still a limit in the minimum thickness that can be achieved with this technique.

Today, making the same soda bottle which takes seconds and costs cents is a major challenge to realize as a metal. The available aluminum soda bottles cannot be fabricated in a single step or piece, taking longer to process, and sometimes costing more than 100 times the cost of their plastic counterpart. Even more important, they're still restricted to simple high symmetry shapes, making the addition of undercuts, asymmetries, or extra features on the surface virtually impossible[2].

The focus of this thesis has been to explore if there are processing methods that allow processing of metals like plastics. To have the ability to merge the best characteristics of both materials and be able to provide new products parts and shapes, that cannot be otherwise obtained for regular metals. By using metallic glasses, which are a new type of materials that could be processed in a similar fashion to plastics while also displaying the strength and structural integrity that the best metals provide, we set to develop a new processing technique that allowed to obtain parts with larger aspect ratios than what was previously possible for metallic glasses.

This can be best appreciated in Figure 1: There exists an ideal region for the properties displayed by the materials/parts under use which polymers cannot achieve, this region is characterized by a high strength/viscosity of the material, hence, processing under this region is not feasible. Metals can be molten to process them, but the viscosity drops too low to be useful for any meaningful forming technique. On the other hand, polymers and metallic glasses can be "softened" to just the right amount, making its viscosity sufficiently low to allow the use of many processing techniques but not so low that there is no control of the deformation process.

In this regard we aimed to develop a new processing technique that allowed for a controlled deformation of the metallic glass while providing access to new options in terms of strains, shapes, and designs.
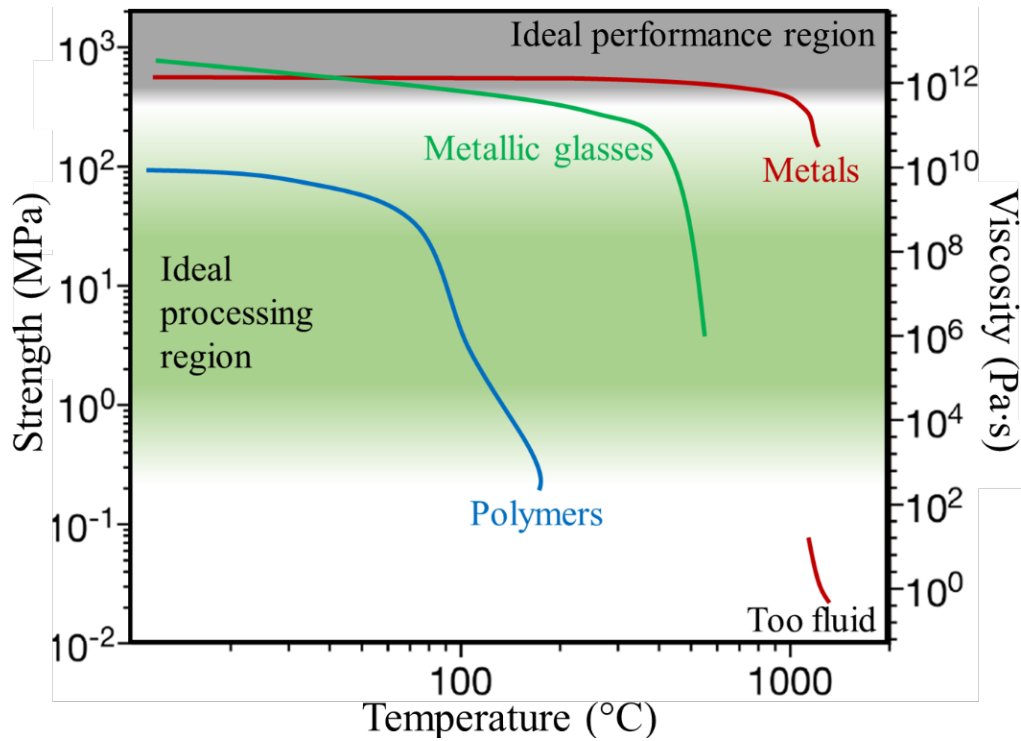
Figure 1. Ideal performance vs. ideal processing regions for polymers, metals, and metallic glasses

Likewise, processing a material is half of the equation, as you will see it is the case for metallic glasses, being able to maintain the properties or improving them once the material is processed is also of paramount importance. We thus, set to find innovative ways to improve the ductility of metallic glasses during the processing and determine the circumstances and conditions that makes it possible.

1.2 Background: Materials Shapes and the Need of a New Kind of Materials

Products that can be obtained and manufactured can be classified in two distinctive groups: one where the thickness is on the same order of magnitude in size with respect to other dimensions which will be called closed shapes (Figure 2). For the closed parts most of the manufacturing technology is already mature and well developed either for polymers or metals. In contrast, parts with cavities and high aspect ratios where the thickness is significantly smaller compared to the rest of the dimensions will be called open shapes. These are in a high demand for use in a wide range of applications, including containers, casings, housings, covers, tubing, hoses, and bellows. While a wide range of processes exists for the fabrication of closed shape articles, including forging, casting, and stamping, processes to fabricate open shape metal parts are limited to high symmetry shapes, which are generally difficult to realize in a metal. CNC can be used in some cases, but the amount of material lost makes it cost prohibitive as the complexity of the part increase. Additive manufacturing alleviates the challenge to some extent; however, closed shape articles are much easier to fabricate than open shape metal articles with a thin wall thickness[3-6].
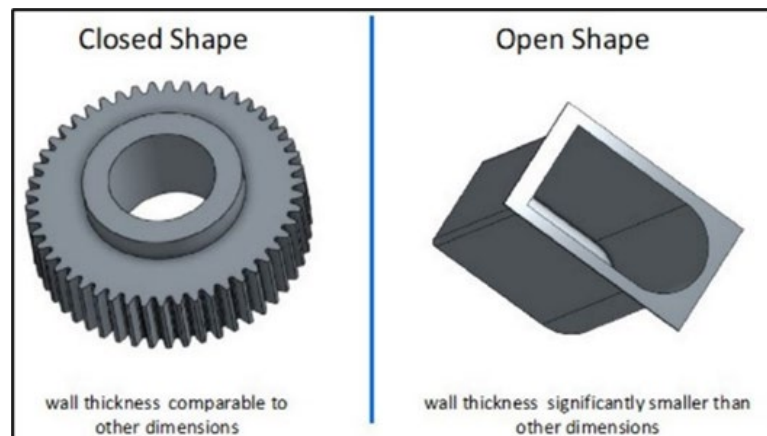
Figure 2.Classification of the obtainable parts according to their final geometry

With the rise of super plastic forming (SPF), some limitations in fabricating open shape metal articles have been overcome in relation to size, thickness, and usable metals[7-10]. Extensive research has concluded however, that SPF suffers from material thinning and is limited to relatively low achievable strain rates[11].

Open shape articles can be readily achieved in thermoplastics[12, 13]. One example is extrusion blow molding, which can fabricate high-strain parts within seconds, as demonstrated by the canonical example of the soda bottle. The reason for such ease is that thermo-plastics exist in a viscosity range on the order of 10^2–10^5 Pa·s, where they can be readily deformed under gas pressure. Such a viscosity range is generally not accessible in metals, which was suggested as the reason for the asymmetry in the difficulty of fabricating metals vs. thermoplastics[14].

1.2.1 Bulk Metallic Glasses: A Versatile Material

A metallic material class that provides access to such a viscosity range is metallic glasses[15-17], being discovered in 1960[18], metallic glasses are relatively new in the material science arena and are the focus of active research; made from multi-metallic alloys, the main element can vary from system to system, Au, Al, Cu, Fe, Zr, Ti, Ni and many more can conform systems of bulk metallic glasses[19-24], but regardless of their composition the fingerprint characteristic is that the internal atomic arrangement is amorphous. This structure is obtained through rapid cooling, there is a critical cooling rate (R_c) that must be achieved to obtain an amorphous structure (Figure 3).
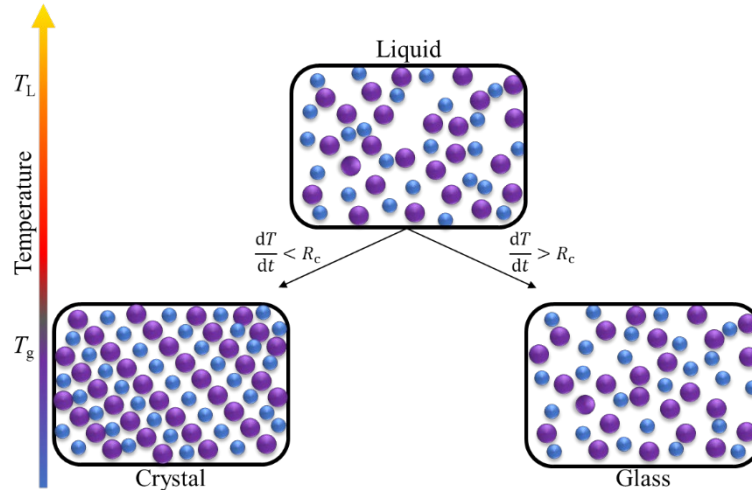
Figure 3.Glass formation from metallic alloys upon cooling, the cooling rate will determine the final structure of the sample.

The critical cooling rate can be determined in a Time-Temperature-Transformation diagram (Figure 4a): conventional metallic systems tend to generate crystalline structures upon cooling from liquidus temperature (T_L) as is the most thermodynamically stable equilibrium state. Metallic glasses avoid crystallization by fast cooling the metallic glass from T_L below a glass transition temperature (T_g) where the material is kinetically impeded to impart periodicity to its atoms, leaving the material in a metastable equilibrium state without any long-range periodicity in three dimensions[25]. Arriving at this crystallization nose, needs to be avoided to obtain an amorphous material, and its exact location is determined experimentally for each metallic glass system[26]. The region between the liquidus temperature and the glass transition temperature is denominated supercooled liquid region (SCLR); although the ability of pure metallic elements to be made amorphous by the same method has been long theorized, the time window to form a glass is very low (Figure 2b), requiring cooling rates close to 10^{12} K/s whereas for metallic glasses the required cooling rate can be on the order of a few K/s. Is only recently in 2014, when it

was demonstrated by ultrafast quenching of Tantalum nanotips, that single pure elements could form glasses[27].
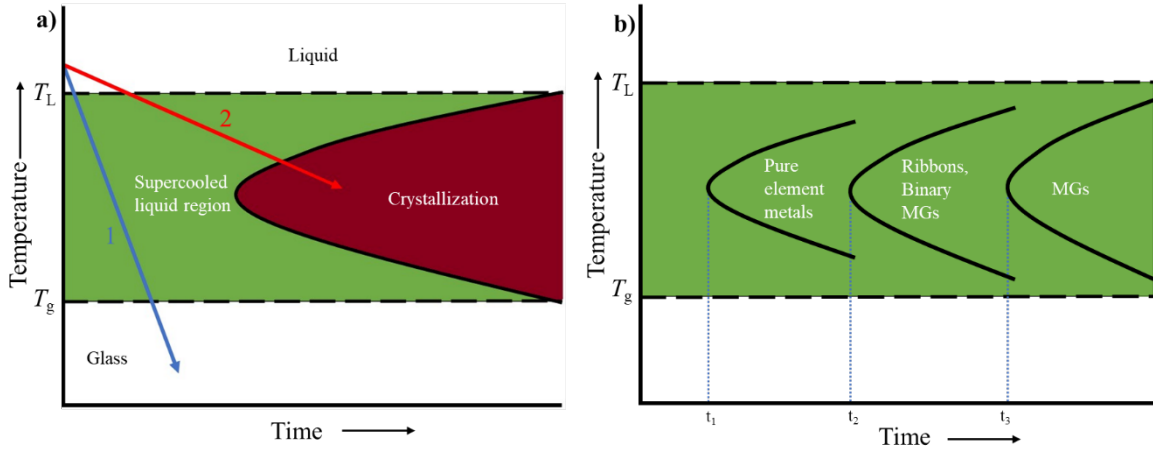
Figure 4. a) Schematic of a TTT diagram, depending on the cooling rate imparted on the alloy from the liquidus temperature, the alloy can (1) crystallize or (2) form a glass b) Schematic of the timescales required to form a glass for pure metals, ribbons, or bulk metallic glasses

1.2.2 The Best Metallic Material in Terms of Processing

When processed in the liquid state, the viscosity of most metals is like that of the water, this provides a facile deformation, but it is too low of a viscosity that the evolution of the deformation process becomes uncertain, reducing the options of processing metals in this condition only to die casting. Plastics have an advantage for this matter, by presenting a T_g they can be softened, but present a viscosity that provides control over the deformation process which increase the processing options. Metallic glasses display the same behavior when heated between T_g and T_L, on the SCLR, the viscosity can drop drastically at a rate of ~1 order of magnitude for every 20 K increased in temperature, making them ideal candidates for processing[16, 28, 29]. There exist however, several differences in the behavior between polymers and metallic glasses while in this softening region; metallic

glasses are considered to behave as a purely Newtonian fluid whereas polymers have a viscoelastic behavior and a viscosity dependance on the shear rate. Also, the viscosities observed differ several orders of magnitude, for perspective Table 1, shows the viscosities of different liquids. Although some non-Newtonian behavior has been observed in metallic glasses, it has been associated with the formation of extra free volume, nanoclusters, or nanocrystals, and not from an intrinsic characteristic of a "pure" metallic glass[30-33].

Table 1.Viscosities of different materials

Material	μ (Pa·s)
Air (0°C)	1.7×10^{-5}
Molten steel (1500°C)	10^{-3}
Water (20°C)	10^{-3}
Mercury (20°C)	1.6×10^{-3}
Oils	10^{-2} to 10^4
Polymer melts	10^2 to 10^4
Molten glass	10^2 to 10^4
Metallic glass in SCLR	10^6 to 10^{12}

The most crucial difference between polymers and metallic glasses is that where polymers cant crystallize to a 100%, metallic glasses will fully crystallize after a certain period of time if left at a temperature between T_g and T_L (chapter 2), leaving a limited amount of time for processing, but nonetheless making them a suitable candidate for the manufacture of parts where the mechanical properties of metals are required[34, 35].

1.2.3 Mechanical properties of metallic glasses: Strength, fracture toughness, and ductility

The superb mechanical properties of metallic glasses derive from its amorphous structure, which prevents the formation of grain boundaries, dislocations and defects that are

otherwise present in crystalline systems. From a structural viewpoint strength and ductility are two characteristics that determine the quality of the service a part will produce. Bulk metallic glasses display a tensile yield strength that compares or surpasses most of the conventional alloys, at the same time, they display an elastic limit around 2% which is on par with polymers and almost 10 times a s those of metals (Figure 5)[36, 37], the metallic glass with the highest strength is known to exceed 5 GPa, while the best Ti and Fe alloys approach 0.5 to 1.5 GPa at most[38].

While strength is of paramount importance to provide structural support, fracture toughness and ductility are also key parameters for the usability of the material. If we define fracture toughness as an indication of the amount of stress that a material can withstand before propagating a preexisting flaw, it becomes evident that it would play a central role as manufacturing processes are far from ideal conditions.
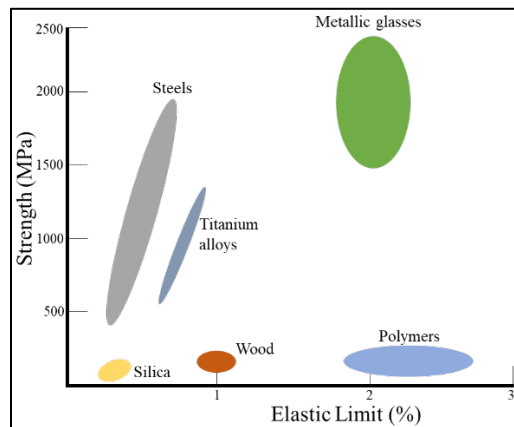
Figure 5. Strength and elastic limits of metallic glasses compared to other materials. Adapted from [36]

Fracture toughness in metallic glasses varies dramatically and has been the subject of a wide range of studies; from a near perfectly brittle behavior of fracture toughness values

of ~2 MPa·m$^{1/2}$ for Mg based metallic glasses[39, 40], to the toughest examples with ~200 MPa· m$^{1/2}$ for a Pd based metallic glass[41]. This phenomenon is present even for a same family of metallic glasses where researchers have obtained different values (Figure 4)[42-46]. This effect has been attributed not only to the randomness of the molecular structure inherent of metallic glasses but also to the procedure used to prepare the samples[47, 48], pointing to processing conditions being of vital importance for the final mechanical properties provided by metallic glasses.
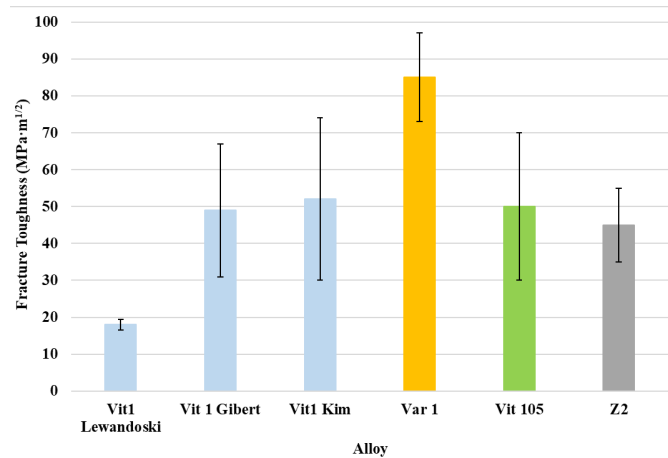
Figure 6. Fracture toughness data from separate research groups for a family of Zr-based alloys. Vit1: $Zr_{41.5}Ti_{13.75}Cu_{12.5}Ni_{10}Be_{22.5}$, Var 1: $Zr_{33.5}Ti_{24}Cu_{15}Be_{27.5}$, Vit 105: $Zr_{52.5}Al_{10}Ti_5Cu_{17.9}Ni_{14.6}$, Z2: $Zr_{55}Cu_{30}Ni_5Al_{10}$ Adapted from [49]

From a structural point of view, ductility is also important to consider as it precludes the material from a catastrophic failure during service. Usually, ductility is provided through a high level of plastic deformation in materials, common alloys and metals display ductility through slipping and twinning; having multiple slip systems from highly symmetrical structures and low resistance from the lattice for dislocation motion can provide most crystalline materials very good plasticity and hence ductility. Bulk metallic glasses lack

these mechanisms due to its amorphous nature, hence suffering from low ductility. A typical stress-strain curve under tension for metallic glasses will display a high level of elasticity and yield strength but a non-existent plastic deformation for all practical purposes, exhibiting brittle behavior (Figure 6a). Ductility can be enhanced in metallic glasses by different means, thermal treatments, mechanical cycling, changes in the geometry or the size of the parts, by introducing heterogeneities, severe plastic deformation, and others[50-54]. In geometries under 1 mm metallic glasses can show ductility due to plastic deformation occurring in a highly localized manner[55](Figure 6b). Ductility in metallic glasses will be explored in more detail in chapter 4.
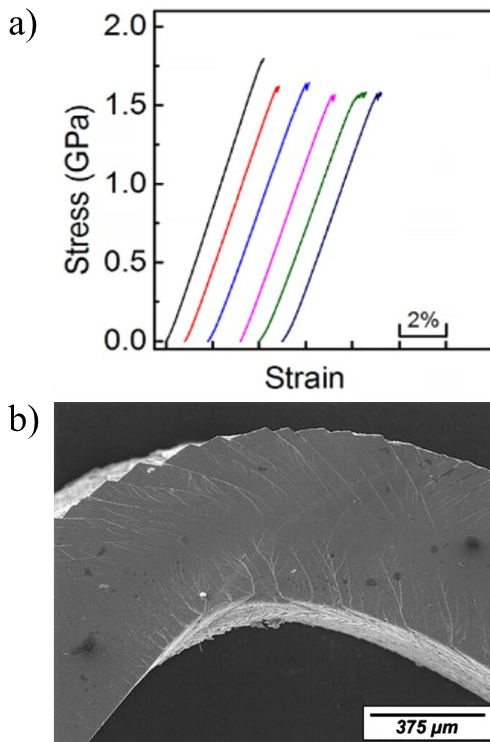
Figure 7. a) Typical tensile stress-strain curve for a metallic glass exhibiting a brittle behavior b) Micrograph of plastic bending of a Zr based metallic glass under 1mm in thickness. Adapted from [55, 56]

1.3 Key Contributions

Although metallurgy and its manufacturing techniques have been a part of the human progress since ancient ages, the development of new processing techniques has slowed tremendously in the past few decades. This can be attributed to the intrinsic characteristics of metals, and it translates to a rather limited portfolio of available shapes and structures that can be formed. By departing from the regular crystalline structure of most metallic alloys, metallic glasses present a new opportunity of developing new processing techniques that increases this portfolio of shapes and structures. By looking at blow molding for plastics, and the form-giving aspects of thermoplastic forming (chapter 2) we were able to develop a new technique for metallic glasses, "Stretch blow molding", which increased the strain rates that could be attained compared to previous techniques from 150% in strain to over 2000% and accessed thicknesses not previously available for metallic parts. We also explored at the thickness distribution models available and develop a new model that better adjust to the process we developed while determine the conditions that provide a better control of the thickness evolution (Chapter 3).

Even though metallic glasses can be processed as plastics, there are some processing aspects on the metallic glasses properties that need to be considered. The presence of a supercooled liquid region, a crystallization nose, and the cooling rate used during processing will all influence the properties of the material. Straining while cooling from the supercooled liquid region, was theorized to affect the mechanical characteristics of the metallic glasses (Chapter 4). We provide direct evidence that ductility can be increased over 3 times by straining under cooling from the SCLR for a $Zr_{44}Ti_{11}Cu_{10}Ni_{10}Be_{25}$ alloy and propose a framework called "Exited liquid cooling mechanism" to define under which

conditions does straining lead to better mechanical properties and how it can be applied to existing processing techniques (Chapter 5).

We also look at the new questions and unknowns that have arisen from this work and those that remain unanswered that will complement it (Chapter 6).

Finally, although not integrated in this thesis, we encourage the reader to read [57] which takes a look on the metallic glasses with the best mechanical properties and where the "Criticality" framework is used to look at the selection of the metallic glass components from an environmental, ecological and political perspective. with the growing interest on using materials that have low environmental and ecological footprint this could be used as a guide for selection and development of metallic glasses from a non-traditional perspective.

Chapter. 2 Form-Giving Aspects of Thermoplastic Forming

2.1 TTT Diagram and Formability

Although being the characteristic that provides an advantage of metallic glasses over regular metals in terms of processing, the appearance of a SCLR and a crystallization nose is also the one that presents the initial hurdle to have an unlimited number of processing steps and maintain the properties of the material through them. Upon cooling from melt, metallic glasses attain a high energy state (metastable). Once reheated from room temperature to a temperature above T_g, the atoms inside a metallic glass have the required kinetic energy to move around and initiate the process to rearrange themselves in a crystalline fashion to lower their energy state. Crystallization of metallic glasses occur between T_g and a crystallization temperature T_x below the liquidus temperature of the alloy and, once crystallized, the alloy (no longer a glass) will lose most of its mechanical properties, rendering it useless. Avoiding crystallization then, is important from the technological perspective and it is one of the major problems to avoid in processing metallic glasses[38, 58, 59].

The temperature range for the SCLR and the size of the crystallization nose will be dependent on the alloy components, making the available time to crystallization at a given temperature from seconds to hours[60-62]. Theoretically, the capacity of the material to be formed can be described by the maximum strain before reaching crystallization, so for an isothermal process, the formability is given by:

$$F_{iso} = \frac{t_{cryst}}{3\eta}$$

Where the isothermal formability (F_{iso}) is dependent of the time to crystallization (t_{cryst}) and the viscosity (η) [63, 64]. The formula reveals a strong dependance on temperature, since the viscosity change for one order of magnitude every 20 K while the crystallization time changes about an order of magnitude every 50 K[65] (Figure 8a), making any error of even 10 K during experimental procedures vary the value obtained quite a lot. The most widely used method to assess formability is a standard method introduced in 2008, where 0.1 cm^3 of material is compressed at a constant load of 4500 N and heated from T_g to T_x at a heating rate of 20 K/min, resulting in discs with different diameters (Figure 8b). This allows a more practical way to determine and compare formability between different systems and their selection[66].
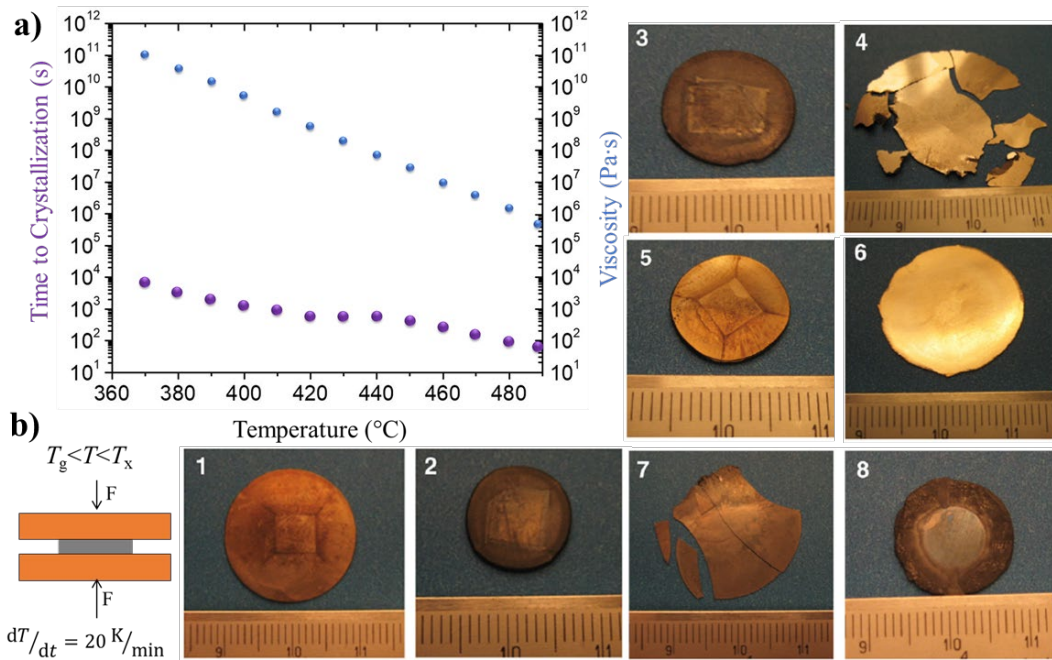
Figure 8. a) TTT diagram vs viscosity for Zr₄₄Ti₁₁Cu₁₀Ni₁₀Be₂₅ b) Formability evaluation of various metallic glasses: (1) Zr₄₄Ti₁₁Cu₁₀Ni₁₀Be₂₅, (2) Zr₅₇Nb₅Cu₁₅.₄Ni₁₂.₆Al₁₀, (3) Zr₅₈.₅Nb₂.₈Ni₁₂.₈Cu₁₅.₆Al₁₀.₃, (4) Pt₅₇.₅Cu₁₄.₇Ni₅.₃P₂₂.₅, (5) Zr₄₁Ti₁₄Cu₁₂Ni₁₀Be₂₃, (6) Au₄₉Ag₅.₅Pd₂.₃Cu₂₆.₉Si₁₆.₃, (7) Pd₄₃Ni₁₀Cu₂₇P₂₀, (8) Zr₆₅Al₁₀Ni₁₀Cu₁₅. The final diameter provides a better indication of formability amongst different metallic glasses. Adapted from [66, 67]

2.2 Die Casting and Thermoplastic Forming

This leaves two approaches for the processing of bulk metallic glasses (Figure 9); the first one consists of directly casting from the melt with methods such as die casting and suction casting[68-70]. One of the benefits of die casting is that bulk metallic glasses present lower shrinkage upon solidification, about 0.5% compared to 5% of regular alloys[71, 72]. It also provides the opportunity to have a high-volume production of small to medium size articles, limited mostly by attaining the required cooling rate throughout the part, the thicknesses would range typically from a few millimeters to 10 centimeters depending on the alloy system.
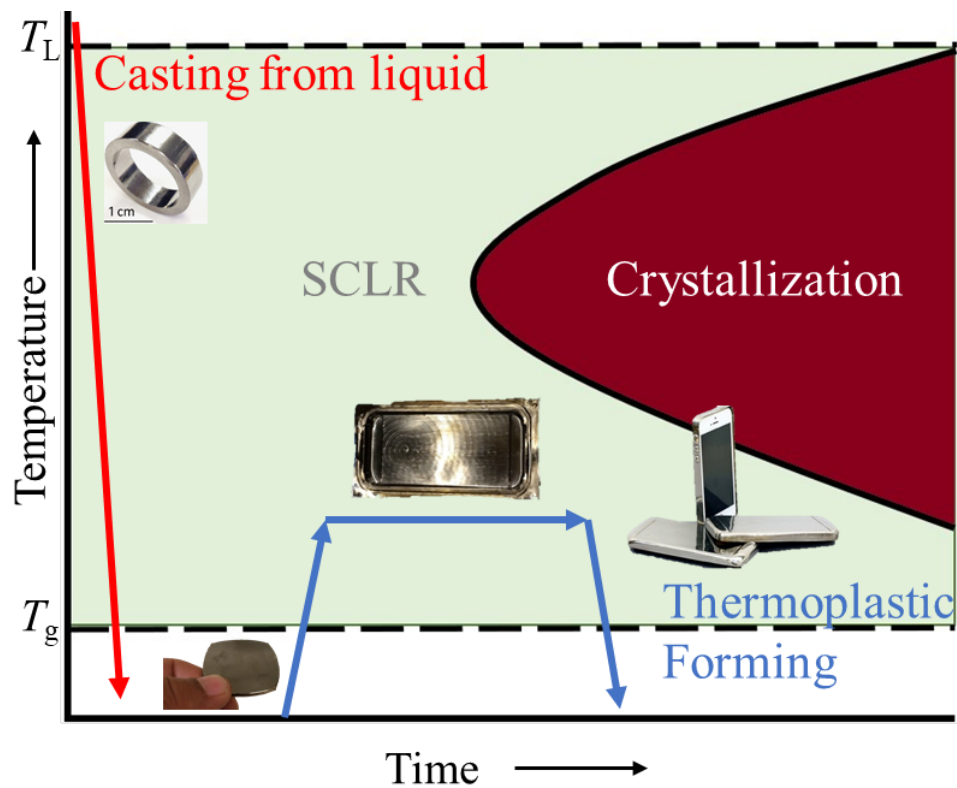
Figure 9. Processing for metallic glasses can be done through casting from the melt or by thermoplastic forming.

16

Having low melting temperatures, it reduces the energy required to process over regular metals, which translates in lower costs due to a shorter heating cycle, lower energy consumption and the need of less specialized tools and molds. Nonetheless, the critical cooling rate (R_c) and the shape of the TTT diagram can be affected by the temperature from where the metallic glass was cooled down. It has been found that for a wide range of glass forming alloys, there exist a threshold temperature that must be exceeded in order to have a metallic glass with good characteristics, this temperature (T_{OH}) is usually 300°C above the liquidus temperature of the metallic glass[73-75], and in some cases overheating the metallic glass can affect the viscosity of the material[73, 76, 77], overall diminishing the benefits of having a low liquidus temperature.

While shrinkage is significative less than with other metals, any gap between the mold and the metallic glass could affect the cooling rate, making this gap the limiting factor for the heat transfer. Also during casting, the metallic glass must be under non-oxidative atmosphere as this promotes crystallization, while depending on the system used, there could be a meaningful correlation between the ability of the alloy to form a glass, and the pressure use during casting[78]. Finally, having the metallic glass forming process coupled with the part shaping, usually means that as the designs become more intricate, the more difficult will be to maintain the mandatory cooling rate through the whole part while assuring a complete filling of the mold[20, 79]. Is for this reasons that direct casting from the liquid will provide a low yield of options besides a few elemental shapes such as rings, rods, or plates.

The second available option consist of thermoplastic forming; by considering the circumstances mentioned before we can decouple the metallic glass forming process from the part shaping: making a preform or stock, while in a separate step heat it above its T_g and deform it to the geometry required if we do not reach crystallization. It has been found that the available time to process metallic glasses is that for samples processed at a single temperature, the time available to the onset of crystallization is additive, but for a multi-step process the time to crystallization severely deviates from an additive behavior[80], so a careful selection of materials and processing steps is needed, but thermoforming has been the preferred method for expanding the options to process metallic glasses.

One such method is hot rolling, this technique has been demonstrated to be useful in producing bulk metallic glass sheets [81]. For example, a disc of 1.7 mm in thickness and 14 mm in diameter can be rolled to obtain a 100 µm thick and an equivalent diameter of 60 mm; the author participated in the development of this technique and is currently under commercial usage[82]. Although hot rolling can be useful to obtain feedstock material for the proposed technique in this prospectus, it is unpractical for using it as the sole medium of production of open shaped parts, since generating parts will require subsequent folding and joining of the material to obtain high aspect ratio parts in three dimensions.

2.3 Compression Molding and No-Slip Conditions

To go from two-dimensional sheets to three-dimensional shapes compression molding has been adapted from polymer processing into metallic glasses. It has been the most used in the formation of closed shapes from gears to net-shape samples that allows consistent

measurement of the fracture toughness of metallic glasses making it the de facto method of processing metallic glasses [19, 21, 47, 48, 83].

During compression molding, a feedstock material is placed between two molds and heated into the SCLR, once the required viscosity is reached, a pressure that exceeds the flow stress of the material is applied to deform into the required shape, this process does not require fast cooling and the part would be useful if is not allowed to crystallize, figure 10 shows an schematic of the process an examples of the versatility of the compression molding process, several parts from a few hundredths of microns to a few centimeters can be achieved. It is also very useful for imprinting and embossing.
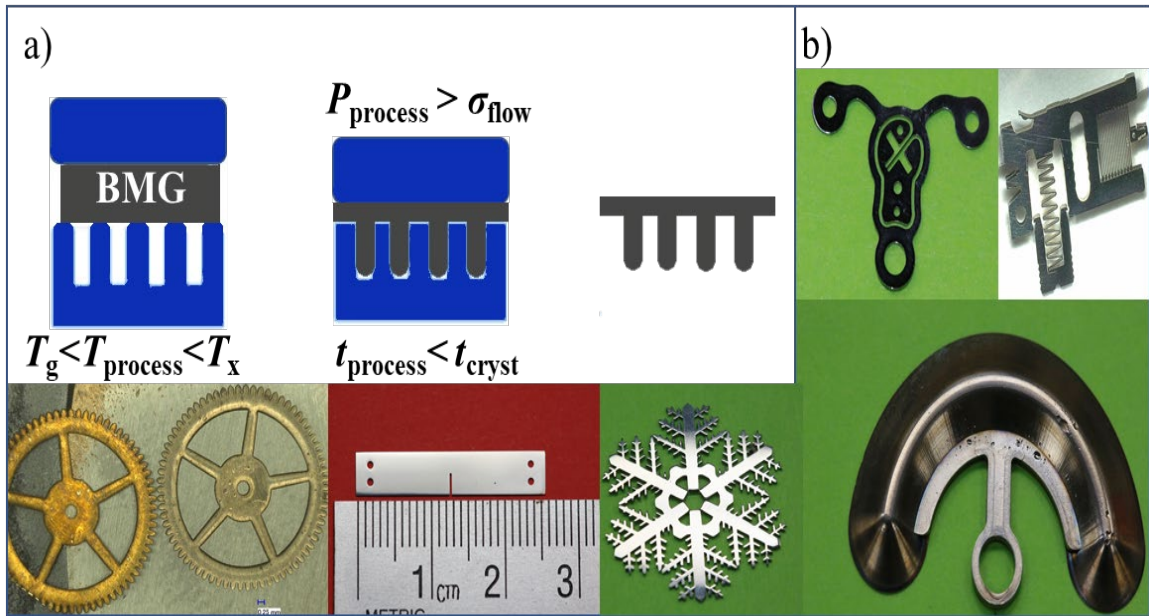
Figure 10. a) Schematics of compression molding b) Examples of the versatility of shapes that can be obtained through compression molding.

In terms of its use for the fabrication of high aspect ratio parts, it has been shown to be useful for making parts with a low aspect ratio (~2) with dimensions of centimeters and where the thickness remains in the order of millimeters [20]. But fabricating thin-walled open shape metallic glass parts with high aspect-ratios is challenging when using techniques like compression molding. This is because during TPF, the metallic glass is subject to perfect stick conditions (zero velocity at metallic glass/mold interface)[84]. The resulting creep-flow exhibits a scaling of forming pressure (P), with wall thickness (d) of:

$$P = 32\frac{\eta v L}{d^2}$$

Where v is velocity, η is viscosity and L the filling depth. Such scaling suggests that compression molding becomes rapidly more difficult when forming articles with thin walls[16, 85]. If we consider the velocity (v) the filling length (L) divided by the maximum time available for the metallic glass to flow, crystallization time (t_{cryst}), we arrive at the equation:

$$L = \sqrt{\frac{P * t_{cryst} * d^2}{32\eta}}$$

Where we can estimate the maximum filling depth for a particular set of conditions.

Figure 11 shows the calculated maximum filling depth for a channel with diameters from 0 to 3 mm. The calculation assumes the use of $Zr_{44}Ti_{11}Ni_{10}Cu_{10}Be_{25}$, which at 460°C has a viscosity of $9.8x10^6$ Pa·s and a crystallization time of 315 s. If we consider a typical pressure used of 15 MPa it is easy to see how obtaining parts with high aspect ratio and reduced thickness becomes harder as we approach smaller sizes. Surprisingly, in the

nanometer size, the use for compression molding has found use to make closed high aspect parts (~20) where the effect of capillary forces drives the material flow [86, 87].

$$L = \sqrt{\frac{P * t_{cryst} * d^2}{32\eta}}$$

Filling depth vs. Diameter
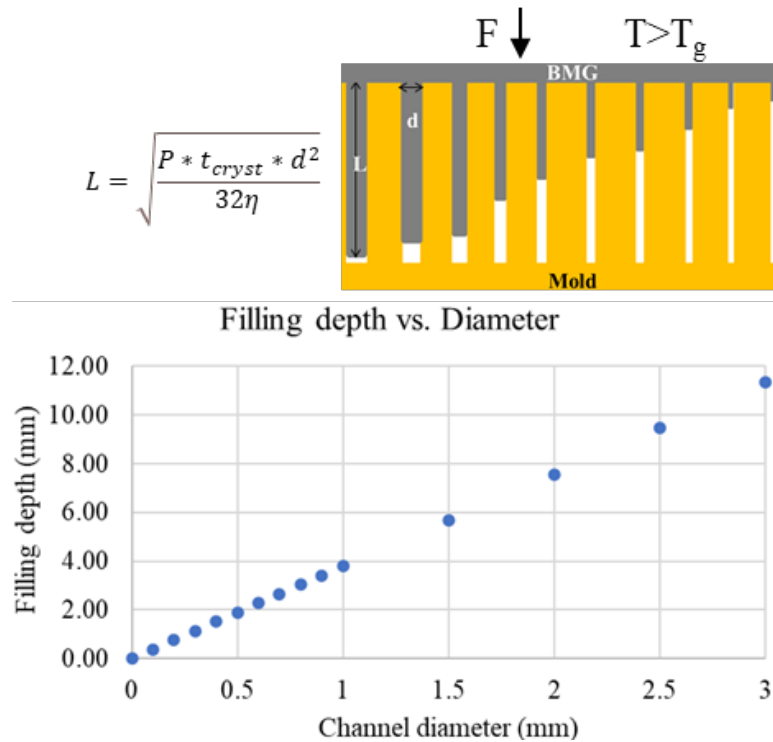
Figure 11. Maximum filling depth for different channel diameters.

In terms of other processing techniques such as extrusion, besides increasing the pressure required as the thickness of the channel decreases, the non-slip condition together with a crystallization time, implies that over time the layer in contact with the mold that did not flow, eventually crystallizes, effectively reducing the channel thickness over time and being the reason why process like extrusion, although very popular for plastics, it has not been adopted for metallic glasses.

2.4 Blow Molding and Delaying Mold Contact

An approach to drastically reduce the required shear strain and shear stress rates for the same geometry is the use of processes where the metallic glass is, for the most part, not in contact with the mold during the shaping operation. One of these processes is blow molding, where low pressures (~1 atm) and short times (~10 s) have been demonstrated to suffice for the fabrication of thin wall open shape articles [88-90]. In the absence of any flow restriction, for a free forming bubble, the pressure required to form it is close to the pressure generated with the human lung (~10^4 Pa). The stress present in the walls of the forming hemisphere can be estimated by:

$$\sigma_H = \Delta P \frac{r}{2t}$$

The stress on the hemisphere wall (σ_H) is defined by the pressure difference (ΔP), the radius of the bubble (r) and inversely proportional to the thickness (t). For a bulk metallic glass to deform in the SCLR, the flow stress must be lower than the stress experienced by the hemisphere wall. Metallic glasses display a Newtonian behavior while at the SCLR, thus the flow stress can be calculated by:

$$\sigma_{flow} = 3\eta\dot{\varepsilon}$$

Where the flow stress (σ_{flow}) is determined by the viscosity of the metallic glass and the straining rate. By using these relationships one can find that indeed, the pressure required to deform a metallic glass sample in the absence of restricting boundaries is very low (Figure 12b), of course higher pressure is possible to use, but this might not be desirable on a working environment.
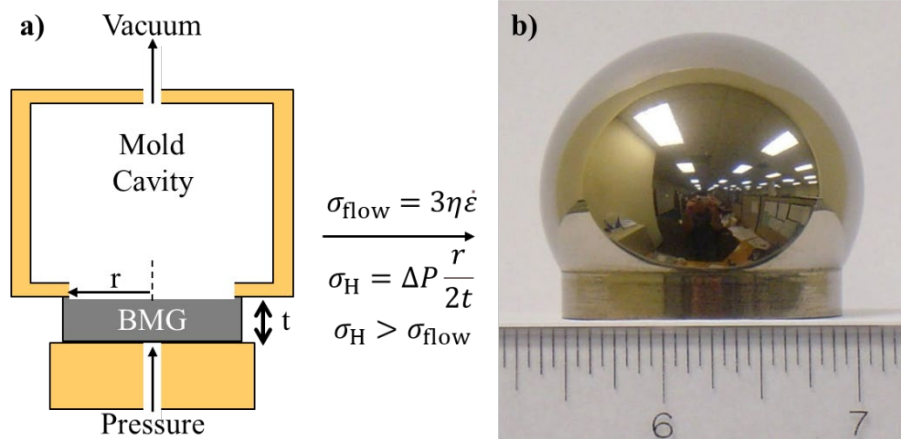
Figure 12. a) Schematic of a setup for free forming a metallic glass bubble, either a pressurized gas from the bottom or a vacuum on the top can be used to deform the metallic glass b) Example of a bubble made from $Zr_{44}Ti_{11}Ni_{10}Cu_{10}Be_{25}$ disk with a diameter of 3.5 mm and a thickness of 0.8mm using 0.2 MPa for 40 s at 460°C under a strain rate of 0.1 s^{-1}(adapted from [88])

Furthermore, material thinning, reflected in the strain rate exponent of unity ($m = \dfrac{d\sigma}{d\varepsilon} = 1$), is essentially absent during blow molding of metallic glasses[91, 92]. However, geometrical thinning limits this process to relatively low strain when using sheet-like feedstock. This issue, present in essentially all blow molding processes, stems from the boundary conditions of the metallic glass to the mold as in compression molding; once the metallic glass touches the mold, it no longer deforms, and the remaining deformation must be accomplished only with the metallic glass that has not yet touched the mold, imposing a higher strain on the metallic glass as it evolves.

Thinning is particularly problematic for parts with high aspect ratios and has therefore limited blow molding to metallic glass parts with a small over-all strain. This can be appreciated in figure 13, where forming a cylinder with an aspect ratio of only 2 (d = 20 mm, h= 40 mm) already presents a highly visible difference in the thickness achieved.
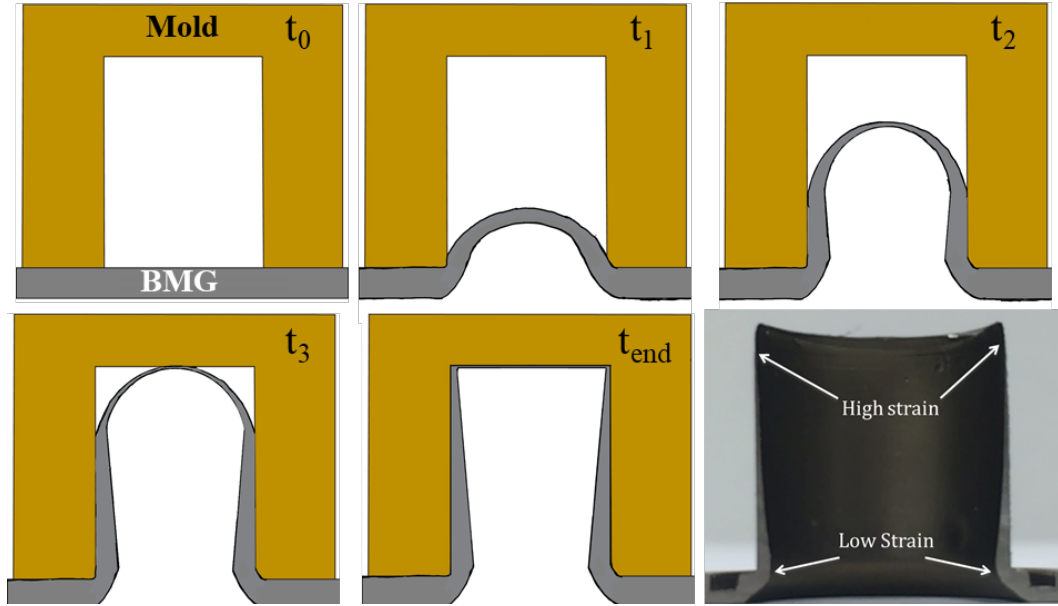
Figure 13.Schematic of the evolution of a metallic glass blow molded piece with an aspect ratio of 2 (d = 20 mm, h = 40 mm) from t = 0 to the end of the process (t_{end}). On the lower right corner, a picture of the actual sample obtained, even for low aspect ratios blow molding is a limited method

By using a kinematic model, we can estimate the thickness variation. We assume an incompressible Newtonian fluid, with a half hemisphere advancing front and with the thickness fixed once the metallic glass touches the mold. Following the previous assumptions, the thickness profile of a blow molded metallic glass in relation to the blow molding depth (z) is given by the initial thickness (t_0) and the radius of the sample (R) (*Supplement 1*):

$$t = \frac{t_0 e^{-\frac{z}{R}}}{1 - \frac{t_0}{2R}(1 - e^{\frac{-z}{R}})}$$

Figure 14 shows the thickness profile calculated for a blow molded sample of 9 mm in diameter up to 140 mm in depth and starting with a thickness of 2.5 mm. Despite that the kinematic model does not consider the pressure or the properties of the material, it is

enough to reveal that regardless of how big the pressure differential we can generate, it will not be possible to obtain a uniform thickness distribution if the no-slip condition is present; preventing us from obtain uniform thin-walled high aspect ratio parts.
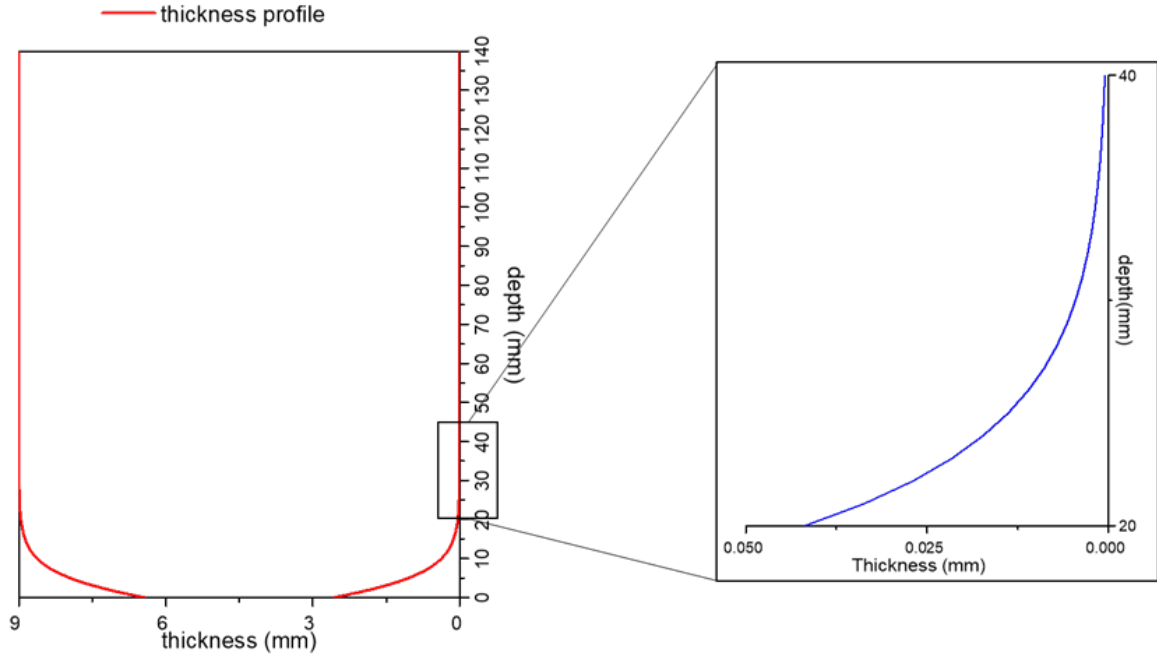
Figure 14. Calculated thickness for a blow molded sample of 9 mm up to 140 mm in depth and starting with a thickness of 2.5 mm

One strategy to overcome geometry limitations due to geometrical thinning is the use of pre-shaped parisons Figure 15a. When using parisons, which resemble the final shape of the article, all parts of the mold are filled at a similar time after a similar amount of strain. Hence, thinning is eliminated, and most of the deformation should be carried out without any contact to the mold. Though effective in realizing complex shapes that require high strains, and permitting hollow, thin, seamless shapes that might require undercuts, the

required additional processing step to fabricate the parison enhances costs, complexity of the process, and consumes thermal budget[14].
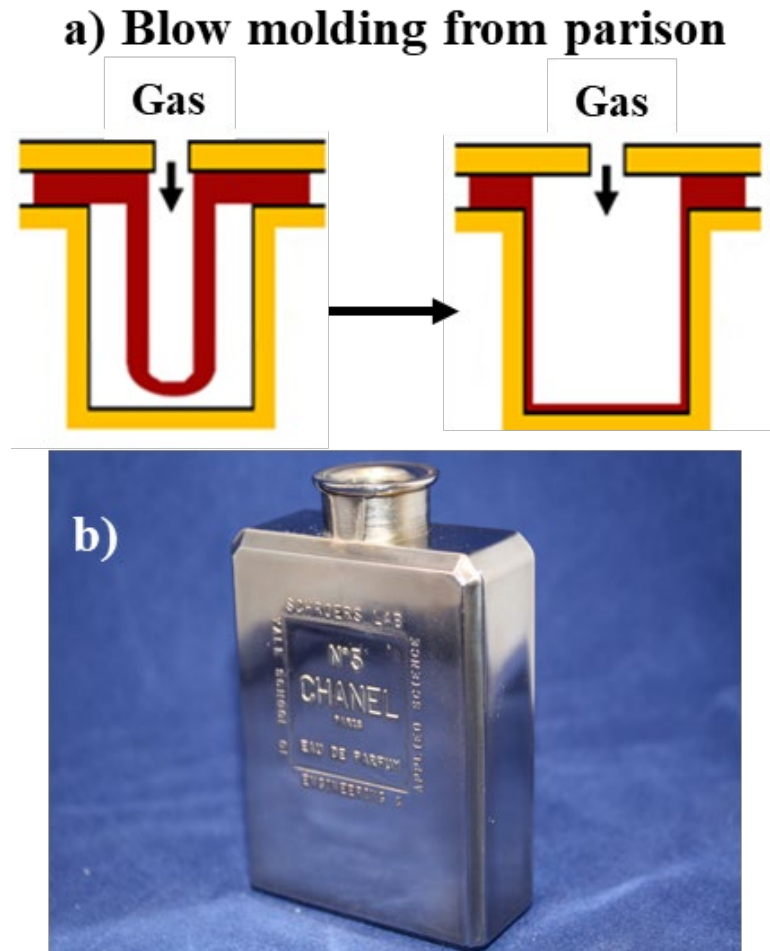
Figure 15. a) Schematic of the thickness distribution by using a preformed parison b) example of a perfume bottle formed by the use of a pre-shape[14]

Summary

One of the challenges of processing metallic glasses in particular, stem from the intrinsic characteristics of the material. Direct casting provides an easy way to shape metallic glasses if only a handful of very simple geometries is sought, but very limited as the metallic glass forming process is coupled with the part shaping aspect. Thermoplastic forming provides a solution by decoupling these two processes by deforming the material while in the SCLR. If we take a careful look at the compromise between the lowest viscosity the metallic glass can display and the time to crystallization, methods like compression molding and blow molding have proven successful in expanding the array of parts that can be obtained. While compression molding is the best choice for closed shaped parts, the required stresses to use it for open shape parts, particularly with thin walls, render it unsuitable for the task due to the no-slip phenomena. Blow molding has helped to increase the aspect ratio of the shapes that can be obtained as it removes for a while the limitation imposed by the mold walls but stills falls short by displaying a thinning effect as the aspect ratio of the parts made is increased. Is considering this that a new method to process metallic glasses is needed.

Chapter 3. Stretching the Limits of Metallic Glasses: Overcoming Geometric Limitations in Metals

3.1 Stretch Blow Molding

Having looked at the advantages and disadvantages of the available processing techniques for metallic glasses, is clear that a new processing technique was needed which could increase the available geometries that can be fabricated especially high aspect-ratio thin-walled parts. As determined in the previous chapter, having the metallic glass deformed in the absence of a restraining boundary, provided the best results in terms of pressure required and thickness distribution. In this work, we overcome the limitations imposed by geometrical thinning and expand the range of achievable shapes that can be realized with metallic glasses by first stretching a sheet-like metallic glass feedstock into the mold cavity (Figure 16). Subsequently, but in the same heating cycle, the stretched feedstock is blow molded against the mold, assuming and replicating its shape.
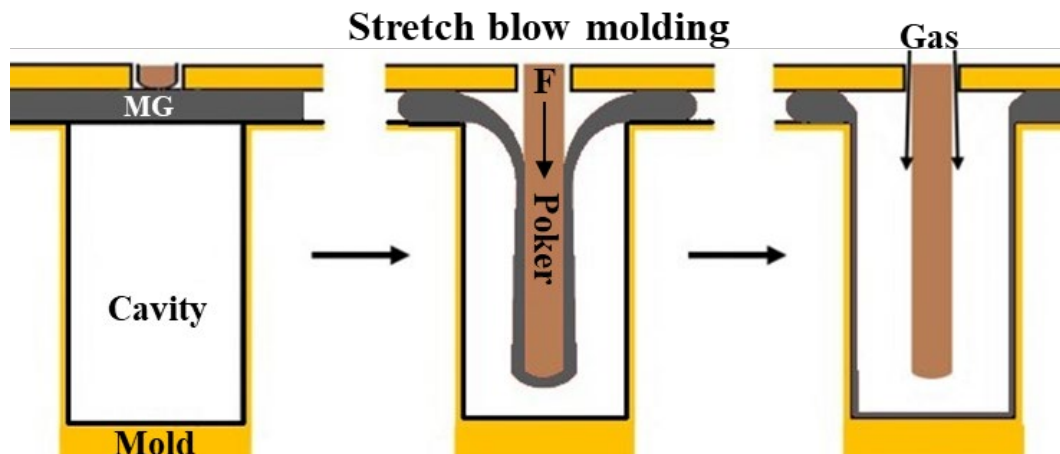
Figure 16. Thickness profile when a sheet-like feedstock is stretched prior to blow molding.

The stretching step creates a pre-shape which can be designed to resemble aspects of the final shape such as length, aspect ratio and/or geometrical features. This allows us to fabricate complex shapes from sheet feedstock with one heating cycle, which we term "stretch blow molding". Such stretch blow molding results in an approximately uniform thickness distribution even for very high overall strains.

3.2 Methods and Materials

There are several requirements for the stretch blow molding process to work:

- A stretching mechanism with a temperature control, to avoid any cooling of the sample through conduction from the metallic glass to the poker.
- Temperature control through the process; we needed to be sure we could obtain the required temperatures to process the material in the stretching and blow molding steps but also to allow for it to cool down before crystallization.
- A holding mechanism that ensured a seamless contact between the metallic glass and the mold to avoid any gas leaking through the blow molding process and did not interfere with the stretching step.
- A method to vary the holding force between the mold and the metallic glass that avoided squeeze flow but also prevented slippage of the sample through the stretching step.

We designed a new equipment to comply with these requirements and test the stretch blow molding process in its full capacity. Two tool steel plates that allowed the insertion of PID controlled cartridge heaters would work as the holding mechanism of the metallic glass

feedstock into the mold. The bottom plate was fixed into an aluminum frame that provided the required rigidity to the whole equipment. The top plate had a circular hole in the center which provided an entrance for the poking mechanism and the blow molding gas; this was attached to a spring mechanism that provided the clamping force require to hold the material and mold in place, while allowing to determine the applied force by measuring its displacement (figure 17a). The poking mechanism consisted of a stainless-steel tube with an interchangeable tip to allow different geometries as poker tips. The poker also allowed the insertion of a cartridge heater to avoid any heat loss from the metallic glass to the equipment, the poker had a concentric cap attached at the top to seal the whole system once the poking step was finished (Figure 17b). This was all mounted in a main lever system that allowed the hot plates to be open or closed as needed (Figure 17c).
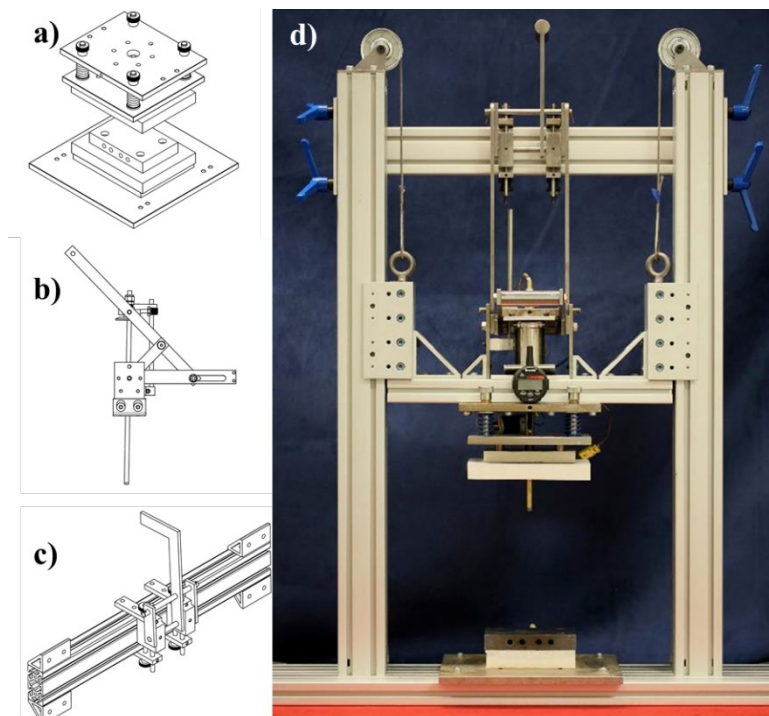
Figure 17. a) hotplates, b) poking mechanism, c) lever mechanism for the setup d) picture of the stretch blow molding equipment.

To stretch blow mold metallic glasses, we developed the following protocol: for metallic glass feedstock we use $Zr_{44}Ti_{11}Cu_{9.8}Ni_{10.2}Be_{25}$, as it has high formability[63, 66], is commercially available, and is widely studied[93-96]. A disc of this metallic glass feedstock is then clamped on top of the mold cavity. Subsequently, the feedstock is heated above the glass transition temperature T_g, where it reaches the supercooled liquid region, at which the feedstock softens and becomes moldable. For the stretch blow molding process, we considered temperatures ranging from 365°C to 430°C. The viscosity of $Zr_{44}Ti_{11}Cu_{9.8}Ni_{10.2}Be_{25}$ in this temperature region ranges from 10^9 Pa·s (365°C) to 10^6 Pa·s (430°C)[28, 65].

A concentric and axisymmetric poker then pushes and stretches the feedstock into the mold with a varying force of approximately 1 N–1500 N and a strain rate of $\sim$0.60 s^{-1}. This stretching is carried out without any contact of the metallic glass to the mold walls and creates a pre-shape (Figure 17). It is this step that enables the fabrication of high-aspect ratio metallic glass articles. Once the metallic glass material has been stretched to its final extension inside the cavity, the gas pressure applied in the subsequent blow molding step separates the metallic glass from the poker and molds it against the mold cavity, replicating its shape. Finally, the sample is cooled down below T_g for extraction from the mold.
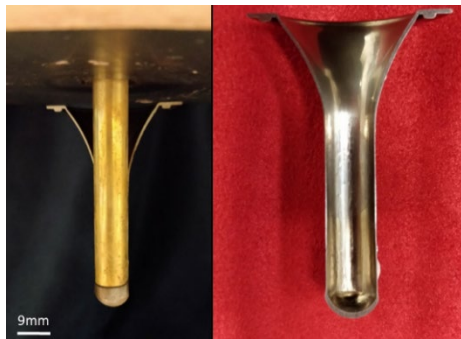
Figure 18. Pre-shape forming with the stretch blow molding equipment before the blow molding step.

The amorphous nature of the material was confirmed to be retained after all processing steps using differential scanning calorimetry (TA instruments Q200) and X-ray diffraction (Rigaku Smart Lab X-ray Diffractometer).

Bending tests were performed on strips from stretch blow molded samples, confirming that the material maintained its mechanical properties during stretch blow molding.

3.3 Thickness Distribution According to Previous Models

Models have been developed for different materials deformed under similar techniques. For polymers the first model was presented by Williams [97]. He shows that large strain solutions may be obtained from approximations of thin membrane theories, with a form of stress-strain relation to predict the profile and thickness variation of blown domes and other axisymmetric shapes. A direct loading was considered with a 2D geometry as shown in figure 19a, together with the variables involved. A strip of width $2b$ is forced upwards centrally by a force (F), with boundaries at $r = a, r = b$ and a strain (λ_H), where H is the poker penetration or height:

$$\lambda_H = \left(\frac{H}{H_0}\right) = 1.$$

From this geometry of the deformation, Williams derived the following ratio for the thickness variation:

$$\frac{t}{t_0} = \lambda_t = \frac{1}{\sqrt{1 + \left(\frac{H}{r \, ln\frac{a}{b}}\right)^2}}$$

The results are shown in Figure 19b. Although Williams shows experimental points in the graph for a PMMA membrane, it does not comment or provide any information on the experimental conditions.
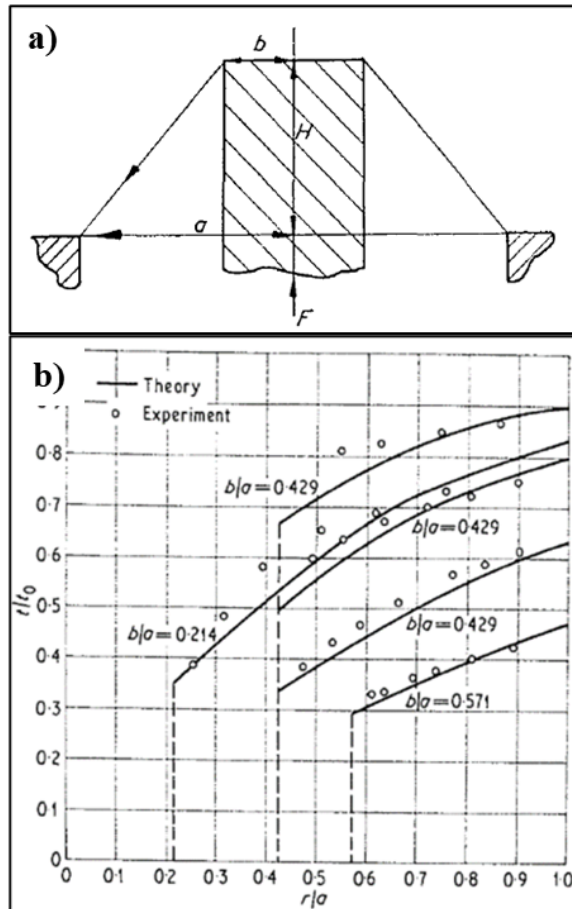
Figure 19. a) Geometry used by Williams for a direct loading of a polymeric sheet b) direct loading forming thickness variations. Adapted from [97]

In light of lack of a through experimental comparison, Throne developed a more robust model including the force require to deform a rubbery sheet, using various plug diameters and two material thicknesses [98]. The results were further compared with the large strain solution from Williams.

Throne analysis shown that plug-assist deformation of rubber sheets results in plane-strain deformation; that is, every point on the undeformed sheet is displaced in the force direction onto the deformed sheet. As a result, the strain in the radial direction is unity everywhere. This can be appreciated in the images in figure 20 which show a top view of a circle pattern draw in the rubber sheet in the unstrained and strained conditions. Eccentric plug-assist deformation yielded plane-strain deformation as well.
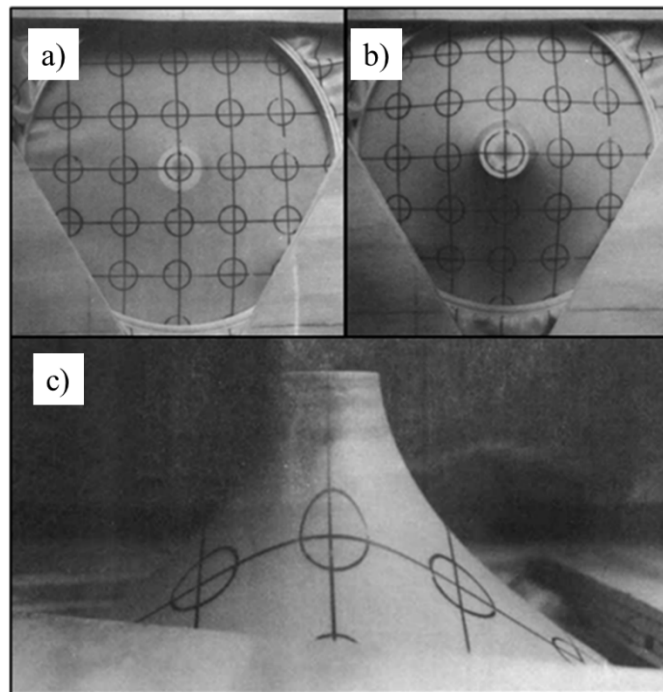
Figure 20. Top view of a) Unstrained rubber sheet. b) Sheet extended 7cm c) Side view of the extended sheet.[98]

Throne also found that the extent of deflection of a rubbery sheet is a linear function of the applied force and that the thickness of the rubbery sheet decreases in a hyperbolic way with decreasing sheet radius from the rim to the plug. The angle the sheet makes with the horizontal also increases with decreasing sheet radius. The approach to the development of the respective equations (Williams and Throne) were based in the figures shown in figure

21a and a comparison of some of the results obtained by Throne and Williams are shown

in Figure 21b. Is interesting to note that although both Williams and Throne, developed a

model for the thermoforming of a plastic membrane with a plug, Williams used a

thermoplastic PMMA membrane for experimental data with the temperature near or at T_m

(160°C) while Throne uses a natural rubber sheet (elastomer) at room temperature, thus a

direct comparison on the applicability of said models is not strictly correct.
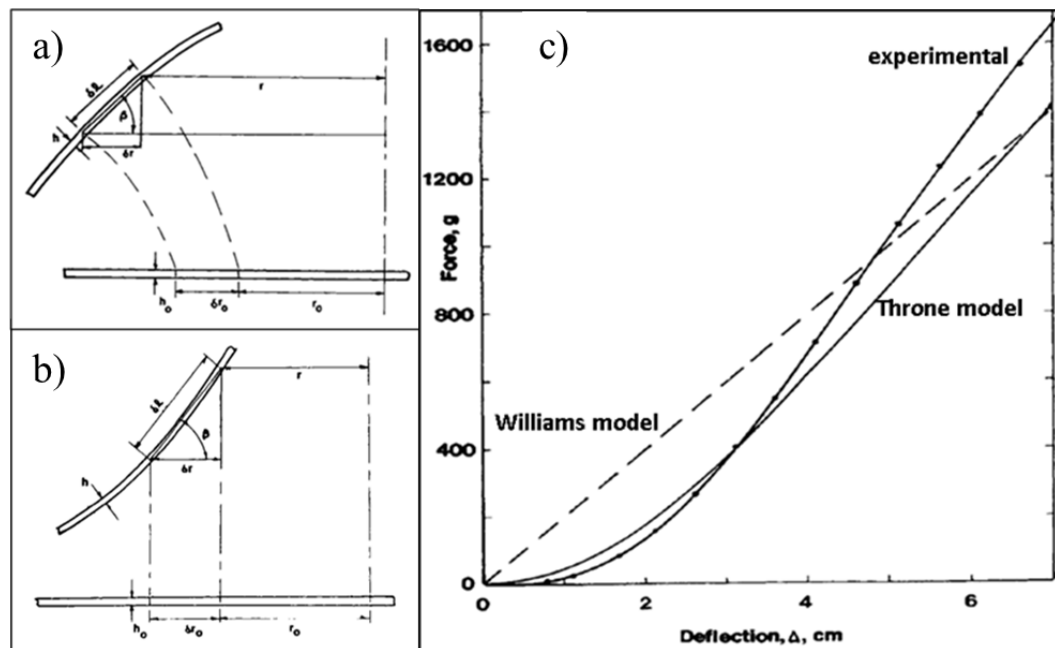
Figure 21. a) Williams coordinate system for the membrane in large strain deformation b)Throne coordinate system for large strain deformations of a rubbery membrane c)comparison of experimental and theoretical force-deflection for a 0.010 in thick rubbery sheet with a plug diameter of 2.1 cm[98]

From the models described before; the closest to the processing characteristics of the

metallic glass is the model proposed by Williams. We calculated the predicted profile and

thickness variation using this model to have an idea of what we should obtain. The results

are shown in Figure 22. The values used for the calculation include the initial thickness of

the disc 1.25 mm, the radius of the poker 4.5 mm, a radius for the disc of 12.25 mm and a

poking depth of 50 mm. Following Williams model, the deflection profile is given by:

$$D = \frac{H}{\ln\frac{a}{b}}\ln\frac{a}{r}$$

Where D is the deflection at a given radius from the center axis, H is the total penetration

depth, a is the radius of the disc (or mold) and b is the radius of the poker.
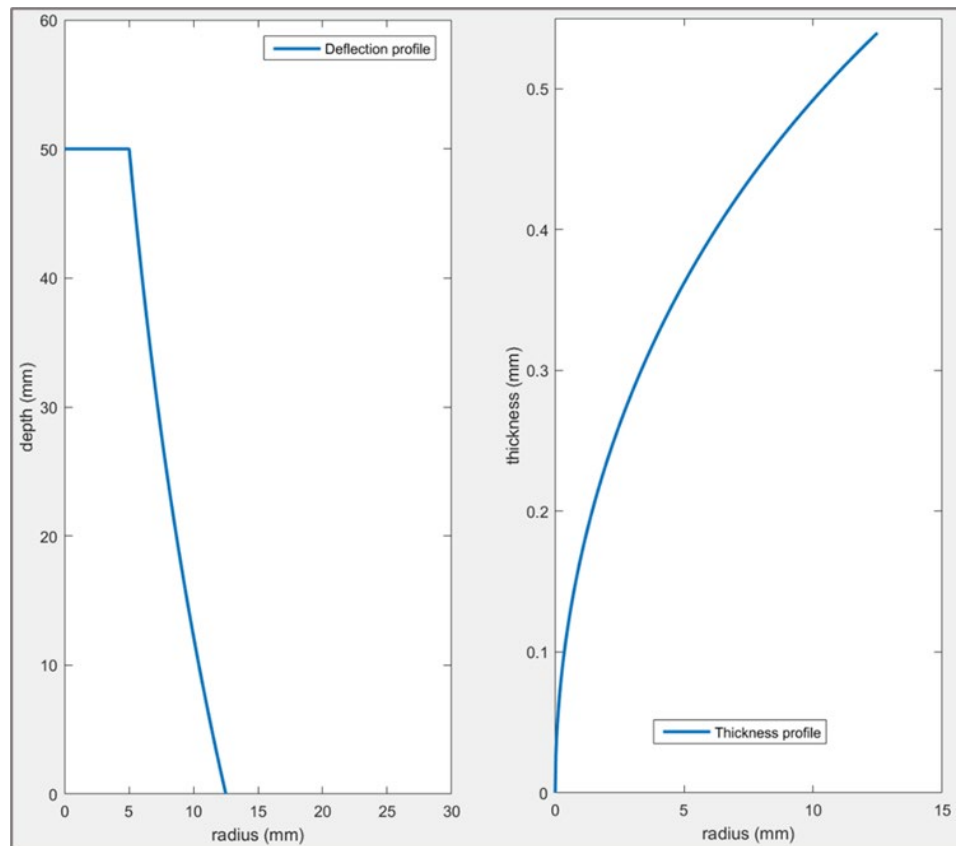
Figure 22. Deflection profile and thickness distribution calculated from Williams's model.

The thickness distribution is given by:

$$t = \frac{t_0}{\sqrt{1 + \left| \dfrac{H}{r \ln\left(\frac{a}{b}\right)} \right|^2}}$$

Where t_0 is the initial thickness. According to Williams's model, we would expect that the material closest to the center to thin out more as it is the one sustaining more strain and displacement. For the deflection profile of the material, we would expect a deflection in a quasi-linear manner where the metallic glass is only in contact with the poker within the surface of the tip.

3.4 Thickness Distribution in Pre-Shape After Stretching

An essential aspect of the introduced stretch blow molding process is the control of the thickness distribution in the pre-shape after stretching. We used feedstock discs (25 mm diameter,1.25 mm thickness) of amorphous $Zr_{44}Ti_{11}Cu_{9.8}Ni_{10.2}Be_{25}$, which were stretched at a temperature of 415°C to various depths of 25 mm, 50 mm, and 75 mm. A circular poker with diameter of 10 mm was used. Two distinctive regions are observed upon stretching (Figure 23). One of these regions, which we refer to as the contact region, is in contact with the poker and exhibits a relatively uniform thickness distribution. The contact region is thickest at the location that first touches the poker and thinnest at the location that last touches the poker. The region that does not touch the poker has a different thickness distribution and is referred to as the non-contact region. The shape and thickness

distribution of the non-contact region is defined by the ratio of the outer rim to the poker diameter, and by the original feedstock thickness and depth of the contact region.
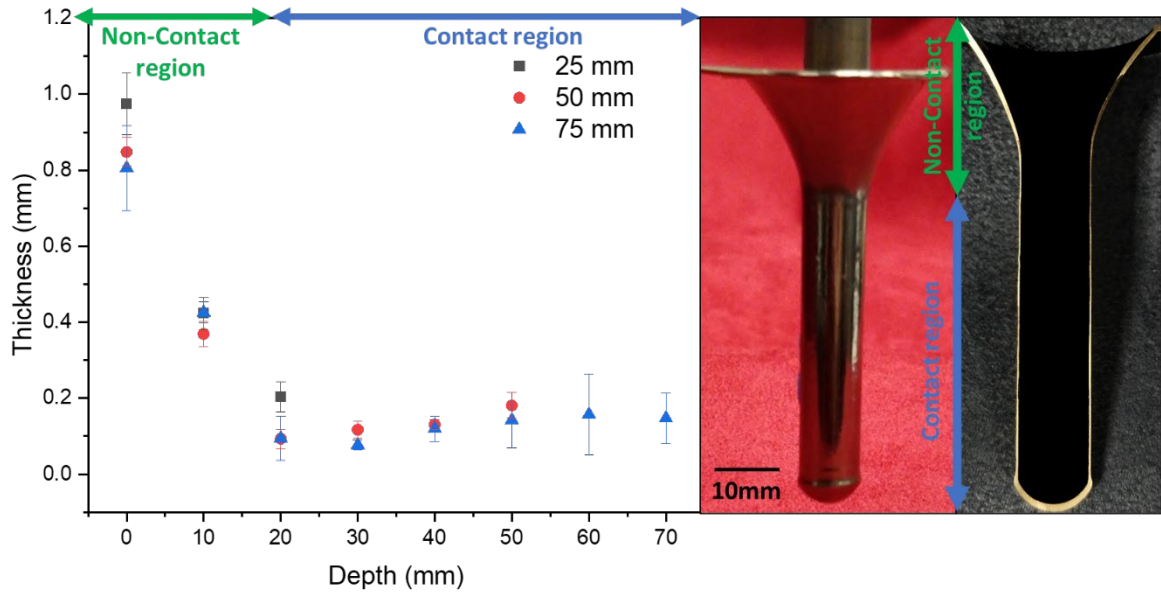
Figure 23. Thickness profile of stretched metallic glass to different stretching depths. Two distinct regions are observed. One is the contact region (blue), which comprises a purely extensional flow prior to contact with the poker and no deformation once the metallic glass touches the poker. The non-contact region (green) is the reservoir of metallic glass that has not touched the poker yet and deforms in a more homogenous fashion.

The non-contact region is characterized by a stretching process undergoing a purely extensional flow(Trouton model)[99]; where the contact region is characterized by a quasi-uniform thickness due to the deformation process being switched from a purely extensional flow to a shear flow enforced by the non-slip condition of the poker surface (Figure 24). These two straining processes compete as the metallic glass is stretched and the thickness values obtained for the contact region suggest that once the metallic glass touches the poker; any further thinning can be neglected as the thickness is similar at any given point in the contact region regardless of the amount stretched.
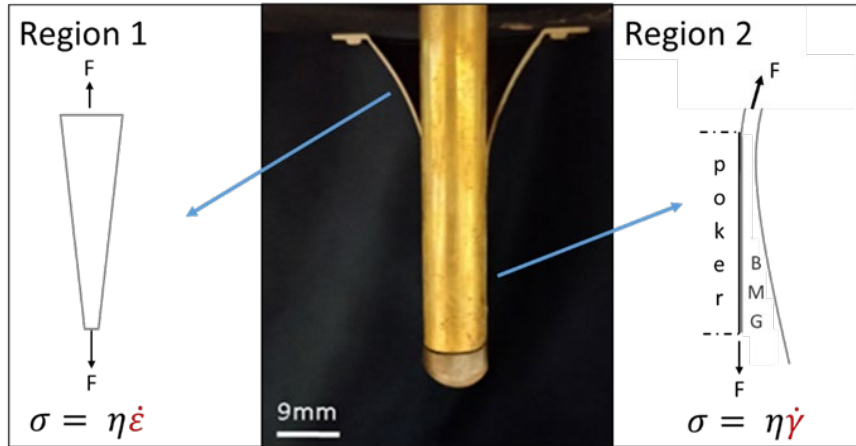
Figure 24. Straining regions developed under axisymmetric stretching

To better explain this, as a simple approximation; we can use the geometry in Figure 25 where we want to double the length and halve the thickness of the specimen shown, this will help to appreciate the difference between the two straining processes.

For a pure extensional flow:

$$\varepsilon = \frac{\Delta L}{L} = \frac{20cm - 10cm}{10cm} = 1 \qquad \text{Assuming we take 10s} \qquad \dot{\varepsilon} = \frac{1}{10s} = 0.1s^{-1}$$

$$\sigma = \eta\dot{\varepsilon}$$

In simple shear:

$$\dot{\gamma} = \frac{V}{h} \qquad V = \frac{10cm}{10s} = 1\,cm/s = 10\,mm/s \qquad \dot{\gamma} = \frac{10\,mm/s}{.5mm} = 20s^{-1}$$

$$\sigma = \eta\dot{\gamma}$$
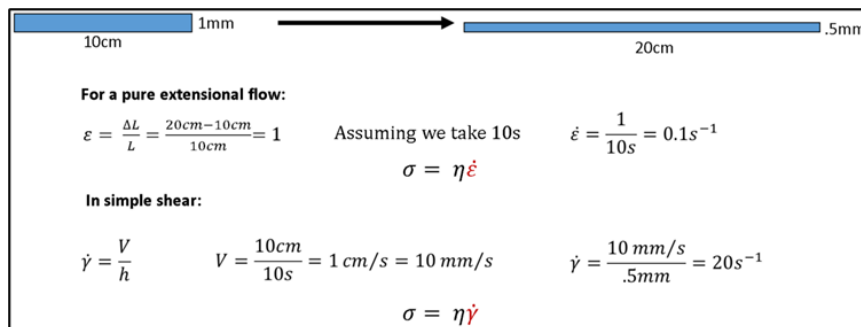
Figure 25. Comparison of the stress required for the same amount of deformation for a pure extensional flow vs. simple shear.

For a pure extensional flow, the extensional stress (σ) is given by[100]:

$$\sigma = \eta\dot{\varepsilon}$$

The material viscosity (η) and the elongational strain rate ($\dot\varepsilon$), with the strain rate defined as:

$$\dot\varepsilon = \frac{d\varepsilon}{dt} = \frac{d}{dt}\left(\frac{L_{(t)} - L_0}{L_0}\right)$$

Measured by the change of the elongation strain (ε) over time, which depends on the original length of the sample (L_0) and the length at time t (L_t). Whereas for simple shear is given by the viscosity (η) and the shear rate ($\dot\gamma$)[100]:

$$\sigma = \eta\dot\gamma$$

Where the sear rate is defined by the change in velocity (v) over the height (h):

$$\gamma = \frac{v}{h}$$

Back to figure 25, assuming we take 10 s to double the length and halve the thickness $\dot\varepsilon = 0.1\ s^{-1}$ but $\dot\gamma = 20\ s^{-1}$ so just by virtue of the difference in the deformation mode; we can appreciate that to impose the same strain, the stress required for the shearing process is at least 200 times that of the pure extensional deformation. Since these both processes compete during stretching, the deformation on the contact region (shear) is negligible.

To quantitatively describe the thickness distribution in the stretched pre-shape, we developed a 3D model of the stretching process (Figure 26) based on the following assumptions:

The depth of the non-contact region remains constant ($Z = P_C$), the thickness in the contact region is defined by the changing thickness of $t = t_c$, and no further deformation occurs for material at $z > P_C$. Finally, we also assume that the material is incompressible. A complete

derivation of the model can be found in *supplement 2*. The model predicts that the thickness

evolution in the contact region decays exponentially with the stretch depth, z:

$$t(z) = t_t e^{-\frac{5}{4}(\frac{D_0 - z}{P_c})}$$

Here, the thickness t at a depth z is a function of a critical point P_c (depth where metallic

glass and poker make contact), the total stretching depth D_o and the thickness value t_t at

the tip (initial thickness at the first point of contact with the poker wall vertically) (Figure

26).
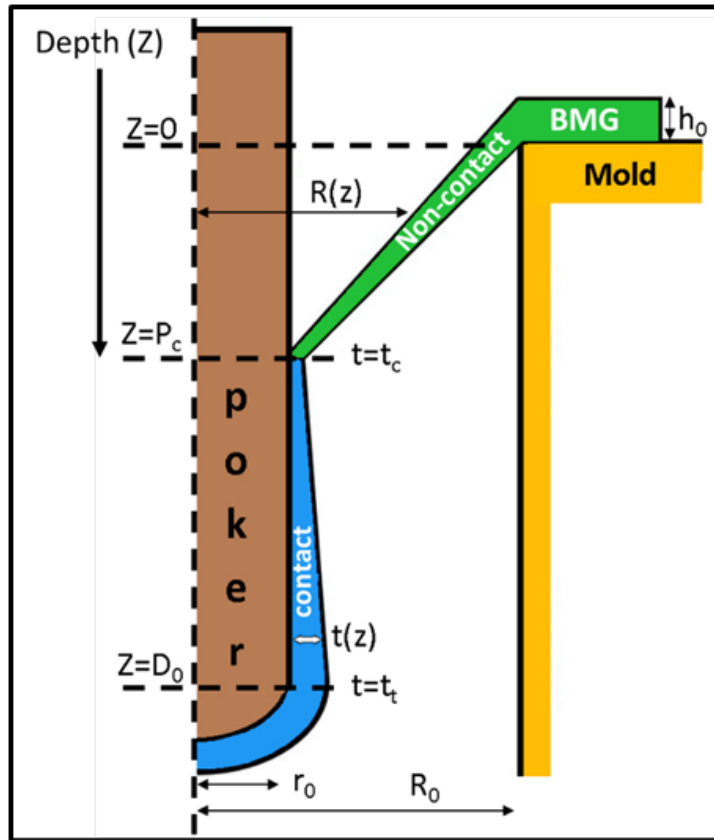
Figure 26. Schematics of the model for the derivation of thickness model. h_0 is the original thickness of the feedstock, R(z) is the radius from the center of the poker to the metallic glass, t_c is the thickness at the critical point where the metallic glass first touches the poker at a depth z = P_c, t(z) is the thickness value at a certain depth, R_0 is the radius of the mold cavity, r_0 is the radius of the poker. The z-axis origin is placed at the top of the mold where the metallic glass is originally placed. Z = D_0 is the final stretching depth.

The model shows reasonable agreement with experimental data (see dashed lines in Figure 27) but overestimates the thickness variations and underestimates the overall thickness. We argue that the model's overrepresentation of the thickness is that it does not consider the tip effect, the rapidly changing contact angle due to the typical hemispherical tip shape of the poker.
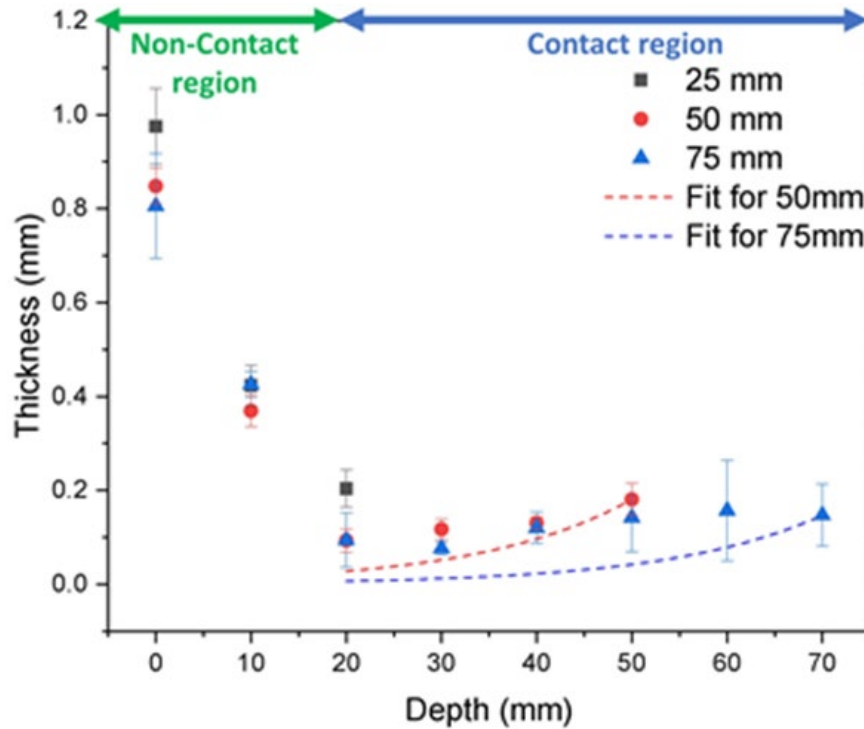
Figure 27. Comparison of the thickness model vs. the actual measurements. Dashed lines represent predicted thickness evolution according to thickness model equation for 50mm (red) and 75mm (blue).

3.5 Controlling the Thickness Profile Distribution

The thickness distribution predicted by our model and experimentally observed in Figure 27 is non-uniform. To control the thickness distribution, we first evaluated using a thermal gradient within the disc feedstock to vary the deformation resistance locally. As a second option, we also evaluated the ability of the poker geometry to manipulate the location of P_c as t is a strong function of z.

3.5.1 Thickness Control Through Thermal Gradient

The strong temperature dependence of the metallic glasses' viscosity [101], so called fragility, can be used as a tool to control the thickness distribution in the stretching step. For example, a change in the temperature in the supercooled liquid region by 20°C results in a change of viscosity by approximately one order of magnitude [65]. The same effect through feedstock geometry (Figure 28a), corresponds to a thickness variation in the initial feedstock of also one order of magnitude, such thickness variation would be difficult to realize and likely result in an instability [88, 102, 103], preventing the usage of highly non-uniform sheet feedstock material.
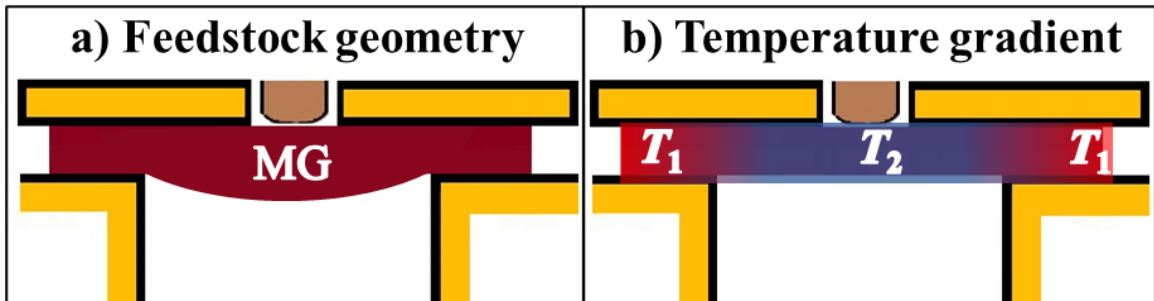
Figure 28. Control of the thickness distribution by a) Modification of the initial thickness/geometry of the feedstock material. b) Imposing a temperature gradient on the feedstock to locally vary the viscosity.

To realize a controlled radial temperature gradient in the disc-shaped feedstock, we control the temperature on the outside of the sample (T_1, clamp temperature) and at the center of the feedstock (T_2, poker temperature) (Figure 28b). To reduce the thickness variation in the stretched pre-shape (Figure 23), a lower temperature in the center of the feedstock material, T_2, should be used relative to the clamp temperature T_1. Therefore, the center

region experiences higher resistance to deformation and thins to a lesser degree than it would when both temperatures are identical. Likewise, the outer region will strain more, hence compensating for the geometrical thinning. Temperature differences T_1-T_2 ranging from 15°C to 65°C were realized and their resulting thickness distribution in the stretched (50 mm deep) pre-shape were determined (Figure 29).
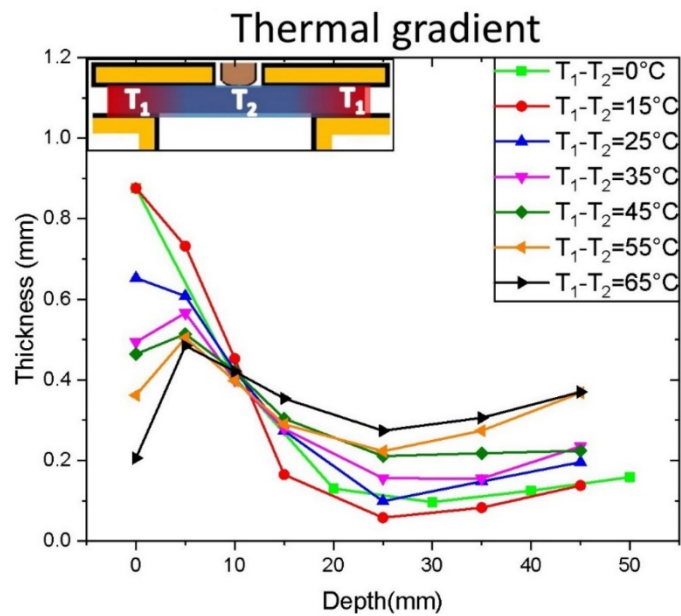
Figure 29.Thickness distribution profile for samples with a radial thermal gradient where the outer temperature T_1 is always higher than the center temperature T_2

Upon stretching, the overall thickness in non-contact region (Figure 23) decreases more quickly as compared to samples where a single uniform temperature was imposed. With increasing temperature gradient from T_1-T_2 = 15°C to T_1-T_2 = 55°C, the thickness becomes more uniform. When further increasing T_1-T_2, the variation in thickness throughout the stretched pre-shape increases again, particularly in the clamped region (depth 0 mm in

Figure 29). Here, the flow resistance at T_1 is overcompensated relative to T_2. By imposing a thermal gradient during the stretching step, however, one must consider the reduced time to the onset of crystallization at the highest temperature used to avoid any unwanted modification in the mechanical characteristics of the part.

3.5.2 Modification of the Point of Contact by Poker Geometry

An alternative approach to control the thickness distribution in the stretched pre-shape is based on the modification of the poker geometry, a schematic illustration is shown in figure 30, where the diagram compares the use of a constant radius poker to a poker with increasing radius.

Point of contact through poker geometry
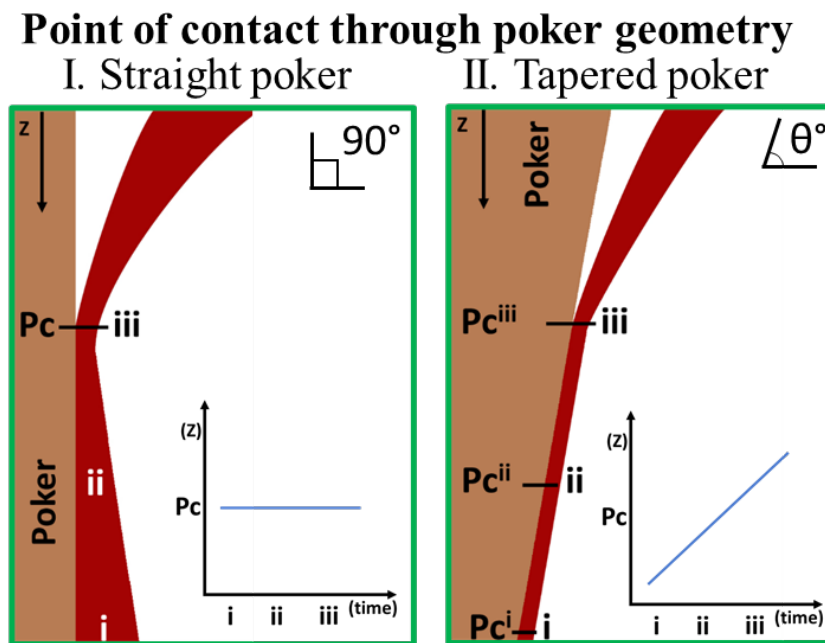
Figure 30. Alteration of the point of contact between the poker and the feedstock; I) shows a zoomed representation of a typical profile obtained using a poker with a constant diameter. Here, the point of contact P_c remains at the same height from time 1 to time 3). II) shows that by using a poker with an increasing diameter (tapered), the amount of metallic glass in contact at a given time can be adjusted. The initial P_c at time 1 is continuously moving upwards at the following times 2 and 3. Thereby, one can use the taper angle of the poker to generate a desired thickness distribution.

By varying the poker geometry, the contact region of the poker with the feedstock metallic glass can be adjusted. For a constant poker radius, at an arbitrary time 1 the poker subtracts a certain amount of metallic glass from the non-contact region. Since the volume of the material is finite at a subsequent step at time 2, the poker subtracts a smaller metallic glass volume. To compensate for this continuous change, we can increase the poker radius to reach for metallic glass material at a higher position by displacing the contact point P_c upwards (Figure 28 II). A tapered poker can therefore result in a more even thickness distribution.

For a cone shaped poker with a round tip, we estimated that an angle of 88.75 degrees would give the most uniform thickness distribution, based on the thickness profile obtained experimentally. Samples of $Zr_{44}Ti_{11}Cu_{9.8}Ni_{10.2}Be_{25}$ with an initial thickness of 1.25mm were stretched to 80 mm in depth.
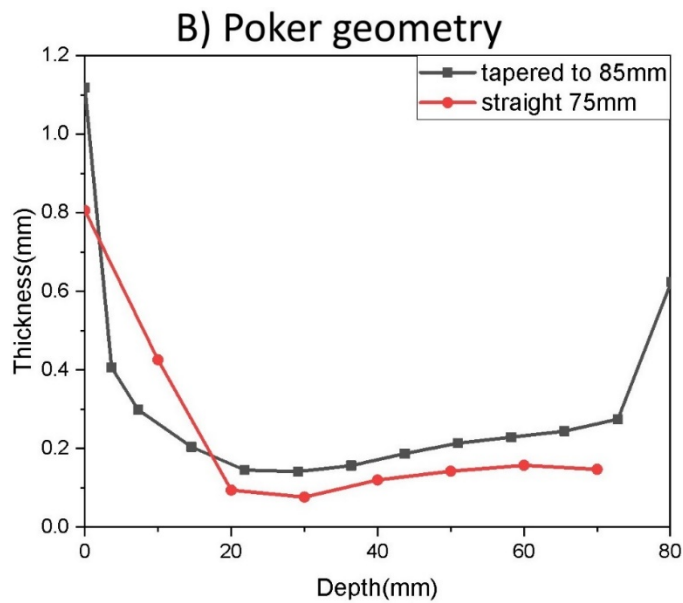
Figure 31. Thickness distribution profiles for samples stretched with a constant radius poker (red) and a poker with increasing poker radius with an angle of 88.75° (black).

Figure 31 shows the comparison of the thickness profile obtained for a sample stretched with a uniform poker radius vs. the thickness profile obtained for a sample stretched with a poker with a tapered angle with increasing radius. With the tapered poker, we obtain a uniform wall thickness across a larger region of the samples.

3.6 Thermal, Structural, and Mechanical Characterization of Stretched Metallic Glass

An important aspect in metallic glass processing is how processing affect properties [16, 104-106] . It has been shown that changes in fictive temperature [107-110] and partial crystallization [111] can have dramatic effects on the metallic glass properties, particularly on their mechanical properties.   In addition, some research has suggested that crystallization can be affected by a strain rate during exposure in the supercooled liquid state [112-115].

To characterize the effect of stretch blow molding on thermal, structural, and mechanical properties we carried out a range of characterization at various stages of the stretch blow molding. To quantify their thermal characteristics, we carried out differential scanning calorimetry (DSC). Specifically, we characterized metallic glass after it was stretch blow molded and used material from various locations (Figure 32a) at different stretched depths (a=15 mm, b=30 mm and c=60 mm, sample cap). Based on their glass transition temperature, T_g, their crystallization temperature, T_x, and their heat of crystallization, ΔH, the thermograms from the samples at the various considered locations after stretch blow molding are indistinguishable from the as cast feedstock material. This suggests that stretch

blow molding can be carried out without introducing crystallization or even consuming large fractions of the thermal budget.

These findings are supported by XRD characterization which reveal an amorphous structure for the stretch blow molded samples, indistinguishable from the as cast feedstock (Figure 32b).
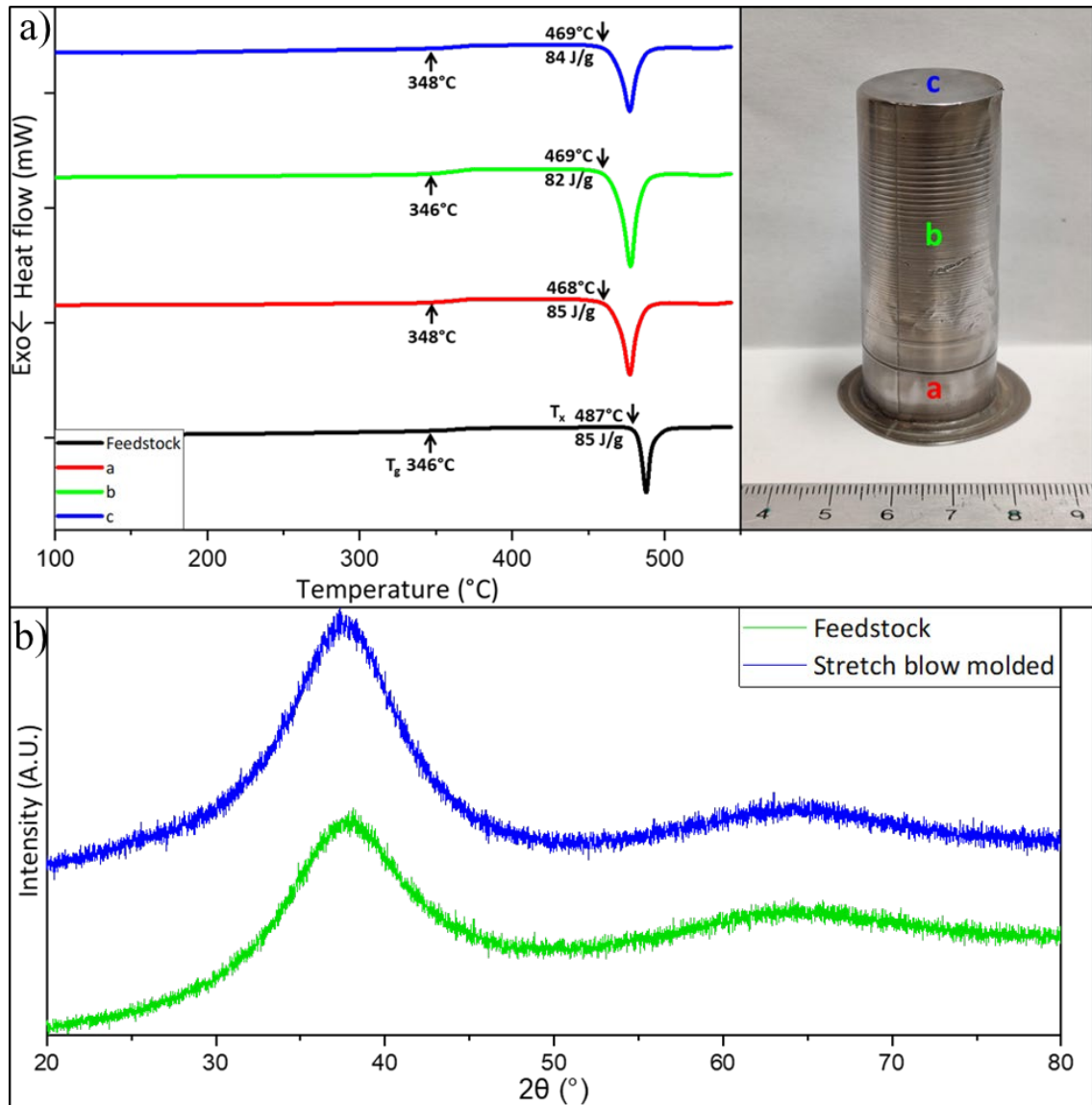
Figure 32. a) DSC thermograms of a stretch blow molded sample taken at three different heights: 15 mm(a), 30 mm (b), and 60 mm (c), and for comparison the thermogram of the feedstock. The thermograms

for the samples from the various locations after stretch blow molding are undistinguishable within experimental error from the as cast feedstock sample judging by their T_g, T_x, and ΔH b) XRD spectra of feedstock and stretched blow molded sample both reveal amorphous structure.

A powerful indicator to determine processing effects on metallic glasses is the bending strain to failure [116, 117]. Whereas metallic glasses typically do not show any tensile ductility in uniaxial loading, they can exhibit significant ductility in bending, particularly when their thickness is below 1 mm [116]. To quantify their bending ductility, bending tests around mandrels with various radii were performed on cut strips from stretch blow molded samples (Figure 33). Strain to failure is calculated by:

$$\epsilon = t/2r$$

where t is the thickness of the sample and r is the bending radius.
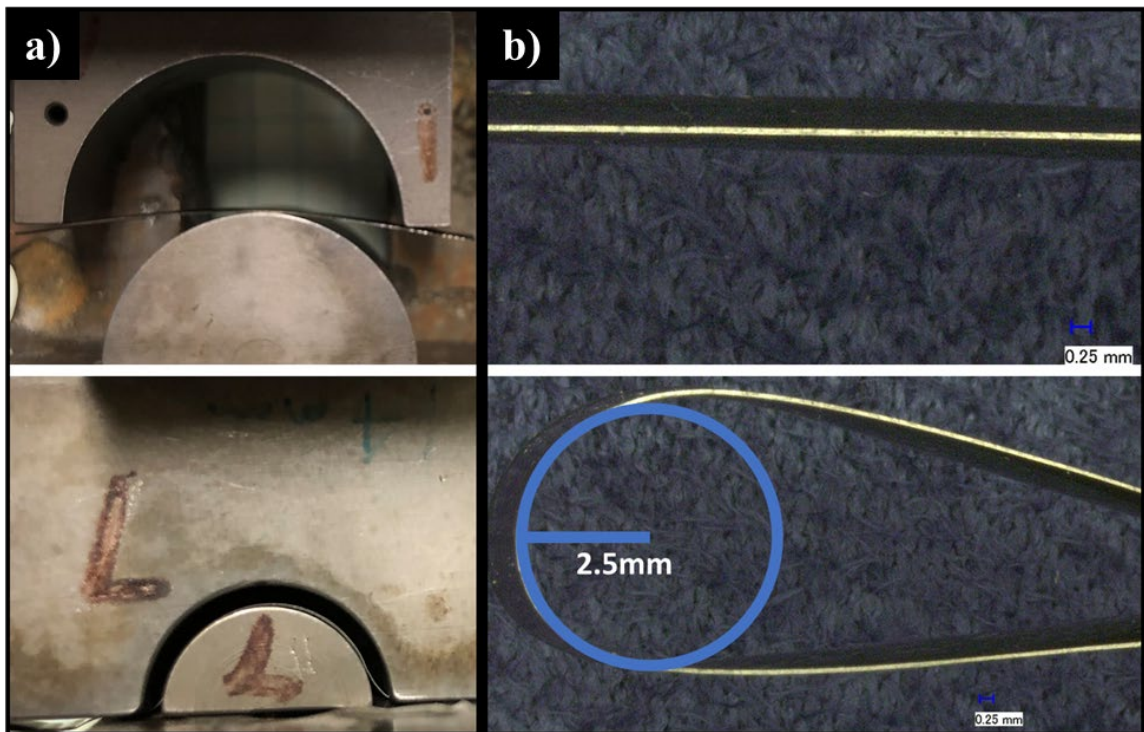
Figure 33 a) mandrels used for ductility analysis of the stretch blow molded and feedstock Zr-Based metallic glass parts b) example of a manually bent metallic glass strip from the stretch blow molded sample.

Stretch blow molded samples, which were taken from various locations as well as samples from as cast feedstock all with an average thickness of ~0.125 mm start to deform plastically at a bending radius of 2.5 mm with a corresponding strain of ~2.5 % and fracture at a bending radius 0.25 mm at a failure strain of 25%. Such large plasticity in all samples further suggests that stretch blow molding can result in metallic glass parts that maintain their high properties during processing.

3.7 Parts Manufactured Through Stretch Blow Molding

Using the strategies described above to control the thickness distribution during the stretching step, we were able to fabricate thin-walled metal parts that are open shaped (Figure 34). Starting with a flat, sheet-like feedstock, strains of up to 2000% and parts with an aspect ratio of four were achieved. It should be mentioned that likely even larger strains and aspect ratios can be achieved; here we were limited by the equipment design. By comparison, blow molding using sheet like feedstock can only provide parts with an aspect ratio of < 1.5 [88]. This technique also allows fabricating single piece geometries with undercuts and side features, which are impossible with conventional metal processing methods such as spinning or deep drawing (Figure 32). For example, the versatility of our process allows to fabricate seamless open shape parts, which are only for high symmetry possible with other metal processing methods. All metallic glass parts replicated the mold surface and details. In fact, recent studies of the fidelity of thermoplastic forming processes suggest that much smaller features can be achieved as the surface appearance [118, 119]. This suggest that surface finishes, for example a mirror finish can be incorporated into the

stretch blow molding processing step, as oppose to conventionally where it is subsequently added at high costs.

Figure 34. Parts obtained through the stretch blow molding process. By starting with a flat sheet-like feedstock with a few mm in thickness as the one shown at the center of the image parts with aspect ratios of 4 and strains over 2000% were obtained.

Summary

We have developed stretch blow molding which allows for the fabrication of high aspect ratio open shape structures from flat, sheet-like bulk metallic glass feedstock. Including a stretching step in the blow molding process eliminates previous limitations such as small aspect ratios and non-uniform thicknesses during blow molding. Achievable overall strains with reasonable thickness variations were increased from ~150% achieved during blow molding to ~2000% when incorporating the stretching processing step. Mechanical, thermal, and structural analysis revealed that during stretch blow molding the amorphous structure is maintained. Hence when using appropriate feedstock metallic glass in sheet-like form, thin-walled shapes, previously unachievable with any metal process can be realized and these shapes exhibit superb mechanical properties.

Open shape geometries are ideal application of metallic glasses, as they yield exceptional bending ductility as long as the wall thickness is below ~1 mm [116]. Additionally, open shape structures utilize less material, which is an important consideration due to the relatively high material costs and criticality of metallic glasses when compared to steel [120]. Therefore, stretch blow molding offers a highly practical and effective method to net-shape complex open shape articles from metallic glasses, and we are looking forward to a broad commercial adaptation of this method, where we currently submitted a patent application (62/641,65). We recommend the reader to watch a neat demonstration of a blow molding process: https://www.youtube.com/watch?v=Bd370rlvT5M and for a demonstration of stretch blow molding use:

https://www.youtube.com/watch?v=iBbpIFwvxwI.

Chapter 4. Processing Aspects on the Metallic Glass Properties

So far, we have focused on the form giving aspects of thermoplastic forming metallic glasses to obtain new parts and shapes; and while we must comply with certain conditions to obtain a glass (cooling rate $> R_c$), and then to process it on the SCLR (avoid the crystallization nose by controlling temperature and time in the SCLR); most of the known metallic glasses lack sufficient ductility or toughness when fabricated under conditions resulting in bulk glass formation. In this regard, improving the mechanical characteristics of metallic glasses while processing and understanding how the processing conditions affect the metallic glasses final properties is of uttermost importance.

4.1 Fictive Temperature and the Energy Landscape

When a metallic glass forming liquid is cooled, its structure continuously reconfigures into a new temperature dependent metastable equilibrium structure. Such reconfiguration, referred to as structural relaxation, proceeds with a characteristic time, τ_{rel} that rapidly increases with decreasing temperature. Reconfiguration occurs if the required time scale for relaxation exceeds the available time, which is usually set by the cooling rate, R; $\tau_{cool} = 1/R$. However, at a certain temperature, usually referred to as the fictive temperature (T_f) or glass transition temperature upon cooling, the metastable liquid can no longer find its metastable equilibrium and freezes into a glass. This fictive temperature is used to describe the structural state of the metallic glass when the liquid falls out of equilibrium, resulting in the liquid and the glass having the same structure, volume and enthalpy at this point (Figure 35)[121].
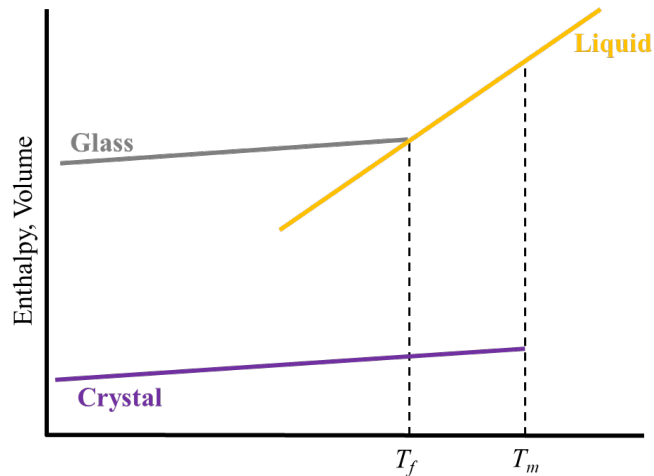
Figure 35. Change in enthalpy or volume according to temperature for a metallic glass

For the same metallic glass, the colling rate from the SCLR will affect the obtained fictive temperature, as the cooling rate is faster, T_f departs from equilibrium to become metastable at a higher temperature, while a slow cooling rate allows for sufficient time for the metallic glass to relax and take more time to depart from equilibrium, translating into a low T_f. For metallic glasses, it has been generally observed that higher fictive temperatures result in higher ductility of the corresponding amorphous structure [105, 109, 122-125], in this regard, processing temperatures and cooling rates start to paint a more complex picture where the displayed properties of metallic glasses are sensitive to the processing conditions[126].

If given the sufficient time, metallic glasses can obtain a different structure or T_f from the one it had before. The time required to do so is defined by the Vogel-Fulcher-Tamman (VFT) equation:

$$\tau_{rel} = \tau_0 \exp\left(\frac{D^* \cdot T_0}{T_f - T_0}\right)$$

54

Where the relaxation time (τ_{rel}) is a function of the relaxation time (τ_0) in the limit as $1/T$ tends to 0 (infinite temperature relaxation time), while (D^*) is the fragility parameter and (T_0) is the temperature where the barrier to flow goes to infinity[127-129]. For Zr based metallic glasses τ_0 has been calculated to be 2.5×10^{-13} s[129].

To better understand the complex phenomenology of the different internal states a metallic glass can attain as an amorphous material a convenient visualization is described through the potential energy landscape (PEL) [130, 131]. The PEL is a multidimensional surface that describes the relationship between the potential energy to the coordinates or configurations of the atoms, and where there are many local optima for particle packaging[132]. In this framework, the state of the system is characterized by the ensemble of energy minima visited by the system[133, 134]. This has also been use to explain the properties of other disordered materials such as colloids, foams and granular materials[135, 136] and although several studies have focused on determine the PEL directly, it remains a difficult task[131, 137, 138], thus, PEL is often presented as an schematic.
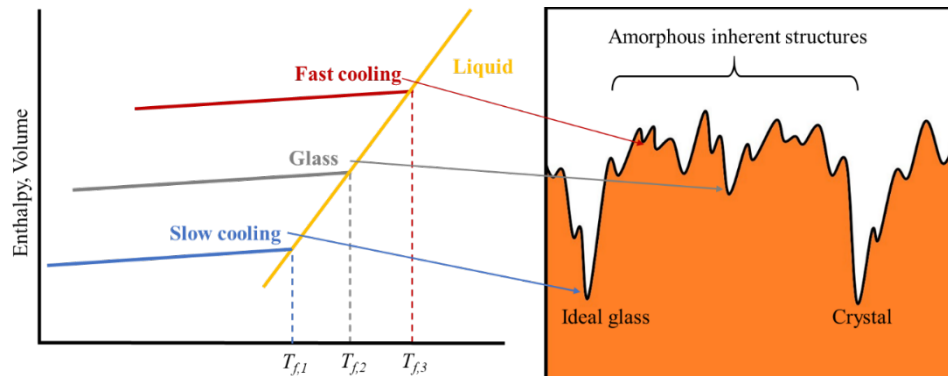
Figure 36.Schematic diagram of the PEL for a metallic glass (right). Depending on where the glass falls out of the equilibrium, is the position/structure that occupies on the energy landscape.

To visualize the different glass states of a metallic glass and the effect of the cooling rate, we can use a one-dimensional PEL (Figure 36), glass in general will arrive at a local minima basin (amorphous inherent structures). A fast cooled glass will present a high fictive temperature and be in a high energy state (red). On the contrary, a slowly cooled glass will be able to minimize its energy, presenting a lower fictive temperature (blue) and tending to an ideal glassy structure, nature however, imposes a strict limit in the cooling rates that can be experimentally achieved.

4.2 Relaxation and Rejuvenation

The most common method to change the metallic glass to a lower structural state is through annealing. If the metallic glass is let at a particular temperature for a time longer that its characteristic relaxation time at that temperature, the metallic glass will achieve this new structural state, or "relax" into it. Annealing will provide enough energy for the atoms in the structure to change it configuration into different wells in the PEL. If annealing is done below T_g, the metallic glass can only reconfigure to adjacent configurations (figure 37). Theoretically, crystallization is possible to attain but highly unlikely, and the time scale to do so is of no practical use. For a temperature between T_g but below T_L the metallic glass has enough energy to sample several configurational states; the minimum energy is still the crystalline state, to which the metallic glass will eventually arrive given sufficient time. Being this the reason of the metallic glasses' crystallization nose on the TTT diagram, and the reason there is a maximum processing time available.
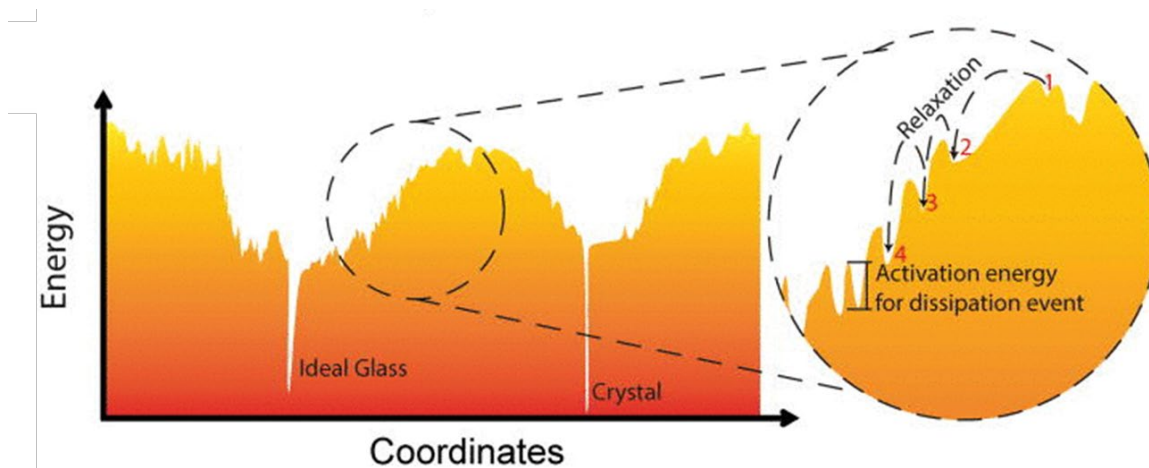
Figure 37. PEL for an arbitrary metallic glass. The close up shows the mechanism of structural relaxation to lower energy levels when done at temperatures lower than T_g , adapted from [139]

Beyond the theoretical approach, there are experimental approaches to quantify these changes in structure, free volume, and enthalpy. One of the most effective tools is the DSC, which is probably the most sensitive tool to energy fluctuation during glass transition and relaxation among all the characterization techniques. Figure 38 depicts a diagram for a DSC obtained for an arbitrary metallic glass. In general, a metallic glass from the as-cast state will undergo a glass transition, where it approaches the SCLR, a crystallization, where the material has achieved enough energy to arrange its atoms in a periodic fashion and finally melting, as it achieves a liquid state. If we zoom in the glass transition region, we can observe changes according to the thermal history of the metallic glass. A relaxed metallic glass will have a lower enthalpy compared to the as-cast material, so as it is heated up in the DSC and it has enough energy to rearrange its atoms, it will experience an excess of enthalpy that it can gain, which it is shown as a positive increase in enthalpy (shaded area).
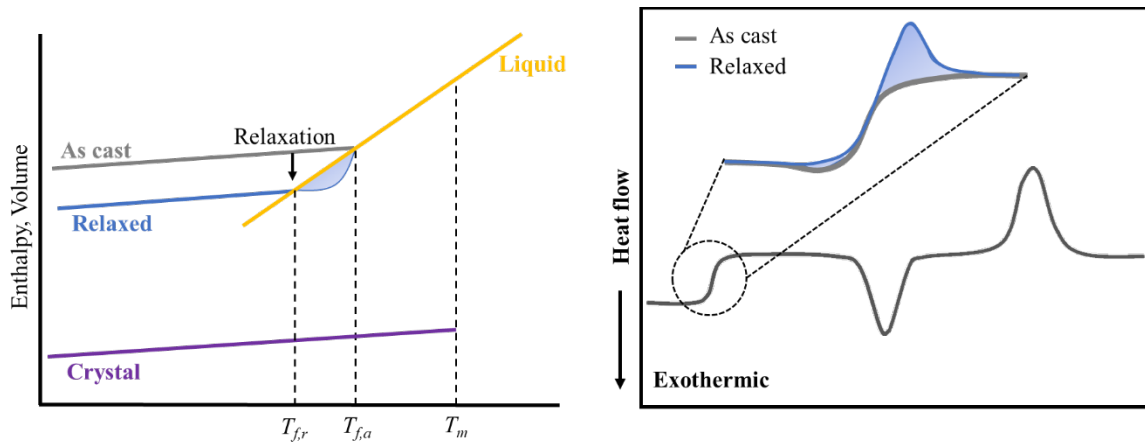
Figure 38. Diagram of a DSC thermogram from an as-cast metallic glass compared to one from a relaxed metallic glass

Early work on relaxation of metallic glasses has shown that it promotes the embrittlement of metallic glasses[123, 140-142], making usage temperatures and times worth of consideration for metallic glass parts.

Like relaxation, which decreases the internal energy of the system, rejuvenation can be used to increase it, this increase in energy has been associated with a more "disordered" system with increased volume, providing an increase in ductility for metallic glasses[143-146]. From the PEL perspective, the rejuvenation of a material would mean a climb to higher levels in the potential landscape. If we look at it through DSC measurements, compared to the as-cast material, the rejuvenated glass will experiment a decrease in heat flow as the system arrives at the glass transition region (Figure 39). In general, it has been shown that these two processes can be reversed, as long as there is no crystallization or damage imposed in the sample[106, 147].
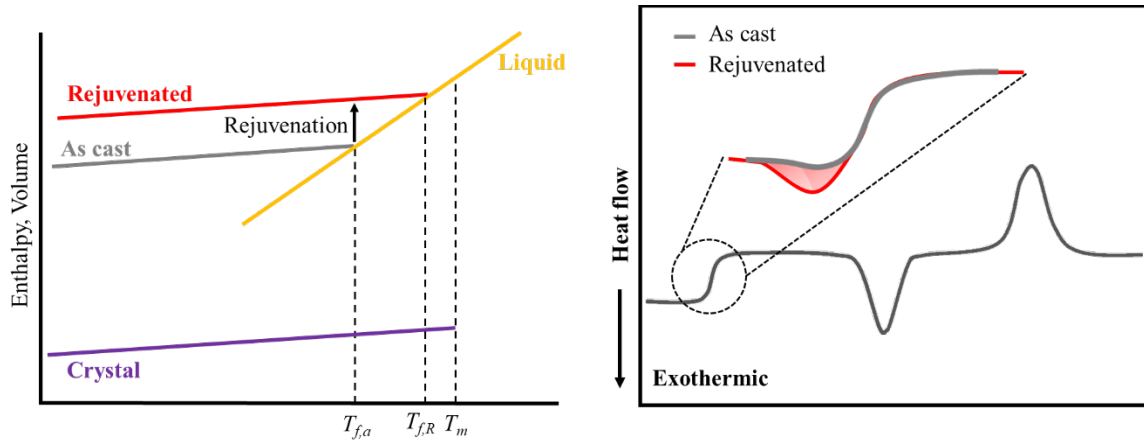
Figure 39. Diagram of a DSC thermogram from an as-cast metallic glass compared to one from a rejuvenated metallic glass

4.3 Deformation and Processing Effects in Bulk Metallic Glasses

Whether a material shows a brittle fracture, or a plastic deformation is of high relevance for its usage. Under tensile stress, most metallic alloys display an elastic region within a strain of usually 0.2% until they yield. Following yielding, regular alloys show plastic deformation by the gliding of dislocations inside the crystals, and finally a catastrophic failure through the propagation of cracks through the grains or grain boundaries. An important phenomenon during its processing is work hardening, where following plastic deformation, more dislocations are generated through the material that impede the continuation of the gliding, generating work hardening behavior. Annealing will usually result in relaxation (recovery) but the only way to substantially reduce the dislocation density is through recrystallization, typically at temperatures above 60% of the absolute melting temperature.

Compared to regular alloys, in metallic glasses the elastic strain is non-affine, meaning that in the atomic level the atoms never occupy equivalent positions to their crystalline counterparts. Rearrangements can occur upon unloading, but the exact structure is not restored, so there is a net structural change. Under the elastic region, soft spots with local plasticity emerge in an apparently rigid matrix, which upon unloading pushes the soft spots roughly back to their original configurations. In general, metallic glasses will show a yield strain of around 2% which is higher than regular metals. Usually, past this point, the metallic glasses will go directly to fracture without showing any macroscopic plastic deformation as in regular metallic alloys. In this regard we can identify two types of plastic deformation in metallic glasses below its glass transition temperature; under a low stress, the metallic glass shows homogeneous deformation, described as creep flow. If the stress increases, the plastic flow is inhomogeneous and localized into shear bands that become part of the fracture mechanism[148].
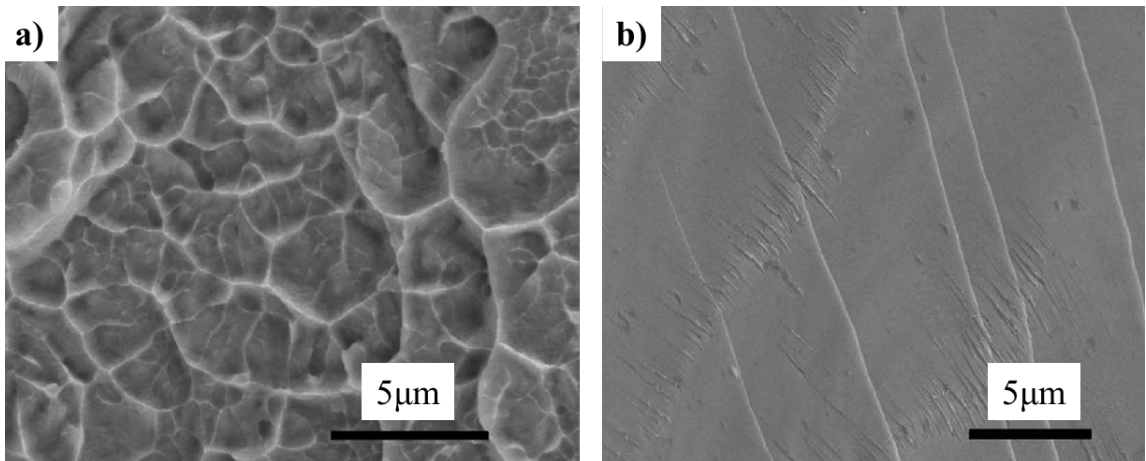
Figure 40. a) Fracture surface of $Zr_{41}Ti_{14}Cu_{12.5}Ni_{10}Be_{22.5}$ showing plastic flow b) Same material after annealing at 623 K for 12 h, the fracture surface shows brittle fracture. Adapted from[149]

Some metallic glasses however, behave brittle both locally and globally, such as magnesium-based alloys with a toughness less than 5 MPa m$^{1/2}$ [39]. Figure 40a shows the surface of a vein pattern that is formed in a Zr-based alloy evidencing high local plasticity. The same alloy was annealed for 12 h at 623 K to relax the material and increase its brittleness. The surface shows a river pattern associated with the fracture of brittle materials (Figure 40b). Once above the glass transition temperature, metallic glasses deform as highly viscous liquids.

4.4 Current Methods to Modify the Structure and Increase Ductility

It has been widely shown that metallic glasses of the same chemistry can have greatly different ductility or fracture toughness[150-152]. Relative to the metallic glass as-cast structure, ductility or fracture toughness can be reduced [151, 153, 154] or enhanced [105, 110]. This can be achieved through thermal treatments such as the use of different cooling rates [105, 155], annealing protocols [109, 153, 156, 157], or mechanical treatments such as quasistatic mechanical loading [158-162], plastic deformation [144, 163-165] , thermal cycling [104, 166-168], shot peening [143] , and radiation damage [169-173] .

For mechanical treatments, the glass itself is manipulated. Manipulation of the glass is often inhomogeneous, most extremely during treatments that generate shear bands where most of the treatment effects are localized in shear bands occupying a very small volume fraction of the sample. For thermal treatments over the glass transition temperature, enable the liquid metallic glass former to be affected before it freezes into a glass, providing a more dramatic effect in the metallic glass properties compare to thermal treatment below

$T_{g[174]}$, Figure 41 shows the normalized notch fracture toughness measured for different metallic glasses, the value increase dramatically as the material is set to fictive temperatures above T_g. A through table in Supplement 3 show a comprehensive list of the available techniques to modify the mechanical properties of metallic glasses.
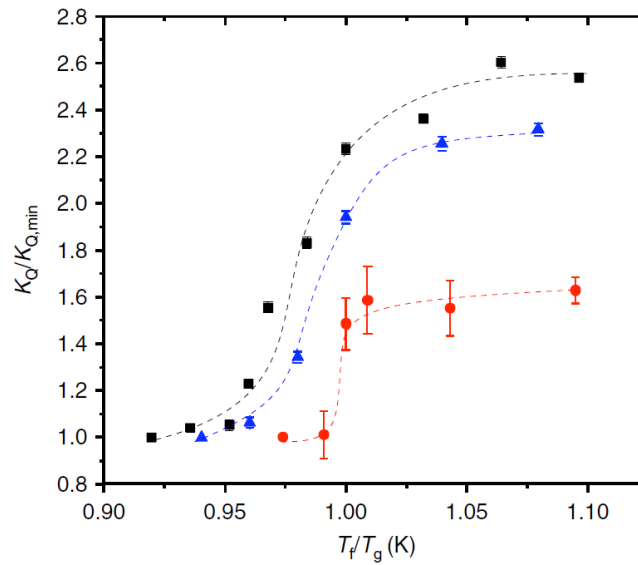
Figure 41. Notch fracture toughness for Zr₄₄Ti₁₁Ni₁₀Cu₁₀Be₂₅ (black squares), Pd₄₃Cu₂₇Ni₁₀P₂₀ (red circles) and Pt₅₇.₅Cu₁₄.₇Ni₅.₃P₂₂.₅ (blue triangles), showing an abrupt change in the normalized values for the notch fracture toughness in the region around the glass transition temperature. From [174]

Summary

Even when complying with the general processing requirements to avoid crystallization and obtain the best processing parameters defined by the TTT diagram of metallic glasses, a more through look reveals that several aspects might affect the final displayed properties of the material. For two different pieces, even if they undergo similar thermoforming processes, they can end with totally different internal structures and characteristics defined by its fictive temperature and where they are in the potential energy landscape, as they have a direct effect in how brittle or ductile the pieces can be. Thanks to the amorphous characteristic of metallic glasses, these properties are not fixed, and they can be modified to a degree by means of relaxation or rejuvenation of the material. Mechanical modification of the properties has been focused on inhomogeneous deformation of the BMG outside the SCLR with limited success and no practical or commercial application outside the laboratory. A new method to improve the properties of metallic glasses while thermoforming is then needed.

Chapter 5. Improving Ductility Through Straining

5.1 Straining at SCLR While Cooling

Realizing a higher T_f and hence a ductile state in a glass upon cooling requires either a slower relaxation process or faster cooling. As the relaxation process of a metallic glass forming liquid is an alloy specific and intrinsic property, only the cooling rate can act as a tool to enhance ductility. As a consequence, ductile states can generally only be realized in thin and simple geometries where sufficiently high cooling rates can be achieved [105], and most metallic glasses in bulk form lack ductility or fracture toughness [175-177].

Recognizing such limitations in realizing a ductile state under metallic glass forming conditions has led to the development of processing strategies to enhance ductility after the glass has already been formed. Such strategies are based on mechanical means [178] and include irradiation [169-173], static loading [158-162], cyclic loading [179], shot peening [143], rolling [180], twin roll casting [181], thermal cycling [104, 166-168], and severe plastic deformation [144, 164]. Among these methods addressing the glass are some that offer practical methods to enhance ductility in metallic glass forming alloys [104]. However, it is unclear for which metallic glasses these techniques lead to rejuvenation or relaxation and hence a more ductile or brittle behavior, respectively [167]. Beyond cooling rate, other strategies that directly affect the liquid prior to glass formation have been explored but remain inconclusive [182].

Here, we strain the supercooled liquid metallic glass former during cooling. The resulting excited liquid originates from the evolving competition between structural relaxation and strain rejuvenation. Upon freezing into a glass, the temperature at which the excited liquid

state has been resumed is the representative fictive temperature of the resulting excited glass. The level to which straining enhances the fictive temperature depends on the difference between the time scales set by the strain rate, which increases the potential energy, and by structural relaxation, which decreases the potential energy. An increase in fictive temperature is reflected in an increase in ductility which we measure in bending.

5.2 Setup and Testing Method

Amorphous $Zr_{44}Ti_{11}Ni_{10}Cu_{10}Be_{25}$ rods of ~1.8 mm in diameter were prepared by copper mold casting. High purity ingots (for all constituent purity higher than 99.99) were arc-melted under argon atmosphere to alloy the constituents; subsequently, the alloy was reheated to a temperature of ~1000 ºC and under an argon gas pressure forced from the quartz nozzle into a copper mold with the final shape (Figure 42). The amorphous condition for the rods was confirmed by thermal analysis on some of the rods, revealing the typical thermogram for a fully amorphous sample which was cooled with a rate ~500 K/sec [109].
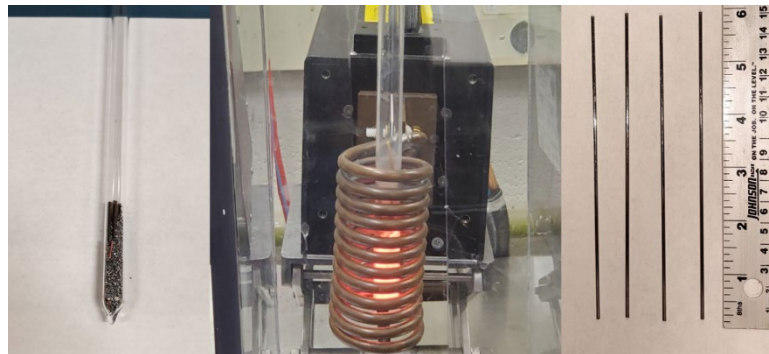
Figure 42. $Zr_{44}Ti_{11}Ni_{10}Cu_{10}Be_{25}$ rods made by allowing the components in a quartz tube and subsequently prepared by copper mold casting

To strain the samples on the SCLR, the amorphous $Zr_{44}Ti_{11}Ni_{10}Cu_{10}Be_{25}$ rods were heated to a temperature 80 K above the calorimetric glass transition temperature (T_g = 623 K) in an induction coil to deform it under a load and air cooling while deforming (Figure 43).
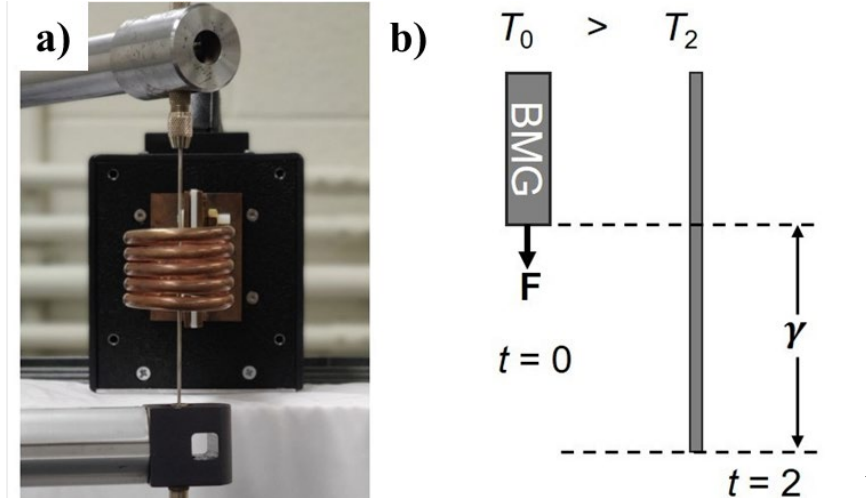
*Figure 43. a) Induction heating is used to heat a metallic glass rod to a desired temperature in the supercooled liquid region b) A constant force, which can vary between 1 and 100 N is applied to strain the sample. Upon straining, the sample is air cooled with a varying cooling rate ranging ~10-100 K/s. The variation of the cooling rate originates from the decreasing diameter of the sample upon straining from initially ~1.8 mm to a final ~ 0.1 mm. Strain, γ, is calculated from the sample's initial length, L_0 and length at time, L(t), by γ(t)=((L(t)-L_0)/L_0) * 100*

To determine when the required temperature is achieved, and have a consistent set of measurements, we rely on the VTF equation for the temperature dependance of the viscosity, where the viscosity (η) of the material can be calculated at a given temperature T with the fragility parameter (D^*), the temperature where barriers with respect to flow would go to infinity (T_0), and η_0 is the high temperature limit of viscosity[183]:

$$\eta_T = \eta_0 \exp\left(\frac{D^* \cdot T_0}{T - T_0}\right)$$

The stress (σ) imposed by the weight on the material is given by the relationship:

$$\sigma = \frac{F}{A}$$

With the force calculated with the weight in use, and the area (A) being the cross-sectional area of the sample. Finally, by substituting both equations in the flow stress of the material:

$$\sigma = \eta\dot{\gamma}$$

we can determine the strain rate imposed on the sample and use it as a proxy for the temperature measurement under a constant load (Figure 42).
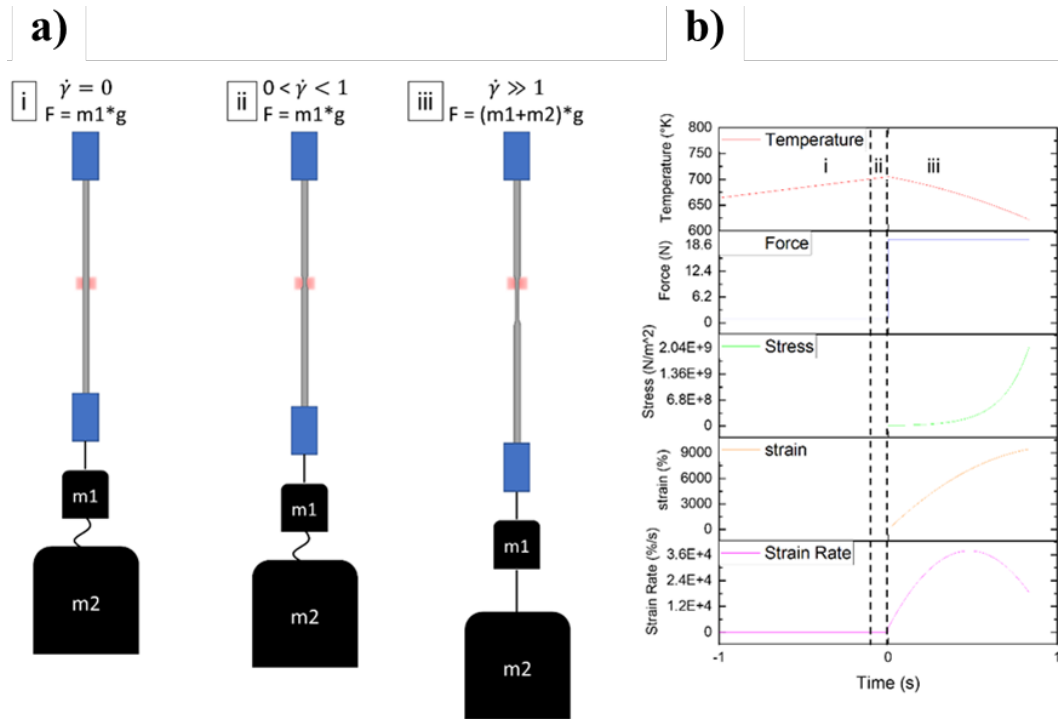
Figure 44. a) A small weight (m1) is used to determine temperature once deformation can be detected. Using the corresponding strain rate ~ $\dot{\gamma} = 0.1\ s^{-1}$ and $\dot{\gamma} * \eta = F/A$ the corresponding viscosity can be determined due to the strong temperature dependence of viscosity [184] b) Variable evolution over time for a sample wire

67

The rod is held from above inside an RF-coil, affixed with a hanging weight (100 g) and a second weight that is suspended not to exert any force on the sample initially (0-10000 g). The RF- coil is turned on, and once the rod deforms sufficiently to lengthen 5mm due to the 100 g force, the larger weight is released and rapidly strains the sample rod into a wire (Figure 45).
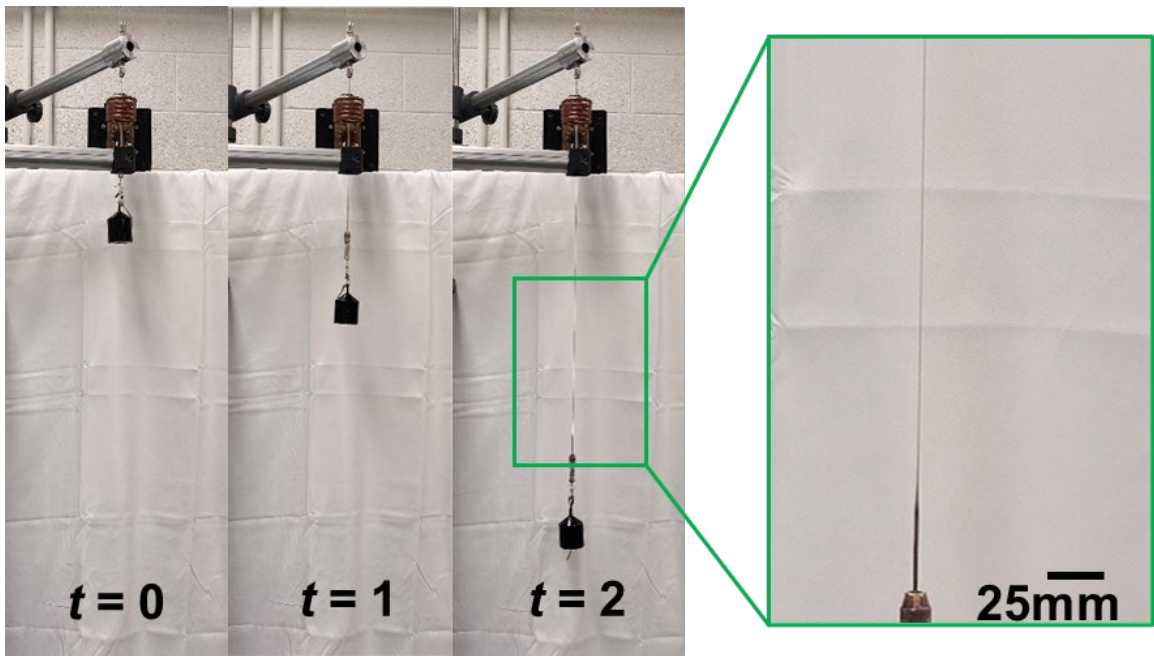
Figure 45. Snapshots of the deforming metallic glass in its supercooled liquid state

By varying the load, the strain rate can be manipulated. The decreasing cross section of the deforming sample and the strong temperature dependence of the viscosity control the evolution of temperature and strain rate profile (Figure 46). As the cross section of the sample continuously decreases, the cooling rate continuously increases (at least for $T > T_g$). Strain rate ($\dot{\gamma}$) under constant applied force is controlled by the time dependent cross-

sectional area and by the temperature dependent viscosity. The later can be approximated with a Vogel-Fulcher-Tammann (VFT) temperature dependence, hence exponentially increasing with decreasing temperature.
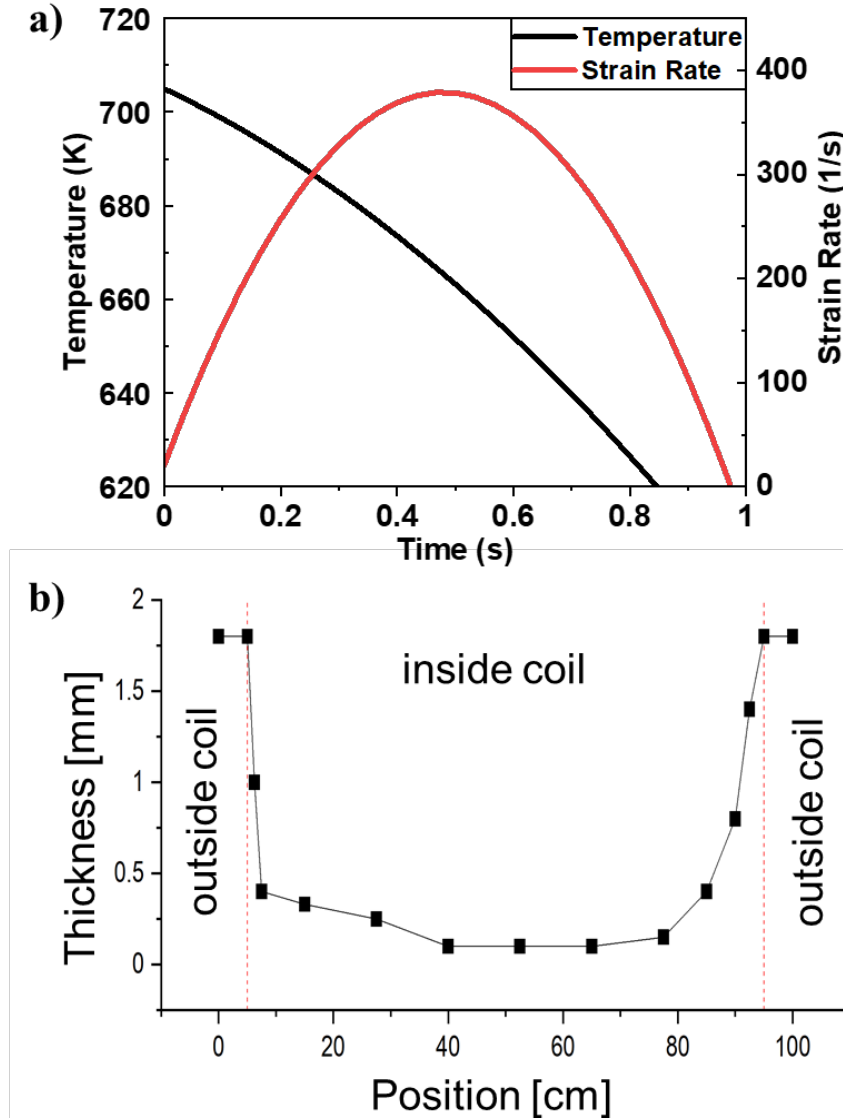
Figure 46. A typical time evolution of temperature and strain. Temperature evolution is estimated assuming convective air cooling and estimated through a lumped-capacitance model, which gives $T(t)=T_{env}+(T_0-T_{env})\ e^{-t/\tau}$, T_{env}: room temperature, T_0 : initial temperature of the sample, τ : time variable of the system, defined by $\tau = mc\ /\ (hA)$; m : mass of the sample, c : specific heat capacity, h : heat transfer coefficient, A : heat transfer surface area (see Supplement 4) b) Thickness distribution within the pulled wire.

Strain rate once the required weight is released after obtaining the required temperature is determined from video analysis and varied by changing the mass of the second weight. The first processing step with the 100 g weight warrants control over the initial temperature as the deformation to 5 mm is predominately controlled by viscosity which is highly temperature sensitive [185].

Qualitatively $\dot{\gamma}(T)$ exhibits a peak with values of several hundred strain per second, before decreasing again (Figure 46a). The sample presents a consistent thickness through the sample but in the region close to the undeformed edges (Figure 46). For a full derivation of the heat transfer during pulling please refer to supplement 4.

5.4 Evaluation of the Effects on Bending Ductility

The samples which were processed according to the simultaneous cooling and straining processing protocol were subsequently characterized to determine their ductility (Figure 45a). We choose bending characterization to determine the metallic glass samples' ductility. Metallic glasses exhibit typically no ductility in tension [176], and ductility measurements in compression are often overshadowed by misalignment and confinement effects [186]. Hardness and modulus trends have been associated with ductility trends and used for experimental convenience; however, these offer indirect information at best. The most reliable quantification of a ductile vs. brittle behavior can be achieved through fracture toughness measurements [187]. As those measurements are not possible due to the samples' geometry after pulling, we carry out bending experiments.

It has been shown that some metallic glasses, including the $Zr_{44}Ti_{11}Ni_{10}Cu_{10}Be_{25}$ alloy considered here, exhibit a well-defined and characteristic bending ductility in geometries where their thickness is below ~1 mm [116, 188, 189]. As the absolute value of the bending ductility is a function of the samples' thickness [116], only samples with similar thickness should be compared.
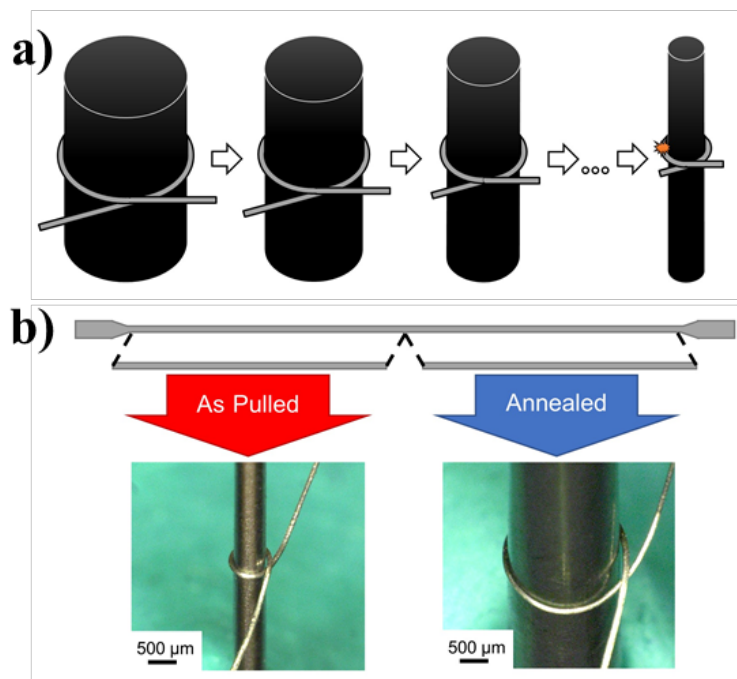
Figure 47. Characterization of the effect of excited liquid cooling on $Zr_{44}Ti_{11}Ni_{10}Cu_{10}Be_{25}$ metallic glass bending ductility a) Wires are mechanically characterized through bending around cylinders of successively small diameter until fracture b) In order to separate the effects of excited liquid cooling from the fast-cooling rate of the small geometry, wires are separated into two, with one segment characterized as pulled and the other annealed.

A challenge is to isolate the effect of the applied strain rate from other effects such as the cooling rate [182]. To be able to separate the effects, wires are divided into roughly equal segments and separated into two categories: as pulled and annealed (Figure 47b). Both sets

of wires are characterized via bending around cylinders of successively smaller diameters until fracture. Fractured wires are measured under an optical microscope to determine thickness and radius of fracture to determine bending plastic strain. This value is then added to the measured elastic strain limit (which is in close agreement with previously reported values [55]) to determine bending fracture strain ε_F^B.

We annealed one half of each wire at $T_g + 60$ K for 180 sec (~500 times the relaxation time [185], Figure 47b) to ensure that any history of the strain rate is erased after annealing, and a glass with the new fictive temperature of $T_g + 60$ K is created while at this elevated temperature[109]. Cooling from $T_g + 60$ K is carried out in the same way as the as-pulled samples, in ambient air, resulting in the same cooling rate as during the wire pulling experiments.
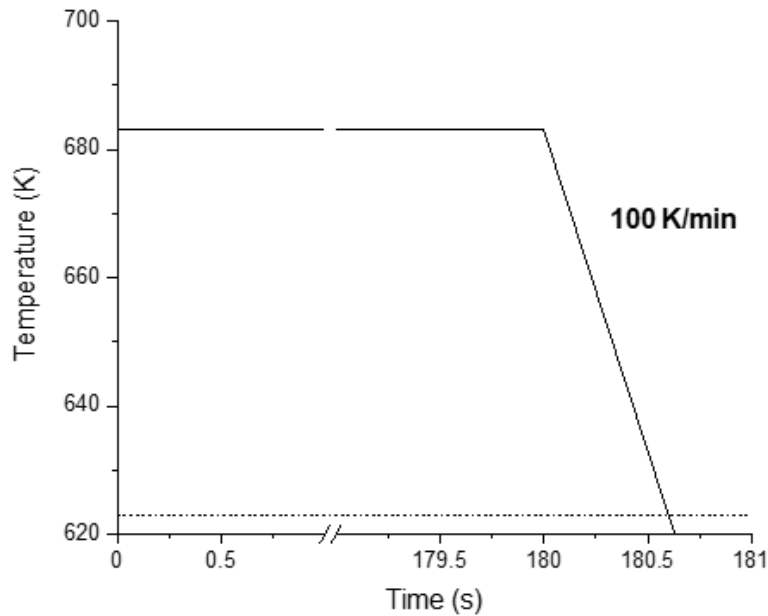
Figure 48. Temperature profile of wire annealing treatment. A salt bath is preheated to 60 K above the calorimetric cooling glass transition temperature (683 K) for at least an hour. Sample wires are submerged in the salt bath for 180 s before being retrieved and allowed to air cool.

72

The history of the straining is erased in the annealed wires while maintaining the same cooling profile as in the as-pulled samples. Subtracting the property values of the annealed samples from those of the as-pulled samples allows us to isolate the effect of strain rate during excited liquid cooling on the ductility, Figure 48 shows the temperature profile for the annealed samples.
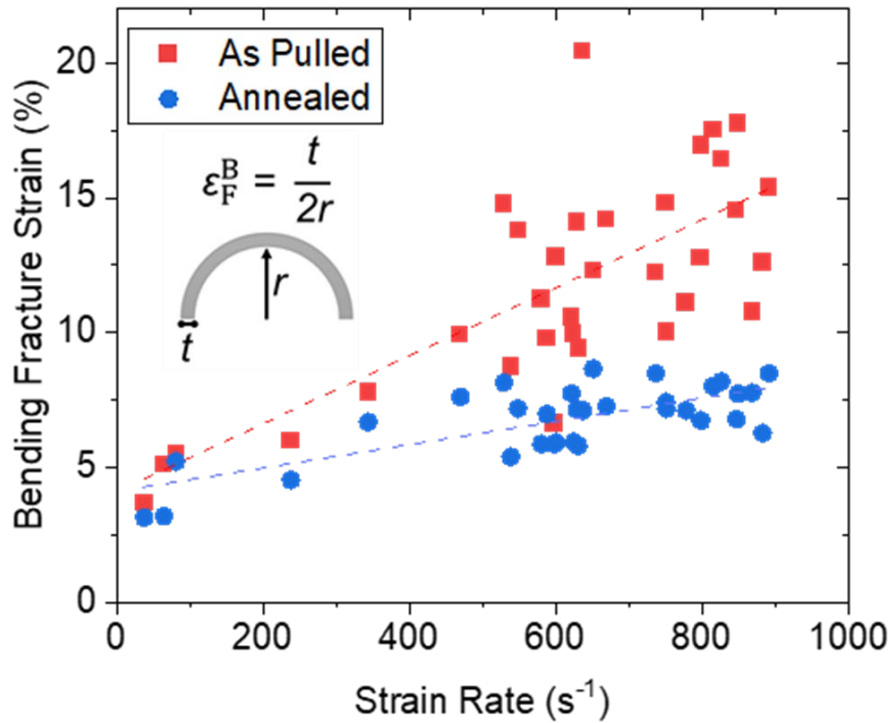
Figure 49. As pulled wires show a positive correlation between maximum strain rate of the pulling process and bending fracture strain. Annealed wires lose the added ductility to approximately the value of the as cast sample. However, as the final wire thickness decreases slightly with increasing strain rate, a small positive correlation between bending fracture strain and applied strain rate is present in the annealed wires, due to geometric effects in determining bending ductility [116].

A summary of the bending characterization of the differently strained metallic glass samples are shown in Figure 49. The bending fracture strain (ε_F^B) increases with increased experimental strain rate. For the same thickness of 100 μm, the as-cast

$Zr_{44}Ti_{11}Ni_{10}Cu_{10}Be_{25}$ exhibits an average $\varepsilon_F^B = 6\%$. With increasing strain rate, ε_F^B increases from ~4% for $\dot{\gamma} \sim 40$ s^{-1} to a maximum value of $\varepsilon_F^B = 16$ % for $\dot{\gamma} = 890$ s^{-1}. In some cases, even higher plastic bending strains of up to $\varepsilon_F^B \sim 20$ % are observed. We contribute the large scatter in the resulting bending fracture strain to the experimental difficulty of our setup in applying strain rate and cooling rate in a controlled synchronized way.

The samples that have been annealed after the pulling process exhibit a slightly higher but very similar $\varepsilon_F^B \sim 7\%$ compared to the as-cast material of ~6%. This suggest that the significant enhancement in ε_F^B measured in the as-pulled samples is predominantly due to the applied strain rate.

5.5 Thermal Characterization

Thermal characterization was also carried out on samples processed through excited liquid cooling (Figure 48). Thermal analysis was conducted using in a TA Q200 differential scanning calorimeter under argon flow with a heating rate of 20 K min^{-1}. All samples were heated through crystallization, subsequently cooled, and then heated again with the same heating rate to establish a baseline to be subtracted from the initial heating run. Measurements for the heat of enthalpy were made by finding the area of the curve with respect to the baseline, shown as a dashed line in Figure 48a.

Specifically, we consider the enthalpy of relaxation, $\Delta H_{rel,}$ which has been used as a thermodynamic measure to quantify the degree of rejuvenation [155, 157, 167, 190, 191]. For the strained samples, an increase in ΔH_{rel} compare to the annealed sample is present

(Figure 50a). Specifically, ΔH_{rel} increases from 0.21 kJ/mol for $\dot{\gamma} = 215$ s^{-1} to 0.81 kJ/mol

for the highest $\dot{\gamma} = 830$ s^{-1} (Figure 48b). The maximum absolute value of ΔH_{rel} of 0.81

kJ/mol is comparable to previously reported sub T_g mechanical rejuvenation techniques

including high pressure torsion and notched triaxial strain [147, 158, 162] and among the

highest reported changes in enthalpy of relaxation when compared to the reference sample.
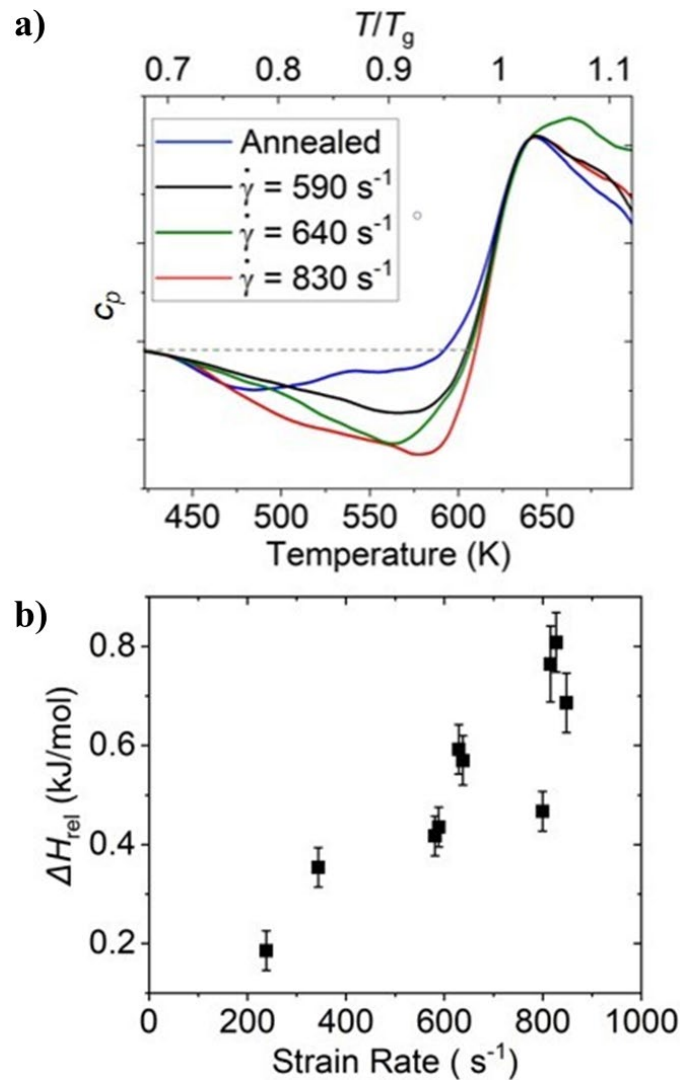
Figure 50. Thermal characterization of Zr$_{44}$Ti$_{11}$Ni$_{10}$Cu$_{10}$Be$_{25}$ metallic glass processed through excited liquid cooling. a) Thermograms measured with differential scanning calorimetry reveal the thermal signal of the excited liquid cooling. b) The enthalpy of relaxation increases with increasing strain rate applied during excited liquid cooling.

5.6 Excited Liquid Cooling Mechanism

The general understanding is that with both thermal and mechanical treatments, the potential energy of the glass can be manipulated. Enhancing the potential energy of a glass structure in the potential energy landscape is equivalent to increasing the fictive temperature of a glass [192]. Further, it has been argued that a high T_f can be generally associated with a larger ductility or fracture toughness [105, 109, 110, 193]. The treatment of excited liquid cooling discussed here directly affects the supercooled liquid.

We argue that the straining of the supercooled liquid is counteracting the relaxation process, preventing the liquid from assuming its metastable equilibrium and hence causing it to assume an excited state (Figure 49). The kinetic freezing of the (supercooled) liquid metallic glass former into a glass originates from the competition of the involved time scales. Under cooling conditions without an imposed strain rate, one of the involved time scales is set be the relaxation time, τ_{rel}, which is the temperature dependent time required for the liquid to assume the (meta)stable equilibrium configuration which continuously changes e.g., with temperature. Widely used to approximate τ_{rel} is the VFT equation: $\tau_{rel} = \tau_0 exp\left(\frac{D^*T_0}{T-T_0}\right)$ with T_0 as the VFT temperature, D^* the VFT fragility parameter, and τ_0 the high temperature limit of the relaxation time. This intrinsic time scale, with its exponential dependence on temperature, must be compared with the extrinsic time scale set by the processing protocol, τ_{cool}. During a typical cooling process, τ_{cool} is defined by the cooling rate, R, and can be described by $\tau_{cool} = \frac{1}{R}$.
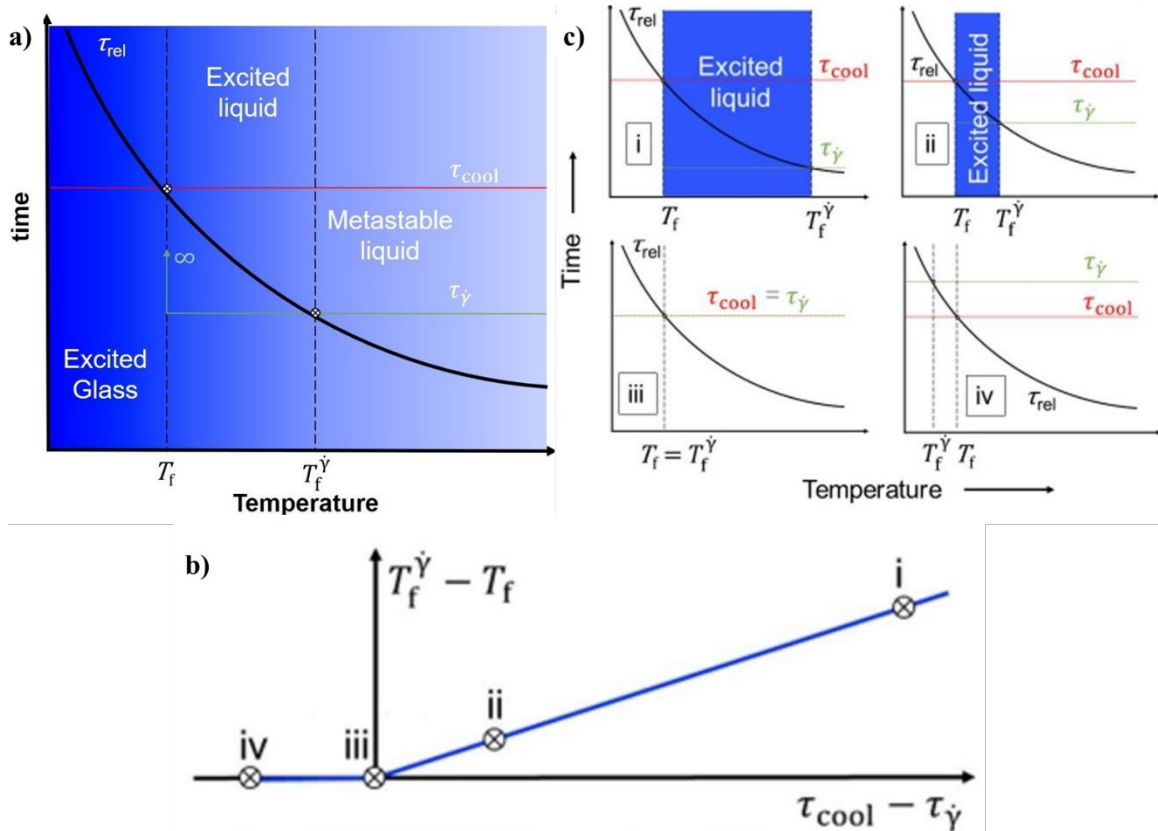
Figure 51. Excited liquid cooling mechanism a) Illustration of the characteristic time scales involved in the excited liquid cooling mechanisms as a function of temperature. The structural relaxation time, τ_{rel}, increases exponentially with decreasing temperature (black curve). A requirement for the excited liquid cooling mechanism is that the time scale set by the strain rate (green line), $\tau_{\dot{\gamma}} = \frac{0.02}{\dot{\gamma}}$ is smaller than the available time set by the cooling rate (red line), $\tau_{cool} = \frac{1}{R}$. Upon cooling, the liquid metallic glass former remains in metastable equilibrium for $\tau_{rel} < \tau_{\dot{\gamma}}$ until $\tau_{rel} = \tau_{\dot{\gamma}}$. Here, an "excited liquid" state is maintained through a competition between straining, causing the potential energy to increase, and relaxation, which decreases the potential energy for $T_f^{\dot{\gamma}} > T > T_f$ ($\dot{\gamma} = 0$). When $\tau_{rel} = \tau_{cool}$, at T_f, the excited liquid can no longer reconfigure on the experimental time scale to maintain its metastable equilibrium and freezes into an excited glass. The structure that freezes into a glass at T_f is that of the excited liquid with a fictive temperature of $T_f^{\dot{\gamma}}$. b and c) The effectiveness of excited liquid cooling is controlled by the relative rates of cooling and straining, inversely related to τ_{cool} and $\tau_{\dot{\gamma}}$. For $\tau_{cool} - \tau_{\dot{\gamma}} > 0$, the enhancement of fictive temperature $T_f^{\dot{\gamma}} - T_f$ scales with $\tau_{cool} - \tau_{\dot{\gamma}}$ (i and ii). For $\tau_{cool} - \tau_{\dot{\gamma}} \leq 0$, structural rearrangements due to $\dot{\gamma}$ do not occur (sufficiently) and hence do not affect fictive temperature or ductility (iii and iv).

At high temperatures, $\tau_{rel} < \tau_{cool}$, and the liquid has sufficient time to reconfigure during cooling to its temperature dependent metastable equilibrium. At lower temperatures $\tau_{rel} > \tau_{cool}$, which is due to the exponential temperature dependence of τ_{rel}, hence the liquid can no longer reconfigure into its temperature dependent metastable equilibrium. Consequently, the liquid falls out of metastable equilibrium at $\tau_{rel} = \tau_{cool}$, and freezes into a glass. The temperature T_f at which this freezing occurs ($\tau_{rel} = \tau_{cool}$) is referred to as the fictive temperature or the glass transition temperature upon cooling. As τ_{rel} is an intrinsic property of the liquid metallic glass former, one is left with only τ_{cool} as a tool to manipulate T_f. A higher cooling rate reduces τ_{cool} and, hence, results in a glass with a higher fictive temperature (Figure 49a).

In the present excited liquid cooling, a strain is applied at a certain rate during cooling of the liquid metallic glass former, working against the liquid's drive to assume a denser packed metastable equilibrium with decreasing temperatures. Straining a supercooled liquid metallic glass former causes it to dilate and loosens its packing [194], which increases its potential energy in opposition to the relaxation process of decreasing potential energy with decreasing temperature. To assign a characteristic time to the straining process we assume a critical strain of 2% which results in a characteristic time, $\tau_{\dot{\gamma}} = \frac{0.02}{\dot{\gamma}}$. Assuming 2% strain as a critical value to cause a "significant" structural change is based on previous work where this strain level has been observed to cause shear transformation zones to become unstable and cause a "significant" structural irreversible change [195]. However, it has also been pointed out that "weak" shear transformations occur at a much lower strain levels [122, 160, 196, 197], however significantly less in number.

When cooling a liquid metallic glass former under a strain rate, all three characteristic time scales, $\tau_{\dot{\gamma}}$, τ_{rel}, and τ_{cool} must be considered (Figure 51). Following the liquid metallic glass former upon cooling, it remains in metastable equilibrium down to $T_{\text{f}}^{\dot{\gamma}}$ (Figure 51). This is because for $T > T_{\text{f}}^{\dot{\gamma}}$ the times scales are such that $\tau_{\text{rel}} < \tau_{\dot{\gamma}} < \tau_{\text{cool}}$ hence, relaxation occurs within the available time. With decreasing temperature, τ_{rel} increases and $\tau_{\text{rel}} = \tau_{\dot{\gamma}}$ at $T = T_{\text{f}}^{\dot{\gamma}}$. For temperatures below $T_{\text{f}}^{\dot{\gamma}}$, the liquid can no longer reconfigure to reach its metastable equilibrium before that relaxation process is disturbed by the strain rate. Hence, the structure of the liquid falls out of metastable equilibrium and resumes an excited structure characterized by $T_{\text{f}}^{\dot{\gamma}}$. It is important to emphasize that the metallic glass is still in a liquid state, meaning that the structure rapidly changes, and these changes take place more rapidly than the available time set by the cooling rate τ_{cool}. This "excited liquid" state which is present between $T_{\text{f}}^{\dot{\gamma}}$ and T_{f} is maintained through a competition between straining, which increases the potential energy, and relaxation, which decreases the potential energy. Upon further cooling $\tau_{\text{rel}} = \tau_{\text{cool}}$ at T_{f}, and the excited liquid is no longer able to reconfigure on the time scale set by the experiments and, consequently, freezes into an excited glass. Even though the excited liquid freezes into a glass at T_{f}, its structural state has been established at a higher temperature $T_{\text{f}}^{\dot{\gamma}}$ which is the underlying mechanism of the excited liquid cooling method to achieve a ductile glass.

The effect of an applied strain rate in excited liquid cooling on increasing the fictive temperature of the glass (and hence ductility) depends on the relative magnitudes of the characteristic time scales. To increase the fictive temperature through an application of a strain rate, meaning $T_{\text{f}}^{\dot{\gamma}} > T_{\text{f}}$ ($\dot{\gamma} = 0$) requires $\tau_{\dot{\gamma}} < \tau_{\text{cool}}$. If $\tau_{\dot{\gamma}} > \tau_{\text{cool}}$, the time required

for structural changes to occur due to straining exceeds the time available during the cooling process and hence, structural changes originating from an applied strain rate do not occur. For example, a strain rate > 2 s^{-1} is required to enhance the fictive temperature and thereby ductility during bulk metallic glass formation at a cooling rate of 100 K/s ($\tau_{cool} = 10^{-2}$ s). The effectiveness of $\dot{\gamma}$ in enhancing fictive temperature scales with $\tau_{cool} - \tau_{\dot{\gamma}}$ (Figure 51 b & c). For $\tau_{cool} - \tau_{\dot{\gamma}} > 0$, the enhancement of fictive temperature $T_f^{\dot{\gamma}}$ - T_f scales with $\tau_{cool} - \tau_{\dot{\gamma}}$. With decreasing strain rate (but the same cooling rate) such that $\tau_{cool} - \tau_{\dot{\gamma}} \leq 0$, structural rearrangements due to $\dot{\gamma}$ can no longer significantly occur on the time scale of experiment. Hence, it is only for combinations of strain rates and cooling rates that fulfil $\tau_{cool} - \tau_{\dot{\gamma}} > 0$ that excited liquid cooling takes place. The effect on ductility increases with increasing $\tau_{cool} - \tau_{\dot{\gamma}}$.

In the proposed mechanism for excited liquid cooling assumptions where made which will now be discussed. Key to excited liquid cooling is the competition between relaxation and straining. Relaxation is a three-dimensional mechanism where atoms under the action of thermal energy (quantified in temperature) probe a vast range of structural states. On the other hand, the strain rate applied here is a one-dimensional mechanism which may even result into anisotropic properties and structure [198, 199]. During excited liquid cooling, the two effects compete with each other. However, structural relaxation is a more efficient mechanism utilizing all three physical dimensions to lower potential energy whereas strain rate only meaningfully accesses one dimension to increase potential energy. This makes a quantitative comparison of both contributions challenging.

Furthermore, in the above discussion on the mechanism of excited liquid cooling, we assumed a constant applied strain rate down to $T = T_f$. In general, such an assumption is oversimplified. Fundamentally, metallic glasses change their deformation behavior as a function of temperature and strain rate. At high temperatures, they deform in a homogenous fashion, essentially entirely affine, whereas at low temperatures, deformation is highly localized and non-affine [200]. To qualitatively represent this dramatic change in behavior as a function of temperature we assume $\dot{\gamma} = const \geq 0$ as a finite and constant strain rate for $T > T_f$ and $\dot{\gamma} = 0$ for $T < T_f$. This behavior is however simplified, as the practically realizable changes in $\dot{\gamma}(T)$ between T_l and T_f are less drastic.

It is generally understood that the viscosity in metallic glass forming liquids for $T > T_f$ is strain rate independent [201, 202] . However, for high strain rates, significant non-Newtonian effects have been observed [114, 115, 203], which may also take place during excited liquid cooling. In addition, straining of the sample may also generate heat which will affect cooling rate. Considering all this, our model to describe excited liquid cooling under the current assumptions offers only a qualitative description. For a quantitative description, more complicated calculations, using more detailed values of evolving process variables, would be required.

To compare the effectiveness of excited liquid cooling with other metallic glasses rejuvenation methods we use the enthalpy of relaxation, ΔH_{rel} which has been reported in most publications on rejuvenation techniques (Supplement 3). Comparison reveals that excited liquid cooling is among the most effective techniques to enhance the potential energy of the glass, offering a considerable increase in the enthalpy of relaxation through a mechanism directly affecting the liquid. It should be mentioned that comparison by their

effect on mechanical properties is not possible, as the reported studies of the various methods use different properties.

5.7 How Can This Be Applied in Processing?

The technological motivation of the various techniques to rejuvenate metallic glasses are to improve mechanical properties [104, 166, 167, 178]. Therefore, such methods, including our excited liquid cooling, will have to be practical to be used as a toughening strategy for metallic glass articles. Key to an effective practical usage of the excited liquid cooling method is a sufficiently high strain rate ($\tau_{cool} - \tau_{\dot{\gamma}} > 0$) present at temperatures including T_f and $T_\text{f}^{\dot{\gamma}}$ and that the excited liquid can be frozen into a glass state. It is important to mention that the absolute strain applied during excited liquid cooling is irrelevant. In the present setup, we use such high strains only for experimental convenience. To generate and freeze an excited liquid, only the strain rate over a narrow temperature interval is relevant. This interval is in the vicinity of T_f, where it sets $T_\text{f}^{\dot{\gamma}}$ and maintains this state until T_f. Such a situation can be realized in several metallic glass fabrication methods (Figure 52). For example, the pulling used here can be utilized to fabricate ductile metallic glass wires as a final product (Figure 52a). Similarly, sheets can be produced. For their synthesis, in addition to regular rolling, a subsequent pulling of the escaping sheet is required to establish a simultaneous straining and cooling. If one establishes $\tau_\text{cool} - \tau_{\dot{\gamma}} > 0$ for temperatures down to T_f, ductile sheets can be fabricated (Figure 52b & d). The requirement of $\tau_\text{cool} - \tau_{\dot{\gamma}} > 0$ for temperatures down to T_f can also be realized during blow molding and thereby net-shape complex metallic glass articles while establishing their ductile state

82

(Figure 52c & e). Here, the metallic glass feedstock is deformed through a gas pressure towards a cold mold. It has been previously determined that once the metallic glass touches the mold, the strain rate drops essentially instantaneous to zero [102, 204]. If the mold is set to a low temperature, and a temperature gradient between deforming feedstock and mold can established through the separating vacuum, the excited liquid can be rapidly frozen into a glass upon touching the mold, hence metallic glass parts can be net-shaped into their ductile state.
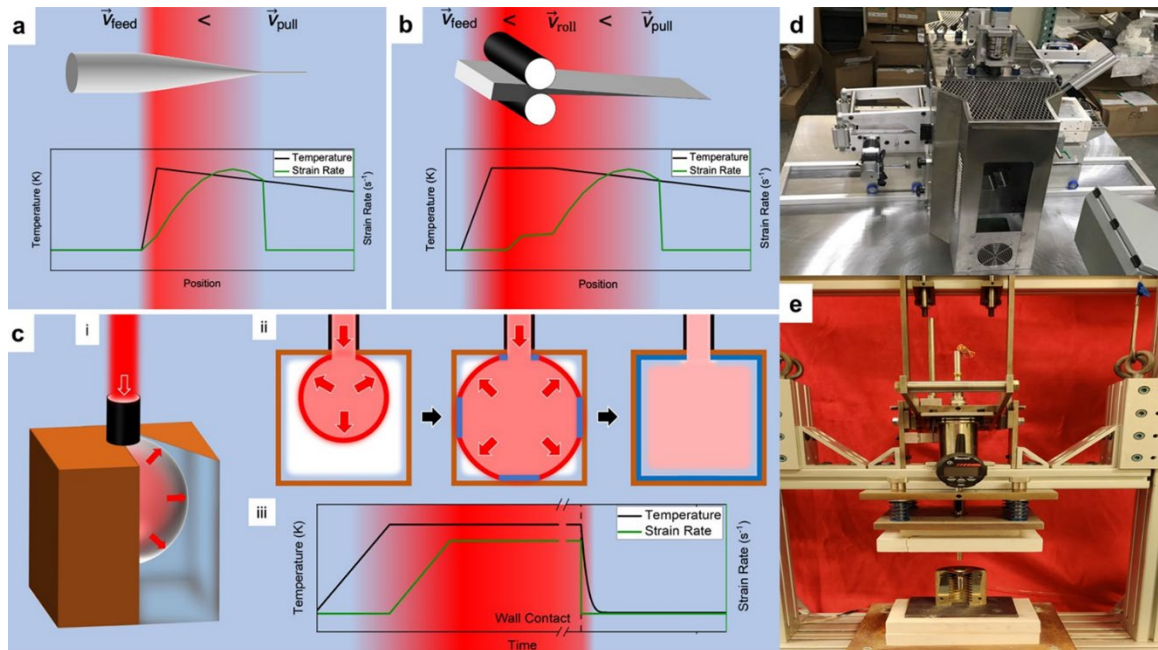
Figure 52. Metallic glass processing techniques that can be extended to incorporate excited liquid cooling a) Wire pulling where the wire ductility is controlled through maximizing $T_f^{\dot{\gamma}}$ - T_f. For a given strain rate, $T_f^{\dot{\gamma}}$ - T_f scales with the steepness of the spatial temperature gradient (From bright red being the highest temperature to blue being any temperature below T_f) b) In order to fabricate ductile sheets, excited liquid cooling can be realized through hot-rolling and subsequent pulling of the escaping sheet down a temperature gradient c) Blow molding [102] against a cold mold results into excited liquid cooling and hence enables to net-shape metallic glass articles into their ductile state d) A hot-rolling mill with a puller to realize b. e) A blow molding machine to realize c

Summary

We show here that an applied strain rate can excite the metallic glass in its liquid state to a higher potential energy. Microscopically, straining causes the structure to dilate, hence "pulls" the structure energetically up the potential energy landscape. Upon further cooling, the resulting excited liquid freezes into an excited glass that can triple its ductility compare to that of the unstrained material. Based on the requirement for the excited liquid cooling, we identify metallic glass processing techniques that allow to shape and net-shape metallic glasses into a complex geometry while assuming a ductile state.

Chapter 6. Conclusions and Outlook

6.1 New Methods to Process Metallic Glasses While Improving Their Ductility

Metallic glasses show promising characteristics that merge the best of two worlds: a high strength and mechanical properties from metals, while being able to process in viscosity ranges that allow for controlled deformations such as in polymers. These characteristics make them good candidates to substitute regular alloys that are limited in the complexity of their shapes that can be formed. By accessing the supercooled liquid region, several processing techniques have been developed for bulk metallic glasses, from flat sheets[82] to processes that enable features integrations[205] and its use as a reusable mold[206]; most of the research have been focused on closed shape or low-aspect ratio parts[207]. In this work we developed a new processing technique that allows bulk metallic glasses to obtain strain rates on the order of 2000% whereas previous techniques allow 150% at most, providing an increase in strain that can be realized by over 13 times; all while preserving the amorphous state and having control on the thickness distribution. Its applicability is demonstrated by its adoption from a Start-up company for its commercialization[208].

Furthermore, there has been an active research on the relationship between the different aspects of bulk metallic glasses and its final mechanical properties displayed, by looking at the effect of chemical composition over fracture toughness[177] and the environmental impact they may have[57], new alloys have been developed using combinatorial techniques[209]. Lately, a look at why the values measured fracture toughness for the same alloy reported by various authors, found that the way that samples were processed had a profound effect on the scattered values[47, 48, 52].

In this regard, several authors have worked on thermally improving the properties of metallic glasses by means of annealing or thermal cycling. In this work we demonstrate that straining a bulk metallic glass while cooling from the supercooled liquid region, "pulls" the material to higher energy states. Such structural changes can improve their ductility by as much as three times over the ductility of the same material, processed under the same conditions but without the application of a strain rate. Likewise, we propose the requirements and conditions under which straining has an effect on structure and properties, and realizing such requirements in thermoplastic processes including stretch-blow molding[204].

6.2 How Far Can These Improvements Go?

While we have shown that straining on the supercooled liquid region while cooling is an effective method to modify the bulk metallic glass properties, it is unclear to what extent this effect can be imposed on bulk metallic glasses or if this effect can be exerted across all the bulk metallic glasses families and compositions. Magnesium based bulk metallic glasses for example, display good corrosion resistance characteristics and are promising candidates for biological implants[210], but they are extremely brittle[57]. Being able to translate to other alloys and predict the outcome, could become a powerful tool to improve properties of some BMGs.

6.3 Anisotropic Properties of Metallic Glasses

In general, metallic glasses are considered isotropic and hence possess isotropic properties. Recent experiments have shown that when uniaxially stressed, metallic glasses show anisotropy in the elasticity they exhibit, with a 4% difference in the young's modulus[211]. While this effect was evaluated by mechanically treating the bulk metallic glasses under their glass transition temperature, it will be interesting to determine if the excited liquid cooling mechanism also induce anisotropy on the bulk metallic glasses, if so to what degree and if the atomic rearrangement is providing this.

6.4 Improving Mechanical Properties While Processing

In the first part of this thesis, we were able to merge the formability of plastics with the superior strength of metals by developing the stretch blow molding for metallic glasses. In the second part, we demonstrated that under the right conditions, it is possible to obtain an excited liquid state and improve the mechanical properties of the metallic glass if the required strain rates are achieved. The final step is to incorporate these improvements on the material while processing. For the case of stretch blow molding, the poker will allow the metallic glass to be at the exact temperature required prior to blow molding. By improving the temperature control of the blow molding process, we could apply strain rates that allow it to maintain an excited liquid configuration and cool it while deforming it, to retain such configuration. If this can be achieved in one single process such as the stretch blow molding, it will be a breakthrough for the commercialization of metallic glasses, as it will provide the material with better mechanical characteristics than what you started with.
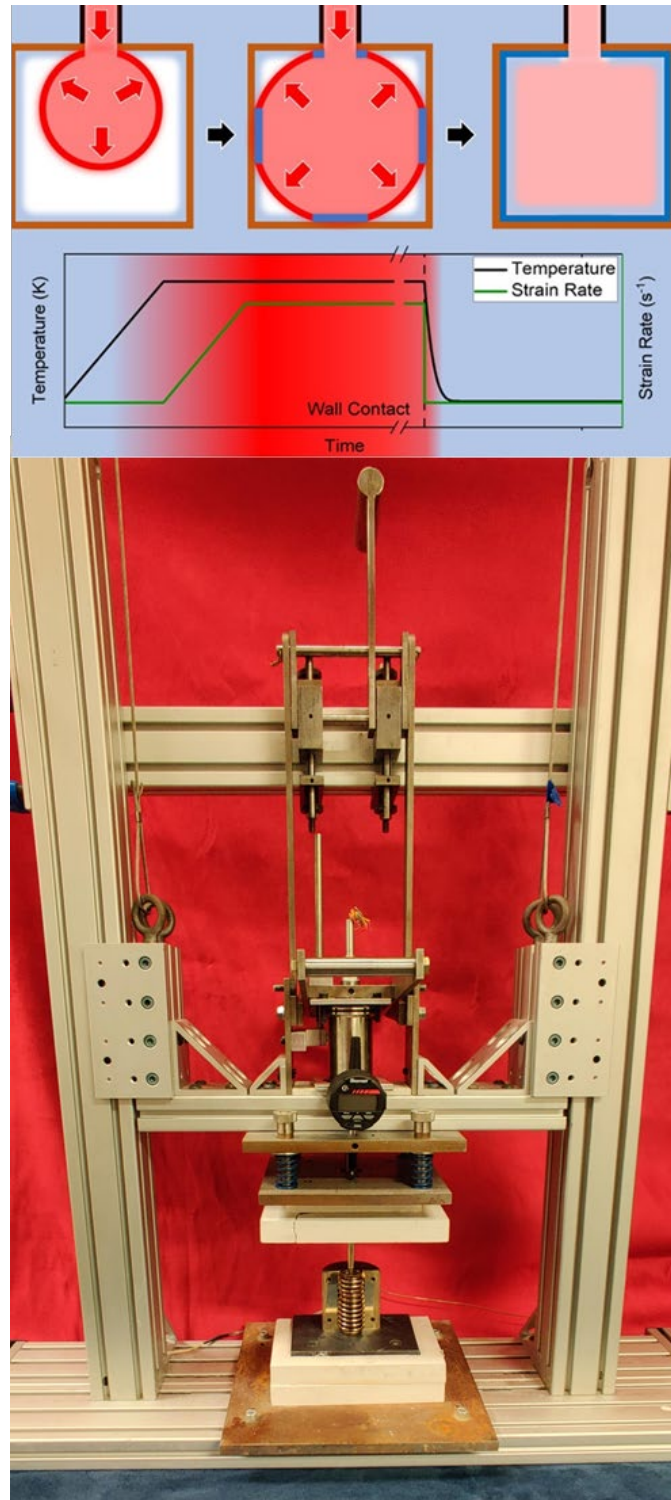
Figure 53. Generating an excited liquid state to improve the material properties while processing. Once the poker has introduced most of the material inside the mold, it can be used to equilibrate the sample temperature to be blow molded at the required strain rates. While cooling during this step, the material is frozen in the excited liquid state once it touches the mold.

Supplement 1. Derivation of a Kinematic Model for the Thickness Evolution of a Metallic Glass in a Cylindrical Mold

A metallic glass disc is held firmly in a cylindrical mold cavity and a pressure difference is applied for blow molding the metallic glass into the mold. Figure 15 shows a schematic of the process.
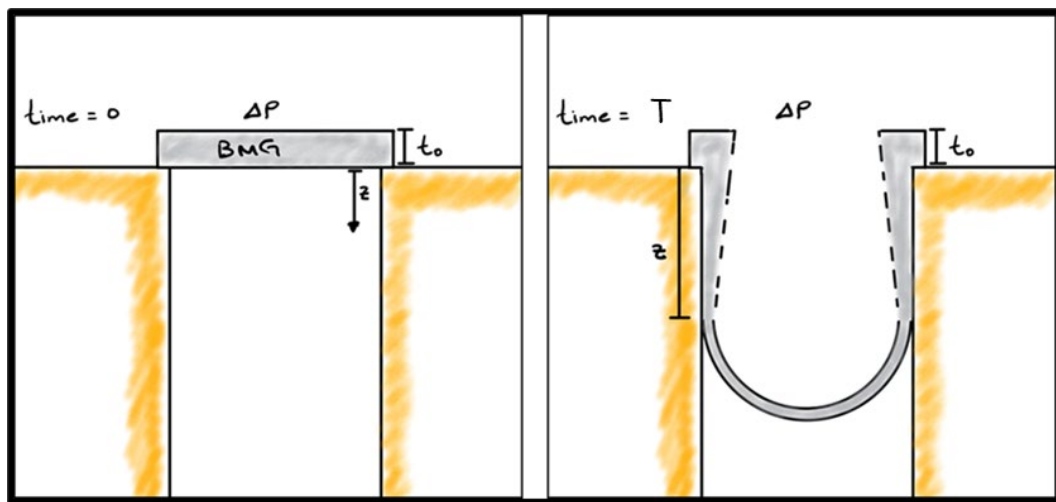
Figure 54. Schematic of the blow molding process. At a time, T=0 and z=0 the thickness is assumed to be equal to the initial thickness. At a time=T, the metallic glass touching the wall observe the no-slipping condition, preventing it from further thinning. We assumed a uniform half sphere advancing front from the free forming volume.

We would assume that the metallic glass is incompressible, that the bubble evolves as an advancing hemisphere front and that the thickness is uniform along this half hemisphere. Since the metallic glass behaves as a Newtonian fluid we will assume no-slip conditions at the boundary which prevents from further thinning of the material once it touches the mold. The volume of the sample is finite and that the thickness at Z_0 will be equal to the thickness at T_0.

The initial volume of the sample is given by:

$$V = \pi t_0 R^2$$

$$= \int_0^z \pi \left[R^2 - (R - t_{(z)})^2 \right] dz + 2\pi R^2 t_{(z)}$$

Since the volume of the material does not change:

$$\frac{dV}{dz} = 0 = \pi[R^2 - (R - t)^2] + 2\pi R^2 t'_{(z)}$$

$$= \pi(2Rt - t^2) + 2\pi R^2 \frac{dt}{dz}$$

$$\frac{dt}{dz} = -\frac{2Rt - t^2}{2R^2}$$

$$\int \frac{dt}{2Rt - t^2} = \int -\frac{dz}{2R^2}$$

$$\ln(t) - \ln(2R - t) = -\frac{z}{R} + C_1$$

By exponentiation of both terms:

$$\frac{t}{2R - t} = C_1 e^{-\frac{z}{R}}$$

$$t = 2RC_1 e^{-\frac{z}{R}} - tC_1 e^{-\frac{z}{R}}$$

$$t \left(1 + C_1 e^{-\frac{z}{R}} \right) = 2RC_1 e^{-\frac{z}{R}}$$

$$t = \frac{2RC_1 e^{-\frac{z}{R}}}{1 + C_1 e^{-\frac{z}{R}}}$$

Knowing that $t=t_0$ at $z=0$ then we can find the value for C_1:

$$t_0 = \frac{2RC_1}{1 + C_1}$$

$$t_0 + C_1 t_0 = 2RC_1$$

$$t_0 = 2RC_1 - C_1 t_0$$

$$t_0 = (2R - t_0)C_1$$

$$C_1 = \frac{t_0}{2R - t_0}$$

And substituting back in the original equation we get:

$$t = \frac{2R \frac{t_0}{2R - t_0} e^{-\frac{z}{R}}}{1 + \frac{t_0}{2R - t_0} e^{-\frac{z}{R}}}$$

Rearranging:

$$t = \frac{2Rt_0 e^{-\frac{z}{R}}}{2R - t_0 + t_0 e^{-\frac{z}{R}}}$$

$$t = \frac{2Rt_0 e^{-\frac{z}{R}}}{2R(1 - \frac{t_0}{2R} + \frac{t_0 e^{-\frac{z}{R}}}{2R})}$$

So, we arrive to the final form of the equation:

$$t = \frac{t_0 e^{-\frac{z}{R}}}{1 - \frac{t_0}{2R}(1 - e^{\frac{-z}{R}})}$$

Supplement 2. Derivation of the Thickness Distribution Model for the Sticking Region.
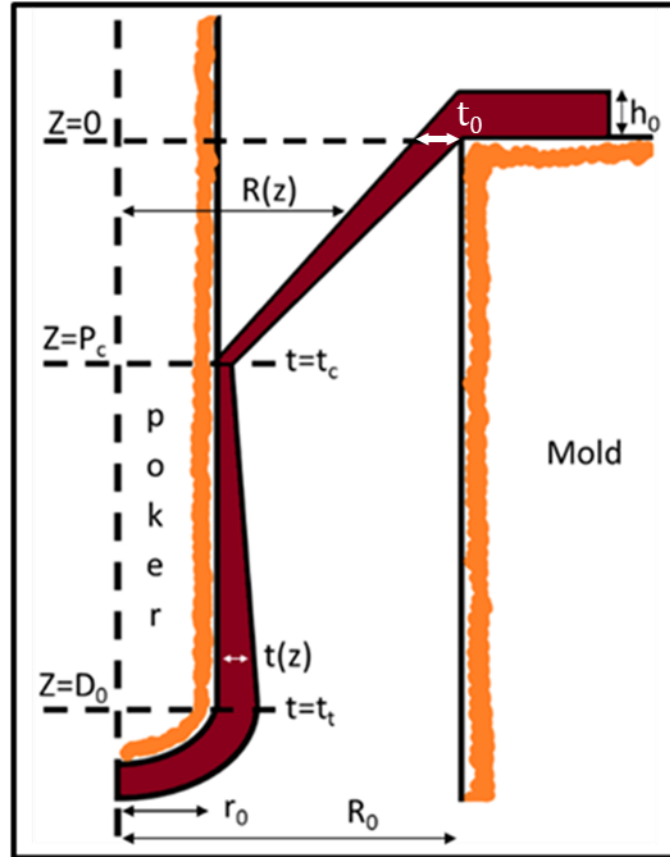
Figure 55. Schematics of the model used for the derivation

Assumptions:

1) Profile of purely extensional region does not change.

$$t_0 = \frac{h_0}{R_0 - r_0} P_c$$

2) Thickness distribution of extensional region is linear.

$$t(z, D) = \frac{z}{P_c} t_c + \frac{P_c - z}{P_c} t_0$$

3) Shape profile of extensional region is a straight line.

$$R(z) = \frac{z}{P_c} r_0 + \frac{P_c - z}{P_c} R_0$$

4) Thickness of poker tip does not change over time.

$$t(D, D) = t(P_c, P_c) = t_c(P_c) = t_t$$

5) The material is uncompressible and once it meets the obstacle, the thickness is
   defined.

$$\frac{dV_{extensional}}{dD} = -[\pi * t_c^2(D) + 2\pi r_0 t_c(D)]$$

Where, to calculate the volume of the purely extensional region:

$$V_{extensional} = \int_0^{P_c} [\pi(R(z) + t)^2 - \pi R^2(z)] \, dz$$

$$= \int_0^{P_c} \left[\pi \left(\frac{t_c - t_0}{P_c} z + t_0 \right)^2 + 2\pi \left(\frac{z}{P_c} r_0 + \frac{P_c - z}{P_c} R_0 \right) \left(\frac{t_c - t_0}{P_c} z + t_0 \right) \right] dz$$

$$= \frac{1}{3} \pi P_c (t_c - t_0)^2 + \pi P_c t_0^2 + \pi P_c t_0 (t_c - t_0) + \frac{2}{3} \pi P_c (r_c - R_0)(t_c - t_0)$$

$$+2\pi P_c r_0 t_0 + \pi P_c R_0 (t_c - t_0) + \pi P_c t_0 (r_c - R_0) \qquad (1)$$

To maintain the total volume:

$$-[\pi \, t_c^2(D) + 2\pi r_0 t_c(D)] = \frac{dV_{extensional}}{dD} \qquad (2)$$

Notice in the equation (1), only t_c is a function of D.

$$\frac{dV_{extensional}}{dD} = \frac{dV_{extensional}}{dt_c} \frac{dt_c}{dD}$$

$$= \frac{d}{dD}\left[\frac{1}{3}\pi P_c(t_c^2 - 2t_0 t_c) + \pi p_c t_0 t_c + \frac{2}{3}\pi P_c(r_0 - R_0)t_c + \pi P_c R_0 t_c\right]$$

$$= \frac{dt_c}{dD}\left[\frac{2}{3}\pi P_c t_c - \frac{2}{3}\pi P_c t_0 + \pi P_c t_0 + \frac{2}{3}\pi P_c(r_0 - R_0) + \pi P_c R_0\right]$$

$$= t_c'\left[\frac{2}{3}\pi P_c t_c + \frac{1}{3}\pi P_c t_0 + \frac{2}{3}\pi P_c r_0 + \frac{1}{3}\pi P_c R_0\right] \qquad (3)$$

Applying equation (3) into equation (2):

$$\frac{dt_c}{dD} = -\frac{\pi t_c^2 + 2\pi r_0 t_c}{\frac{1}{3}P_c(2t_c + t_0 + 2r_0 + R_0)}$$

The equation above leads to:

$$\left(\frac{Y}{t_c} + \frac{X}{t_c + 2r_0}\right)dt_c = dD \qquad (4)$$

Where:

$$\begin{cases} X = -\frac{1}{6}P_c(2 - \frac{t_0}{r_0} - \frac{R_0}{r_0}) \\ Y = -\frac{1}{6}P_c(\frac{t_0}{r_0} + 2 + \frac{R_0}{r_0}) \end{cases}$$

Solving equation (4) we have:

$$D = Constant + X\ln(t_c + 2r_0) + Y\ln(t_c)$$

Which can be written as:

$$e^{\frac{Const-D}{-X}} = (t_c + 2r_0)t_c^{(Y/X)}$$

By Applying the initial conditions when D=P$_c$ then t$_c$=t$_t$ so:

$$e^{\frac{Const-P_c}{-X}-\frac{D-P_c}{-X}} = \frac{(t_c + 2r_0)t_c^{(Y/X)}}{e^{\frac{D-P_c}{-X}}}$$

$$= (t_c(D) + 2r_0)[t_c(D)]^{\frac{Y}{X}}$$

So, we have:

$$[t_c(D)]^{\frac{Y}{X}} = \frac{t_t + 2r_0}{t_c(D) + 2r_0}/e^{\frac{D-P_c}{-X}} * t_t^{\frac{Y}{X}}$$

Since t$_c$ < t$_t$ << 2r$_0$

$$[t_c(D)] = \left\{ t_t^{Y/X}/e^{\frac{D-P_c}{-X}} \right\}^{X/Y}$$

$$= t_t \Big/ e^{\frac{-(D-P_c)}{Y}}$$

By applying the conditions in our procedure, t$_t$=.2mm, t$_0$=1.5mm, R$_0$/r$_0$=2.4, r$_0$=5mm

$$Y = -\frac{1}{6} * \frac{23.5}{5}P_c \approx -\frac{4}{5}P_c$$

$$t_c(D) = t_t e^{-\frac{5}{4}(\frac{D}{P_c}-1)}$$

So, the thickness of the sticking region is approximated by:

$$t = t(z) = t_t e^{-\frac{5}{4}(\frac{D_0-z}{P_c})} \tag{5}$$

Supplement 3. Previous Methods of Ductility Enhancement

Table 2. Summary of previous methods for manipulating metallic glasses properties

Method Description	Effect on glass or liquid	Effect	Mechanical tests	Homogeneous/ Inhomogeneous	Alloys	Change in thermal signal	Reference
High temperature creep	Glass	Increased plasticity (in some samples)	Compression	Homogenous deformation, possible anisotropy	$Zr_{50}Cu_{40}Al_{10}$ $Zr_{65}Cu_{17}Ni_8Al_{10}$ $Zr_{55}Cu_{30}Ni_5Al_{10}$	No difference observed vs. as-cast	[212, 213]
Elastostatic loading	Glass	Condition dependent rejuvenation or relaxation	Nanoindentation	Homogenous	$Cu_{57}Zr_{43}$ $Zr_{35}Ti_{30}Be_{27.5}Cu_{7.5}$	0.247-0.4 kJ/mol	[214-216]
Hot rolling	Liquid	Unstudied	N/A	Homogenous	$Zr_{44}Ti_{11}Cu_{10}Ni_{10}Be_{25}$	N/A	[81]
Twin roll casting	Liquid	Rejuvenation	Hardness	Homogenous	$Zr_{41.2}Ti_{13.8}Cu_{12.5}Ni_{10}Be_{22.5}$	0.2 kJ/mol	[181]
Notched uniaxial compression (Triaxial)	Glass	Rejuvenation, decreased hardness, increased plasticity	Tensile and hardness	Inhomogeneous	$Zr_{64.13}Cu_{15.75}Ni_{10.12}Al_{10}$	0.59 kJ/mol	[53, 54]
High pressure annealing	Glass	Rejuvenation, increased density, shear, and elastic modulus	N/A	N/A	$La_{60}Ni_{15}Al_{25}$	0.1-0.9 kJ/mol	[217]
High pressure torsion	Glass	Rejuvenation	Nanoindentation	Inhomogeneous	$Zr_{50.7}Cu_{28}Ni_9Al_{12.3}$ $Zr_{50}Cu_{40}Al_{10}$	0.5-1.1 kJ/mol	[147, 216, 218]
Cyclic nanoindentation	Glass	Increased hardness	Nanoindentation	Inhomogeneous	$Fe_{41}Co_7Cr_{15}Mo_{14}C_{15}B_6Y_2$	N/A	[219]
Uniaxial compression	Glass	Increase in plastic strain	Uniaxial compression	Homogenous	$Ni_{62}Nb_{38}$	.179 (from as cast) (.3 total) kJ/g	[220]
Dynamic excitation upon cooling	Glass	Rejuvenation	DMA	Homogenous	$Zr_{58.5}Cu_{15.6}Ni_{12.8}Al_{10.3}Nb_{2.8}$ $Zr_{66.5}Cu_{33.5}$ $Pd_{77.5}Cu_6Si_{16.5}$	.5 to 5 kJ/mol	[221]
Cyclic compression	Glass	Rejuvenation elastic, plastic anisotropy	Compression testing Vickers hardness	Inhomogeneous	$Zr_{61}Cu_{27}Fe_2Al_{10}$	0.25 kJ/mol	[222]
Laser shock peening. Shockwave imparted by a laser	Glass	Rejuvenation	Compression testing	Inhomogeneous	$Zr_{52.5}Cu_{17.9}Ni_{14.6}Al_{10.0}Ti_{5.0}$ $Zr_{41.2}Ti_{13.8}Cu_{12.5}Ni_{10}Be_{22.5}$	N/A	[223, 224]

Table 2 Cont'd. Summary of previous methods for manipulating metallic glasses properties.

Method Description	Effect on glass or liquid	Effect	Mechanical tests	Homogeneous/ Inhomogeneous	Alloys	Magnitude of thermal signal	Reference
Shot peening	Glass	Increased plasticity (hardening by residual stress, softening by sheer bands)	Microhardness, compression	Inhomogeneous	$Zr_{41.25}Ti_{13.75}Ni_{10}Cu_{12.5}Be_{22.5}$	N/A	[143, 225]
Shock compression	Glass	Rejuvenation	N/A	Inhomogeneous	$Zr_{55}Cu_{30}Ni_5Al_{10}$	.423 to 1.32 kJ/mol	[216]
Thermal cycling	Glass	Rejuvenation, increased plasticity, decreased hardness	Uniaxial compression, hardness	Inhomogeneous	$Cu_{46}Zr_{46}Al_7Gd_1$ $La_{55}Ni_{20}Al_{25}$ (ribbon) $La_{55}Ni_{10}Al_{35}$ $Zr_{62}Cu_{24}Fe_5Al_9$ ZrCuNiAl(Nb) ZrTiCuNiBe PdNiCuP PtNiCuP	(1.08-.74) = .34 kJ/mol	[226-228] [166, 167, 229]
Cold wire drawing	Glass	Decrease in yield stress, increase in fracture stress and plasticity	Tensile testing	Inhomogeneous	$Pd_{77.5}Cu_6Si_{16.5}$	N/A	[230]
Cold rolling	Glass	Increased ductility Work-hardening rejuvenation	Nanoindentation, ultrasonic testing	Inhomogeneous	$Zr_{55}Cu_{30}Ni_5Al_{10}$ $Cu_{47.5}Zr_{47.5}Al_5$ $Zr_{46.5}Cu_{45}Al_7Ti_{1.5}$	.3-.5 kJ/mol	[231-233]
Ball milling	Glass	rejuvenation	None	Inhomogeneous	$Pd_{40}Cu_{30}Ni_{10}P_{20}$ $Zr_{70}Cu_{20}Ni_{10}$	<.1 kJ/g	[234, 235]
Neutron and high energy particles irradiation	Glass	Rejuvenation or relaxation, increased ductility	Bending and Tension	Homogenous	many	N/A	[171, 236-238]
Fatigue coaxing	Glass	Increase in fatigue limit	3-point bending	Inhomogeneous	$Zr_{41.8}Ti_{12.9}Ni_{9.5}Cu_{12}Be_{23.8}$	N/A	[239]
Equal channel angular processing	Glass	Decreased yield strength, increased plasticity, likely due to shear banding not rejuvenation	Uniaxial compression	Inhomogeneous	$Zr_{57}Cu_{20}Al_{10}Ni_8Ti_5$	N/A	[240, 241]
Hot Wire Drawn	Liquid	Decreased modulus and hardness	Nanoindentation	Homogeneous	$Pd_{40}Cu_{30}Ni_{10}P_{20}$	28% increase from as cast	[182]
Static mechanical loading	glass	Strain hardening Increased plasticity	Tension, compression	Shear Transformation Zones	various	40%	[158, 162, 242]

| Cooling rate and annealing temperature | liquid | Density, Hardness, Modulus | | Homogenous | Cu-based, ZrCuNiAl, MgCuY | yes | [155, 157, 191] |

Supplement 4. Cooling Rate for Pulled Wires.

Assuming that the temperature is uniform throughout the wire deforming region, varying with time (relative position) but not with absolute position, and a constant heat transfer coefficient; we can use the lumped capacitance model to obtain the change in temperature.

From newton's law of cooling:

$$\dot{Q} = h * A * (T(t) - T\_env) = h * A * \Delta T(t)$$

Where:

$\dot{Q}$ is the heat rate transfer out of the body

h is the heat transfer coefficient

A is the heat transfer surface area

$T(t)$ is the temperature of the object's surface

T_{env} is the environment or room temperature

In the case of an incompressible material with a total internal energy U characterized by a single uniform temperature T(t), The heat capacity of the body C is $\frac{dU}{dT}$. The internal energy may be written in terms of the temperature of the body, the heat capacitance, and a reference temperature at which the internal energy is zero:

$$U = C(T - T_{ref})$$

Differentiating U with respect to time:

$$\frac{dU}{dt} = C\frac{dT}{dt}$$

If no work is exerted, by the first law of thermodynamics:

$$\frac{dU}{dt} = -Q$$

Thus:

$$\frac{dT(t)}{dt} = -\frac{hA}{C}(T(t) - T_{env}) = -\frac{1}{\tau}\Delta T(t)$$

Where:

$$\tau = \frac{C}{(hA)} = \frac{mc}{(hA)}$$

τ is the time constant of the system

C is the heat capacity

m is the mass of the material

c is the material specific heat capacity

When the environmental temperature is constant with time, we can define $\Delta T(t) = T(t) - T_{env}$ and the equation becomes:

$$\frac{dT(t)}{dt} = \frac{d\Delta T(t)}{dt} = \frac{1}{\tau}\Delta T(t)$$

Which solution by integration from the initial condition is:

$$\Delta T(t) = \Delta T(0)e^{-t/\tau}$$

Where $\Delta T(0)$ is the temperature difference at time 0, and to obtain the temperature at a given time t:

$$T(t) = T_{env} + (T_0 - T_{env})e^{-t/\tau}$$

Which becomes a function of the time and the heat transfer surface area.

If we assume that the region of interest from the wire it is a cylinder-shaped region with constant volume, we can obtain the change in surface area with respect to the change in length.

The volume of a cylinder is given by:

$$V = \pi r^2 L$$

Where:

r is the radius

L is the length of the wire

Solving for the radius we get:

$$r = \sqrt{\frac{V}{\pi L}}$$

The curved surface area of the cylinder is given by:

$$A = 2\pi r L$$

and so:

$$r = \frac{A}{2\pi r}$$

So, we can stablish:

$$\frac{A}{2\pi r} = \sqrt{\frac{V}{\pi L}}$$

Finally:

$$A = 2\sqrt{\pi L V}$$

Where the volume (V) is constant, and the length (L) varies with time.

References.

1. Mitchell, B.S., *An introduction to materials engineering and science for chemical and materials engineers*. 2004: John Wiley & Sons.

2. Chupak, T., *Aluminum receptacle with threaded outsert*, USPTO, Editor. 2004, Exal Corp: U.S.

3. Pauly, S., et al., *Processing metallic glasses by selective laser melting.* Materials Today, 2013. **16**(1-2): p. 37-41.

4. King, W.E., et al., *Laser powder bed fusion additive manufacturing of metals; physics, computational, and materials challenges.* Applied Physics Reviews, 2015. **2**(4): p. 041304.

5. Herzog, D., et al., *Additive manufacturing of metals.* Acta Materialia, 2016. **117**: p. 371-392.

6. Gibson, M.A., et al., *3D printing metals like thermoplastics: Fused filament fabrication of metallic glasses.* Materials Today, 2018. **21**(7): p. 697-702.

7. Backofen, W., I. Turner, and D. Avery. *Superplasticity*. in *JOM-Journal Of Metals*. 1964. Metallurgical Soc Amer Inst Mining Metall Petrol Eng Inc

8. Hamilton, C., A. Ghosh, and M. Mahoney. *SUPERPLASTICITY AND SUPERPLASTIC FORMING OF HIGH-STRENGTH ALUMINUM-ALLOYS*. in *Journal Of Metals*. 1980. Minerals Metals Materials Soc

9. Chokshi, A.H., A.K. Mukherjee, and T.G. Langdon, *Superplasticity in advanced materials.* Materials Science and Engineering: R: Reports, 1993. **10**(6): p. 237-274.

10. Zwigl, P. and D.C. Dunand, *Transformation superplasticity of zirconium.* Metallurgical and Materials Transactions A, 1998. **29**(10): p. 2571-2582.

11. Barnes, A., *Superplastic forming 40 years and still growing.* Journal of Materials Engineering and performance, 2007. **16**(4): p. 440-454.

12. Ashby, M.F., Y. Brechet, and D. Cebon, *Selection strategies for materials and processes.* Advanced engineering materials, 2002. **4**(6): p. 327-334.

13. Baird, D.G. and D.I. Collias, *Polymer processing: principles and design*. 2014: John Wiley & Sons.

14. Schroers, J., et al., *Thermoplastic blow molding of metals.* Materials Today, 2011. **14**(1): p. 14-19.

15. Kawamura, Y., et al., *Newtonian and non-Newtonian viscosity of supercooled liquid in metallic glasses.* Materials Science and Engineering: A, 2001. **304**: p. 674-678.

16. Schroers, J., *Processing of Bulk Metallic Glass.* Advanced Materials, 2010. **22**(14): p. 1566-1597.

17. Kato, H., et al., *Fragility and thermal stability of Pt-and Pd-based bulk glass forming liquids and their correlation with deformability.* Scripta Materialia, 2006. **54**(12): p. 2023-2027.

18. Klement, W., R. Willens, and P. Duwez, *Non-crystalline structure in solidified gold–silicon alloys.* Nature, 1960. **187**(4740): p. 869-870.

19. Nishiyama, N. and A. Inoue, *Glass transition behavior and viscous flow working of Pd40Cu30Ni10P20 amorphous alloy.* Materials Transactions, JIM, 1999. **40**(1): p. 64-71.

20. Schroers, J., et al., *Precious bulk metallic glasses for jewelry applications.* Materials Science and Engineering: A, 2007. **449**: p. 235-238.

21. Inoue, A., B. Shen, and A. Takeuchi, *Fabrication, properties and applications of bulk glassy alloys in late transition metal-based systems.* Materials Science and Engineering: A, 2006. **441**(1): p. 18-25.

22. Xu, D., et al., *Bulk metallic glass formation in binary Cu-rich alloy series–Cu100−xZrx (x= 34, 36, 38.2, 40 at.%) and mechanical properties of bulk Cu64Zr36 glass.* Acta Materialia, 2004. **52**(9): p. 2621-2624.

23. Kim, K., et al., *Effect of Sn on microstructure and mechanical properties of (Ti–Cu)-based bulk metallic glasses.* Philosophical Magazine Letters, 2006. **86**(8): p. 479-486.

24. Inoue, A., et al., *Cu-based bulk glassy alloys with high tensile strength of over 2000 MPa.* Journal of non-crystalline solids, 2002. **304**(1-3): p. 200-209.

25. Browne, D.J., Z. Kovacs, and W.U. Mirihanage, *Comparison of nucleation and growth mechanisms in alloy solidification to those in metallic glass crystallisation—relevance to modeling.* Transactions of the Indian Institute of Metals, 2009. **62**(4): p. 409-412.

26. Schroers, J., et al., *Continuous refinement of the microstructure during crystallization of supercooled Zr 41 Ti 14 Cu 12 Ni 10 Be 23 melts.* Applied physics letters, 1999. **74**(19): p. 2806-2808.

27. Zhong, L., et al., *Formation of monatomic metallic glasses through ultrafast liquid quenching.* Nature, 2014. **512**(7513): p. 177-180.

28. Busch, R., E. Bakke, and W. Johnson, *Viscosity of the supercooled liquid and relaxation at the glass transition of the Zr46. 75Ti8. 25Cu7. 5Ni10Be27. 5 bulk metallic glass forming alloy.* Acta Materialia, 1998. **46**(13): p. 4725-4732.

29. Mukherjee, S., et al., *Viscosity and specific volume of bulk metallic glass-forming alloys and their correlation with glass forming ability.* Acta materialia, 2004. **52**(12): p. 3689-3695.

30. Nieh, T., et al., *Plasticity and structural instability in a bulk metallic glass deformed in the supercooled liquid region.* Acta Materialia, 2001. **49**(15): p. 2887-2896.

31. Reger-Leonhard, A., M. Heilmaier, and J. Eckert, *Newtonian flow of Zr55Cu30Al10Ni5 bulk metallic glassy alloys.* Scripta materialia, 2000. **43**(5): p. 459-464.

32. Oh, H.S., et al., *A criterion of ideal thermoplastic forming ability for metallic glasses.* Scripta Materialia, 2020. **187**: p. 221-226.

33. Kawamura, Y., T. Nakamura, and A. Inoue. *Superplasticity in Pd40Ni40P20 metallic glass.* in *Materials science forum.* 1999.

34. Schroers, J., *Bulk metallic glasses.* Physics today, 2013. **66**(2): p. 32.

35. Khan, M.M., et al., *Recent advancements in bulk metallic glasses and their applications: a review.* Critical Reviews in Solid State and Materials Sciences, 2018. **43**(3): p. 233-268.

36. Telford, M., *The case for bulk metallic glass.* Materials today, 2004. **7**(3): p. 36-43.

37. Ashby, M. and A.L. Greer, *Metallic glasses as structural materials.* Scripta Materialia, 2006. **54**(3): p. 321-326.

38. Johnson, W., *Science and technology.* Mrs Bull, 1999. **24**: p. 42.

39. Xi, X., et al., *Fracture of brittle metallic glasses: Brittleness or plasticity.* Physical review letters, 2005. **94**(12): p. 125510.

40. Wang, G., et al., *Nanoscale periodic morphologies on the fracture surface of brittle metallic glasses.* Physical review letters, 2007. **98**(23): p. 235501.

41. Demetriou, M.D., et al., *A damage-tolerant glass.* Nature materials, 2011. **10**(2): p. 123-128.

42. Gilbert, C., R. Ritchie, and W. Johnson, *Fracture toughness and fatigue-crack propagation in a Zr–Ti–Ni–Cu–Be bulk metallic glass.* Applied Physics Letters, 1997. **71**(4): p. 476-478.

43. Lowhaphandu, P. and J.J. Lewandowski, *Fracture toughness and notched toughness of bulk amorphous alloy: Zr-Ti-Ni-Cu-Be.* Scripta Materialia, 1998. **38**(12).

44. Kim, C.P., et al., *Fracture toughness study of new Zr-based Be-bearing bulk metallic glasses.* Scripta Materialia, 2009. **60**(2): p. 80-83.

45. Schneibel, J., J. Horton, and P. Munroe, *Fracture toughness, fracture morphology, and crack-tip plastic zone of a Zr-based bulk amorphous alloy.* Metallurgical and Materials Transactions A, 2001. **32**(11): p. 2819-2825.

46. Kawashima, A., et al., *Fracture toughness of Zr55Al10Ni5Cu30 bulk metallic glass by 3-point bend testing.* Materials transactions, 2005. **46**(7): p. 1725-1732.

47. Chen, W., et al., *Does the fracture toughness of bulk metallic glasses scatter?* Scripta Materialia, 2015. **107**: p. 1-4.

48. Chen, W., et al., *Flaw tolerance of metallic glasses.* Acta Materialia, 2016. **107**: p. 220-228.

49. Xu, J., U. Ramamurty, and E. Ma, *The fracture toughness of bulk metallic glasses.* Jom, 2010. **62**(4): p. 10-18.

50. Sarac, B. and J. Schroers, *Designing tensile ductility in metallic glasses.* Nature communications, 2013. **4**(1): p. 1-7.

51. Sarac, B., et al., *Honeycomb structures of bulk metallic glasses.* Advanced Functional Materials, 2012. **22**(15): p. 3161-3169.

52. Liu, Z., et al., *3D metallic glass cellular structures.* Acta Materialia, 2016. **105**: p. 35-43.

53. Pan, J., et al., *Extreme rejuvenation and softening in a bulk metallic glass.* Nature communications, 2018. **9**(1): p. 1-9.

54. Pan, J., et al., *Strain-hardening and suppression of shear-banding in rejuvenated bulk metallic glass.* Nature, 2020. **578**(7796): p. 559-562.

55. Conner, R., et al., *Shear bands and cracking of metallic glass plates in bending.* Journal of applied physics, 2003. **94**(2): p. 904-911.

56. Ma, C., et al., *Improving plasticity of metallic glass by electropulsing-assisted surface severe plastic deformation.* Materials & Design, 2019. **165**: p. 107581.

57. Mota, R.M.O., et al., *Criticality in Bulk Metallic Glass Constituent Elements.* JOM, 2017. **69**(11): p. 2156-2163.

58. Shen, Y., L. Xing, and K. Kelton, *Formation and crystallization of ZrCuTi metallic glasses.* Philosophical Magazine, 2005. **85**(31): p. 3673-3682.

59.   Kelton, K.F., et al., *Mechanisms for nanocrystal formation in metallic glasses.* Journal of non-crystalline solids, 2003. **317**(1-2): p. 71-77.

60.   Schroers, J., et al., *Transition from nucleation controlled to growth controlled crystallization in Pd43Ni10Cu27P20 melts.* Acta Materialia, 2001. **49**(14): p. 2773-2781.

61.   Schroers, J., Y. Wu, and W.L. Johnson, *Heterogeneous influences on the crystallization of Pd43Ni10Cu27P20.* Philosophical Magazine A, 2002. **82**(6): p. 1207-1217.

62.   Schroers, J., et al., *Crystallization behavior of the bulk metallic glass forming Zr41Ti14Cu12Ni10Be23 liquid.* Materials Science and Engineering: A, 2001. **304**: p. 287-291.

63.   Bryn Pitt, E., G. Kumar, and J. Schroers, *Temperature dependence of the thermoplastic formability in bulk metallic glasses.* Journal of Applied Physics, 2011. **110**(4): p. 043518.

64.   Johnson, W.L., et al., *Beating crystallization in glass-forming metals by millisecond heating and processing.* Science, 2011. **332**(6031): p. 828-833.

65.   Waniuk, T., J. Schroers, and W.L. Johnson, *Timescales of crystallization and viscous flow of the bulk glass-forming Zr-Ti-Ni-Cu-Be alloys.* Physical Review B, 2003. **67**(18): p. 184203.

66.   Schroers, J., *On the formability of bulk metallic glass in its supercooled liquid state.* Acta Materialia, 2008. **56**(3): p. 471-478.

67.   Schroers, J., Q. Pham, and A. Desai, *Thermoplastic forming of bulk metallic glass— a technology for MEMS and microstructure fabrication.* Journal of microelectromechanical systems, 2007. **16**(2): p. 240-247.

68.   Inoue, A. and T. Zhang, *Fabrication of bulky Zr-based glassy alloys by suction casting into copper mold.* Materials Transactions, JIM, 1995. **36**(9): p. 1184-1187.

69.   Laws, K., B. Gun, and M. Ferry, *Effect of die-casting parameters on the production of high quality bulk metallic glass samples.* Materials Science and Engineering: A, 2006. **425**(1-2): p. 114-120.

70.   Laws, K.J., B. Gun, and M. Ferry, *Influence of casting parameters on the critical casting size of bulk metallic glass.* Metallurgical and Materials Transactions A, 2009. **40**(10): p. 2377-2387.

71.   Davis, J.R. and A.I.H. Committee, *Metals Handbook Desk Edition 2nd Edition.* 1998: Taylor & Francis.

72.   Schroers, J., *The superplastic forming of bulk metallic glasses.* Jom, 2005. **57**(5): p. 35-39.

73.   Mukherjee, S., et al., *Overheating threshold and its effect on time–temperature-transformation diagrams of zirconium based bulk metallic glasses.* Applied Physics Letters, 2004. **84**(24): p. 5010-5012.

74.   WL, J. and R. WK, *Effect of oxygen impurity on crystallization of an undercooled bulk glass forming Zr–Ti–Cu–Ni–Al alloy.* Materials Transactions, JIM, 1997. **38**(5): p. 473-477.

75.   Wall, J., et al., *Heterogeneous nucleation in a glass-forming alloy.* Applied Physics Letters, 2008. **92**(24): p. 244106.

76.	Way, C., P. Wadhwa, and R. Busch, *The influence of shear rate and temperature on the viscosity and fragility of the Zr41. 2Ti13. 8Cu12. 5Ni10. 0Be22. 5 metallic-glass-forming liquid.* Acta Materialia, 2007. **55**(9): p. 2977-2983.

77.	Lohwongwatana, B., J. Schroers, and W.L. Johnson, *Strain rate induced crystallization in bulk metallic glass-forming liquid.* Physical review letters, 2006. **96**(7): p. 075503.

78.	Setyawan, A.D., et al., *Glass formation dependence on casting-atmosphere pressure in Zr 65 Al 7.5 Ni 10 Cu 17.5− x Pd x (x= 0–17.5) alloy system: A resultant effect of quasicrystalline phase transformation and cooling mechanism during mold-casting process.* Journal of Applied Physics, 2008. **103**(4): p. 044907.

79.	Schroers, J. and N. Paton, *Amorphous metalalloys.* Advanced Materials & Processes, 2006: p. 61.

80.	Bordeenithikasem, P., et al., *Protocols for multi-step thermoplastic processing of metallic glasses.* Scripta Materialia, 2015. **104**: p. 56-59.

81.	Martinez, R., G. Kumar, and J. Schroers, *Hot rolling of bulk metallic glass in its supercooled liquid region.* Scripta Materialia, 2008. **59**(2): p. 187-190.

82.	Schroers, J., et al., *Method and System for Fabricating Bulk Metallic Glass Sheets*. 2016, Google Patents.

83.	Li, N., W. Chen, and L. Liu, *Thermoplastic micro-forming of bulk metallic glasses: a review.* Jom, 2016. **68**(4): p. 1246-1261.

84.	Chiu, H.M., et al., *Thermoplastic extrusion of bulk metallic glass.* Scripta Materialia, 2009. **61**(1): p. 28-31.

85.	Kumar, G., J. Blawzdziewicz, and J. Schroers, *Controllable nanoimprinting of metallic glasses: effect of pressure and interfacial properties.* Nanotechnology, 2013. **24**(10): p. 105301.

86.	Liu, Z. and J. Schroers, *General nanomoulding with bulk metallic glasses.* Nanotechnology, 2015. **26**(14): p. 145301.

87.	Kumar, G., H.X. Tang, and J. Schroers, *Nanomoulding with amorphous metals.* Nature, 2009. **457**(7231): p. 868-872.

88.	Schroers, J., et al., *Blow molding of bulk metallic glass.* Scripta Materialia, 2007. **57**(4): p. 341-344.

89.	Kanik, M., et al., *Metallic glass hemispherical shell resonators.* Journal of Microelectromechanical Systems, 2015. **24**(1): p. 19-28.

90.	Sarac, B., et al., *Three-dimensional shell fabrication using blow molding of bulk metallic glass.* Journal of Microelectromechanical Systems, 2011. **20**(1): p. 28-36.

91.	Lu, J., G. Ravichandran, and W.L. Johnson, *Deformation behavior of the Zr41. 2Ti13. 8Cu12. 5Ni10Be22. 5 bulk metallic glass over a wide range of strain-rates and temperatures.* Acta materialia, 2003. **51**(12): p. 3429-3443.

92.	Yang, F., *Plastic flow in bulk metallic glasses: Effect of strain rate.* Applied Physics Letters, 2007. **91**(5): p. 051922.

93.	Zumkley, T., et al., *Effect of reversible structural relaxation on diffusion in a ZrTiCuNiBe bulk glass.* Scripta materialia, 2001. **45**(4): p. 471-477.

94.	Wang, W.H., et al., *Stability of ZrTiCuNiBe bulk metallic glass upon isothermal annealing near the glass transition temperature.* Journal of materials research, 2002. **17**(6): p. 1385-1389.

95.   Wang, W.H. *Crystallization of ZrTiCuNiBe bulk metallic glasses*. in *Annales de Chimie Science des Materiaux*. 2002. Elsevier.

96.   Jing, Q., et al., *Thermal expansion behavior and structure relaxation of ZrTiCuNiBe bulk amorphous alloy*. Scripta materialia, 2003. **49**(2): p. 111-115.

97.   Williams, J., *A method of calculation for thermoforming plastics sheets*. Journal of Strain Analysis, 1970. **5**(1): p. 49-57.

98.   Throne, J.L., *Modeling plug-assist thermoforming*. Advances in Polymer Technology, 1989. **9**(4): p. 309-320.

99.   Trouton, F.T., *On the coefficient of viscous traction and its relation to that of viscosity*. Proceedings of the Royal Society of London. Series A, 1906. **77**(519): p. 426-440.

100.   Agassant, J.-F., et al., *Polymer processing: principles and modeling*. 2017: Carl Hanser Verlag GmbH Co KG.

101.   Busch, R., J. Schroers, and W.H. Wang, *Thermodynamics and kinetics of bulk metallic glass*. Mrs Bulletin, 2007. **32**(8): p. 620-623.

102.   Schroers, J., et al., *Thermoplastic blow molding of metals*. Materials Today, 2011. **14**(1-2): p. 14-19.

103.   Sarac, B., et al., *Three-Dimensional Shell Fabrication Using Blow Molding of Bulk Metallic Glass*. Journal of Microelectromechanical Systems, 2011. **20**(1): p. 28-36.

104.   Ketov, S.V., et al., *Rejuvenation of metallic glasses by non-affine thermal strain*. Nature, 2015. **524**(7564): p. 200-+.

105.   Fan, M., et al., *Effects of cooling rate on particle rearrangement statistics: Rapidly cooled glasses are more ductile and less reversible*. Physical Review E, 2017. **95**(2).

106.   Ketkaew, J., et al., *The effect of thermal cycling on the fracture toughness of metallic glasses*. Acta Materialia, 2020. **184**.

107.   Kumar, G., et al., *Critical Fictive Temperature for ductility in metallic glasses*. Nature Communications, 2013. **4**: p. 1536.

108.   Magagnosc, D.J., et al., *Effect of Ion Irradiation on Tensile Ductility, Strength, and Fictive Temperature in Metallic Glass Nanowires*. Acta Materialia, 2014. **74**: p. 165.

109.   Ketkaew, J., et al., *Mechanical glass transition revealed by the fracture toughness of metallic glasses*. Nature Communications, 2018. **9**.

110.   Louzguine-Luzgin, D.V., et al., *Influence of cooling rate on the structure and properties of a Cu-Zr-Ti-Ag glassy alloy*. Journal of Materials Research, 2008. **23**(2): p. 515-522.

111.   Ketkaew, J., et al., *Critical Crystallization for Embrittlement in Metallic Glasses*. Physical Review Letters, 2015. **115**(26).

112.   Sun, J.F., M. Yan, and J. Shen, *High strain rate induced embrittlement of Zr-based bulk metallic glass*. Transactions of Nonferrous Metals Society of China, 2005. **15**: p. 115-119.

113.   Jiang, W.H., F.E. Pinkerton, and M. Atzmon, *Effect of strain rate on the formation of nanocrystallites in an Al-based amorphous alloy during nanoindentation*. Journal of Applied Physics, 2003. **93**(11): p. 9287-9290.

114. Lohwongwatana, B., J. Schroers, and W.L. Johnson, *Strain rate induced crystallization in bulk metallic glass-forming liquid.* Physical Review Letters, 2006. **96**(7).

115. Shao, Z., et al., *Shear-accelerated crystallization in a supercooled atomic liquid.* Physical Review E, 2015. **91**(2).

116. Conner, R.D., et al., *Shear bands and cracking of metallic glass plates in bending.* Journal of Applied Physics, 2003. **94**(2): p. 904-911.

117. Kumar, G., et al., *Embrittlement of Zr-based bulk metallic glasses.* Acta Materialia, 2009. **57**(12): p. 3572-3583.

118. Kumar, G., et al., *Atomically smooth surfaces through thermoplastic forming of metallic glass.* Applied Physics Letters, 2010. **97**(10).

119. Li, R., et al., *Atomic imprinting into metallic glasses.* Communications Physics, 2018. **1**.

120. Mota, R.M.O., et al., *Criticality in Bulk Metallic Glass Constituent Elements.* Jom, 2017. **69**(11): p. 2156-2163.

121. Tool, A.Q., *Relaxation of stresses in annealing glass.* J. Res. Natl. Bur. Stand.(US), 1945. **34**(2): p. 199-211.

122. Fan, Y., T. Iwashita, and T. Egami, *How thermally activated deformation starts in metallic glass.* Nature Communications, 2014. **5**.

123. Ketkaew, J., et al., *Structural relaxation kinetics defines embrittlement in metallic glasses.* Scripta Materialia, 2018. **149**: p. 21-25.

124. Fan, Y., T. Iwashita, and T. Egami, *Crossover from Localized to Cascade Relaxations in Metallic Glasses.* Physical Review Letters, 2015. **115**(4).

125. Ashwin, J., E. Bouchbinder, and I. Procaccia, *Cooling-rate dependence of the shear modulus of amorphous solids.* Physical Review E, 2013. **87**(4).

126. Sun, Y., A. Concustell, and A.L. Greer, *Thermomechanical processing of metallic glasses: extending the range of the glassy state.* Nature Reviews Materials, 2016. **1**(9): p. 1-14.

127. Legg, B.A., J. Schroers, and R. Busch, *Thermodynamics, kinetics, and crystallization of Pt57. 3Cu14. 6Ni5. 3P22. 8 bulk metallic glass.* Acta materialia, 2007. **55**(3): p. 1109-1116.

128. Gallino, I., J. Schroers, and R. Busch, *Kinetic and thermodynamic studies of the fragility of bulk metallic glass forming liquids.* Journal of Applied Physics, 2010. **108**(6): p. 063501.

129. Shadowspeaker, L. and R. Busch, *On the fragility of Nb-Ni-based and Zr-based bulk metallic glasses.* Applied physics letters, 2004. **85**(13): p. 2508-2510.

130. Stillinger, F.H., *A topographic view of supercooled liquids and glass formation.* Science, 1995. **267**(5206): p. 1935-1939.

131. Sastry, S., P.G. Debenedetti, and F.H. Stillinger, *Signatures of distinct dynamical regimes in the energy landscape of a glass-forming liquid.* Nature, 1998. **393**(6685): p. 554-557.

132. Heuer, A., *Exploring the potential energy landscape of glass-forming systems: from inherent structures via metabasins to macroscopic transport.* Journal of Physics: Condensed Matter, 2008. **20**(37): p. 373101.

133. Stillinger, F.H. and T.A. Weber, *Packing structures and transitions in liquids and solids.* Science, 1984. **225**(4666): p. 983-989.

134. Debenedetti, P.G. and F.H. Stillinger, *Supercooled liquids and the glass transition.* Nature, 2001. **410**(6825): p. 259-267.

135. Liu, A.J. and S.R. Nagel, *Jamming is not just cool any more.* Nature, 1998. **396**(6706): p. 21-22.

136. Sollich, P., et al., *Rheology of soft glassy materials.* Physical review letters, 1997. **78**(10): p. 2020.

137. Heuer, A., *Properties of a glass-forming system as derived from its potential energy landscape.* Physical review letters, 1997. **78**(21): p. 4051.

138. Sastry, S., et al., *Potential energy landscape signatures of slow dynamics in glass forming liquids.* Physica A: Statistical Mechanics and its Applications, 1999. **270**(1-2): p. 301-308.

139. Kanik, M., et al., *High quality factor metallic glass cantilevers with tunable mechanical properties.* Applied Physics Letters, 2014. **105**(13): p. 131911.

140. Deng, D. and A. Argon, *Structural relaxation and embrittlement of Cu59Zr41 and Fe80B20 glasses.* Acta Metallurgica, 1986. **34**(10): p. 2011-2023.

141. Murali, P. and U. Ramamurty, *Embrittlement of a bulk metallic glass due to sub-Tg annealing.* Acta Materialia, 2005. **53**(5): p. 1467-1478.

142. Rycroft, C.H. and E. Bouchbinder, *Fracture toughness of metallic glasses: Annealing-induced embrittlement.* Physical review letters, 2012. **109**(19): p. 194301.

143. Concustell, A., et al., *Structural relaxation and rejuvenation in a metallic glass induced by shot-peening.* Philosophical Magazine Letters, 2009. **89**(12): p. 831-840.

144. Dmowski, W., et al., *Structural rejuvenation in a bulk metallic glass induced by severe plastic deformation.* Acta Materialia, 2010. **58**(2): p. 429-438.

145. Bian, X., et al., *Cryogenic-temperature-induced structural transformation of a metallic glass.* Materials Research Letters, 2017. **5**(4): p. 284-291.

146. Ge, T., et al., *Unusual energy state evolution in Ce-based metallic glass under high pressure.* Journal of Applied Physics, 2017. **121**(20): p. 205109.

147. Meng, F., et al., *Reversible transition of deformation mode by structural rejuvenation and relaxation in bulk metallic glass.* Applied Physics Letters, 2012. **101**(12): p. 121914.

148. Spaepen, F., *A microscopic mechanism for steady state inhomogeneous flow in metallic glasses.* Acta metallurgica, 1977. **25**(4): p. 407-415.

149. Lewandowski*, J., W. Wang, and A. Greer, *Intrinsic plasticity or brittleness of metallic glasses.* Philosophical Magazine Letters, 2005. **85**(2): p. 77-87.

150. Wu, T.W. and F. Spaepen, *The Relation between Embrittlement and Structural Relaxation of an Amorphous Metal.* Philosophical Magazine B-Physics of Condensed Matter Statistical Mechanics Electronic Optical and Magnetic Properties, 1990. **61**(4): p. 739-750.

151. Gilbert, C.J., R.O. Ritchie, and W.L. Johnson, *Fracture toughness and fatigue-crack propagation in a Zr-Ti-Ni-Cu-Be bulk metallic glass.* Applied Physics Letters, 1997. **71**(4): p. 476-478.

152. Rycroft, C.H. and E. Bouchbinder, *Fracture Toughness of Metallic Glasses: Annealing-Induced Embrittlement.* Physical Review Letters, 2012. **109**(19).

153. Wu, T.W. and F. Spaepen, *Embrittlement of Metallic Glasses.* Journal of Metals, 1984. **36**(12): p. 54-54.

154. Pampillo, C.A. and D.E. Polk, *Annealing Embrittlement in an Iron-Nickel-Based Metallic Glass.* Materials Science and Engineering, 1978. **33**(2): p. 275-280.

155. Saida, J., et al., *Thermal rejuvenation in metallic glasses.* Science and Technology of Advanced Materials, 2017. **18**(1): p. 152-162.

156. Murah, P. and U. Ramamurty, *Embrittlement of a bulk metallic glass due to sub-T-g annealing.* Acta Materialia, 2005. **53**(5): p. 1467-1478.

157. Guo, W., et al., *Thermal Rejuvenation of an Mg-Based Metallic Glass.* Metallurgical and Materials Transactions a-Physical Metallurgy and Materials Science, 2019. **50a**(3): p. 1125-1129.

158. Pan, J., et al., *Extreme rejuvenation and softening in a bulk metallic glass.* Nature Communications, 2018. **9**.

159. Park, K.W., et al., *Elastostatically induced structural disordering in amorphous alloys.* Acta Materialia, 2008. **56**(19): p. 5440-5450.

160. Ju, J.D., et al., *An atomically quantized hierarchy of shear transformation zones in a metallic glass.* Journal of Applied Physics, 2011. **109**(5).

161. Ju, J.D. and M. Atzmon, *A comprehensive atomistic analysis of the experimental dynamic-mechanical response of a metallic glass.* Acta Materialia, 2014. **74**: p. 183-188.

162. Pan, J., et al., *Strain-hardening and suppression of shear-banding in rejuvenated bulk metallic glass.* Nature, 2020. **578**(7796): p. 559-+.

163. Zhou, H.B., et al., *Two-stage rejuvenation and the correlation between rejuvenation behavior and the boson heat capacity peak of a bulk metallic glass.* Acta Materialia, 2019. **179**: p. 308-316.

164. Wang, X.D., et al., *Atomic-level structural modifications induced by severe plastic shear deformation in bulk metallic glasses.* Scripta Materialia, 2011. **64**(1): p. 81-84.

165. Ryu, W., R. Yamada, and J. Saida, *Tailored hardening of ZrCuAl bulk metallic glass induced by 2D gradient rejuvenation.* Npg Asia Materials, 2020. **12**(1).

166. Li, B.S., S.H. Xie, and J.J. Kruzic, *Toughness enhancement and heterogeneous softening of a cryogenically cycled Zr-Cu-Ni-Al-Nb bulk metallic glass.* Acta Materialia, 2019. **176**: p. 278-288.

167. Ketkaew, J., et al., *The effect of thermal cycling on the fracture toughness of metallic glasses.* Acta Materialia, 2020. **184**: p. 100-108.

168. Das, A., E.M. Dufresne, and R. Maass, *Structural dynamics and rejuvenation during cryogenic cycling in a Zr-based metallic glass.* Acta Materialia, 2020. **196**: p. 723-732.

169. Baumer, R.E. and M.J. Demkowicz, *Radiation response of amorphous metal alloys: Subcascades, thermal spikes and super-quenched zones.* Acta Materialia, 2015. **83**: p. 419-430.

170. Raghavan, R., et al., *Ion irradiation enhances the mechanical performance of metallic glasses.* Scripta Materialia, 2010. **62**(7): p. 462-465.

171. Magagnosc, D.J., et al., *Effect of ion irradiation on tensile ductility, strength and fictive temperature in metallic glass nanowires.* Acta Materialia, 2014. **74**: p. 165-182.

172. Ebner, C., et al., *Electron beam induced rejuvenation in a metallic glass film during in-situ TEM tensile straining.* Acta Materialia, 2019. **181**: p. 148-159.

173. Sun, K., et al., *Structural rejuvenation and relaxation of a metallic glass induced by ion irradiation.* Scripta Materialia, 2020. **180**: p. 34-39.

174. Ketkaew, J., et al., *Mechanical glass transition revealed by the fracture toughness of metallic glasses.* Nature communications, 2018. **9**(1): p. 1-7.

175. Ashby, M.F. and A.L. Greer, *Metallic glasses as structural materials.* Scripta Materialia, 2006. **54**(3): p. 321-326.

176. Schuh, C.A., T.C. Hufnagel, and U. Ramamurty, *Overview No.144 - Mechanical behavior of amorphous alloys.* Acta Materialia, 2007. **55**(12): p. 4067-4109.

177. Shao, L., et al., *Effect of chemical composition on the fracture toughness of bulk metallic glasses.* Materialia, 2020. **12**.

178. Sun, Y.H., A. Concustell, and A.L. Greer, *Thermomechanical processing of metallic glasses: extending the range of the glassy state.* Nature Reviews Materials, 2016. **1**(9).

179. Packard, C.E., L.M. Witmer, and C.A. Schuh, *Hardening of a metallic glass during cyclic loading in the elastic range.* Applied Physics Letters, 2008. **92**(17): p. -.

180. Lee, M.H., et al., *Improved plasticity of bulk metallic glasses upon cold rolling.* Scripta Materialia, 2010. **62**(9): p. 678-681.

181. Zhang, L., et al., *Rejuvenated metallic glass strips produced via twin-roll casting.* Journal of Materials Science & Technology, 2020. **38**: p. 73-79.

182. Dong, J., et al., *Rejuvenation in Hot-Drawn Micrometer Metallic Glassy Wires.* Chinese Physics Letters, 2020. **37**(1).

183. Glade, S. and W. Johnson, *Viscous flow of the Cu 47 Ti 34 Zr 11 Ni 8 glass forming alloy.* Journal of Applied Physics, 2000. **87**(10): p. 7249-7251.

184. Waniuk, T., J. Schroers, and W.L. Johnson, *Timescales of crystallization and viscous flow of the bulk glass-forming Zr-Ti-Ni-Cu-Be alloys.* Physical Review B, 2003. **67**(18).

185. Gallino, I., J. Schroers, and R. Busch, *Kinetic and thermodynamic studies of the fragility of bulk metallic glass forming liquids.* Journal of Applied Physics, 2010. **108**(6).

186. Wu, W.F., Y. Li, and C.A. Schuh, *Strength, plasticity and brittleness of bulk metallic glasses under compression: statistical and geometric effects.* Philosophical Magazine, 2008. **88**(1): p. 71-89.

187. Lewandowski, J.J., W.H. Wang, and A.L. Greer, *Intrinsic plasticity or brittleness of metallic glasses.* Philosophical Magazine Letters, 2005. **85**(2): p. 77-87.

188. Chen, W., et al., *Test sample geometry for fracture toughness measurements of bulk metallic glasses.* Acta Materialia, 2018. **145**: p. 477-487.

189. Nollmann, N., et al., *Impact of micro-alloying on the plasticity of Pd-based bulk metallic glasses.* Scripta Materialia, 2016. **111**: p. 119-122.

190. Cangialosi, D., *Dynamics and thermodynamics of polymer glasses.* Journal of Physics-Condensed Matter, 2014. **26**(15).

191. Wakeda, M., et al., *Controlled Rejuvenation of Amorphous Metals with Thermal Processing.* Scientific Reports, 2015. **5**.

192. Debenedetti, P.G., F.H. Stillinger, and M.S. Shell, *Model energy landscapes.* Journal of Physical Chemistry B, 2003. **107**(51): p. 14434-14442.

193. Shen, J., Y.J. Huang, and J.F. Sun, *Plasticity of a TiCu-based bulk metallic glass: Effect of cooling rate.* Journal of Materials Research, 2007. **22**(11): p. 3067-3074.

194. Spaepen, F., *Metallic glasses: Must shear bands be hot?* Nature Materials, 2006. **5**(1): p. 7-8.

195. Johnson, W.L. and K. Samwer, *A universal criterion for plastic yielding of metallic glasses with a (T/T-g)(2/3) temperature dependence.* Physical Review Letters, 2005. **95**(19): p. -.

196. Atzmon, M. and J.D. Ju, *Microscopic description of flow defects and relaxation in metallic glasses.* Physical Review E, 2014. **90**(4).

197. Fan, M., et al., *Particle rearrangement and softening contributions to the nonlinear mechanical response of glasses.* Physical Review E, 2017. **96**(3).

198. Sun, Y., et al., *Flow-induced elastic anisotropy of metallic glasses.* Acta Materialia, 2016. **112**: p. 132-140.

199. Wu, B., T. Iwashita, and T. Egami, *Anisotropy of stress correlation in two-dimensional liquids and a pseudospin model.* Physical Review E, 2015. **92**(5): p. 052303.

200. Spaepen, F., *Microscopic Mechanism for Steady-State Inhomogeneous Flow in Metallic Glasses.* Acta Metallurgica, 1977. **25**(4): p. 407-415.

201. Kawamura, Y. and A. Inoue, *Newtonian viscosity of supercooled liquid in a Pd40Ni40P20 metallic glass.* Applied Physics Letters, 2000. **77**(8): p. 1114-1116.

202. Lu, J., G. Ravichandran, and W.L. Johnson, *Deformation behavior of the Zr41.2Ti13.8CU12.5Ni10Be22.5 bulk metallic glass over a wide range of strain-rates and temperatures.* Acta Materialia, 2003. **51**(12): p. 3429-3443.

203. Langer, J.S. and T. Egami, *Glass dynamics at high strain rates.* Physical Review E, 2012. **86**(1).

204. Mota, R.M.O., et al., *Overcoming geometric limitations in metallic glasses through stretch blow molding.* Applied Materials Today, 2020. **19**: p. 100567.

205. Schroers, J., et al., *Property enabled feature integration strategies and their fabrication methods for metallic glasses.* 2018, Google Patents.

206. Schroers, J., et al., *Molding and De-Molding of Metallic Glass Using Non-Disposable Molds.* 2016, Google Patents.

207. Rodrigo Miguel Ojeda Mota, J.K., Wen Chen, Jan Schroers. *Yale professor makes the case for Supercool Metals.* 2014; Available from: https://news.yale.edu/2014/09/04/yale-professor-makes-case-supercool-metals.

208. metals, S.; Available from: https://www.supercoolmetals.com/.

209. Liu, N., et al., *Combinatorial measurement of critical cooling rates in aluminum-base metallic glass forming alloys.* Scientific Reports, 2021. **11**(1): p. 3903.

210. Dambatta, M., et al., *Mg-based bulk metallic glasses for biodegradable implant materials: A review on glass forming ability, mechanical properties, and biocompatibility.* Journal of Non-Crystalline Solids, 2015. **426**: p. 110-115.

211. Concustell, A., et al., *Induced elastic anisotropy in a bulk metallic glass.* Scripta Materialia, 2011. **64**(12): p. 1091-1094.

212. Tong, Y., et al., *Recovering compressive plasticity of bulk metallic glasses by high-temperature creep.* Scripta Materialia, 2013. **69**(8): p. 570-573.

213. Tong, Y., et al., *Mechanical rejuvenation in bulk metallic glass induced by thermo-mechanical creep.* Acta Materialia, 2018. **148**: p. 384-390.

214. Lee, J.-C., *Calorimetric study of β-relaxation in an amorphous alloy: An experimental technique for measuring the activation energy for shear transformation.* Intermetallics, 2014. **44**: p. 116-120.

215. Zhang, M., et al., *Mechanical relaxation-to-rejuvenation transition in a Zr-based bulk metallic glass.* Scientific Reports, 2017. **7**(1): p. 1-12.

216. Ding, G., et al., *Ultrafast extreme rejuvenation of metallic glasses by shock compression.* Science advances, 2019. **5**(8): p. eaaw6249.

217. Wang, C., et al., *High stored energy of metallic glasses induced by high pressure.* Applied Physics Letters, 2017. **110**(11): p. 111901.

218. Wang, Y., et al., *Introducing a strain-hardening capability to improve the ductility of bulk metallic glasses via severe plastic deformation.* Acta materialia, 2012. **60**(1): p. 253-260.

219. Packard, C., L. Witmer, and C. Schuh, *Hardening of a metallic glass during cyclic loading in the elastic range.* Applied Physics Letters, 2008. **92**(17): p. 171911.

220. Lee, S.-C., et al., *Microstructural evolution of an elastostatically compressed amorphous alloy and its influence on the mechanical properties.* Scripta Materialia, 2008. **58**(7): p. 591-594.

221. Küchemann, S. and R. Maaß, *Gamma relaxation in bulk metallic glasses.* Scripta Materialia, 2017. **137**: p. 5-8.

222. Louzguine-Luzgin, D., et al., *On room-temperature quasi-elastic mechanical behaviour of bulk metallic glasses.* Acta Materialia, 2017. **129**: p. 343-351.

223. Liang, M., et al., *Effect of laser shock peening and its size-dependence on the compressive plasticity of Zr-based bulk metallic glass.* Journal of Materials Processing Technology, 2018. **251**: p. 47-53.

224. Cao, Y., et al., *Laser shock peening on Zr-based bulk metallic glass and its effect on plasticity: experiment and modeling.* Scientific reports, 2015. **5**: p. 10789.

225. Zhang, Y., W. Wang, and A. Greer, *Making metallic glasses plastic by control of residual stress.* Nature materials, 2006. **5**(11): p. 857-860.

226. Ketov, S., et al., *Rejuvenation of metallic glasses by non-affine thermal strain.* Nature, 2015. **524**(7564): p. 200-203.

227. Guo, W., R. Yamada, and J. Saida, *Rejuvenation and plasticization of metallic glass by deep cryogenic cycling treatment.* Intermetallics, 2018. **93**: p. 141-147.

228. Tong, Y., et al., *Structural rejuvenation in bulk metallic glasses.* Acta Materialia, 2015. **86**: p. 240-246.

229. Guo, W., et al., *Rejuvenation of Zr-based bulk metallic glass matrix composite upon deep cryogenic cycling.* Materials Letters, 2019. **247**: p. 135-138.

230. Takayama, S., *Drawing of Pd77. 5Cu6Si16. 5 metallic glass wires.* Materials Science and Engineering, 1979. **38**(1): p. 41-48.

231. Chen, H., *Stored energy in a cold-rolled metallic glass.* Applied Physics Letters, 1976. **29**(6): p. 328-330.

232. Liu, J., et al., *Shear band evolution and hardness change in cold-rolled bulk metallic glasses.* Acta materialia, 2010. **58**(14): p. 4827-4840.

233. Song, K., et al., *Significant tensile ductility induced by cold rolling in Cu47. 5Zr47. 5Al5 bulk metallic glass.* Intermetallics, 2011. **19**(10): p. 1394-1398.

234. Yavari, A.R., et al., *Excess free volume in metallic glasses measured by X-ray diffraction.* Acta Materialia, 2005. **53**(6): p. 1611-1619.

235. Shao, H., et al., *High density of shear bands and enhanced free volume induced in Zr70Cu20Ni10 metallic glass by high-energy ball milling.* Journal of alloys and compounds, 2013. **548**: p. 77-81.

236. Gerling, R., F.-P. Schimansky, and R. Wagner, *Restoration of the ductility of thermally embrittled amorphous alloys under neutron-irradiation.* Acta Metallurgica, 1987. **35**(5): p. 1001-1006.

237. Baumer, R. and M. Demkowicz, *Radiation response of amorphous metal alloys: Subcascades, thermal spikes and super-quenched zones.* Acta Materialia, 2015. **83**: p. 419-430.

238. Magagnosc, D.J., et al., *Tunable Tensile Ductility in Metallic Glasses.* Scientific Reports, 2013. **3**.

239. El-Shabasy, A.B. and J.J. Lewandowski, *Fatigue coaxing experiments on a Zr-based bulk-metallic glass.* Scripta Materialia, 2010. **62**(7): p. 481-484.

240. Lee, C.-M., K.-W. Park, and J.-C. Lee, *Plasticity improvement of a bulk amorphous alloy based on its viscoelastic nature.* Scripta materialia, 2008. **59**(8): p. 802-805.

241. Tong, Y., et al., *Residual elastic strain induced by equal channel angular pressing on bulk metallic glasses.* Acta materialia, 2013. **61**(4): p. 1204-1209.

242. Wang, Z.T., et al., *Densification and Strain Hardening of a Metallic Glass under Tension at Room Temperature.* Physical Review Letters, 2013. **111**(13).